LBNL-45379

# Ernest Orlando Lawrence Berkeley National Laboratory

# Ultrafast Excited State Dynamics of Tris-(2,2'-Bipyridine) Ruthenium(II)

Alvin T. Yeh

**Materials Sciences Division**

March 2000

Ph.D. Thesis

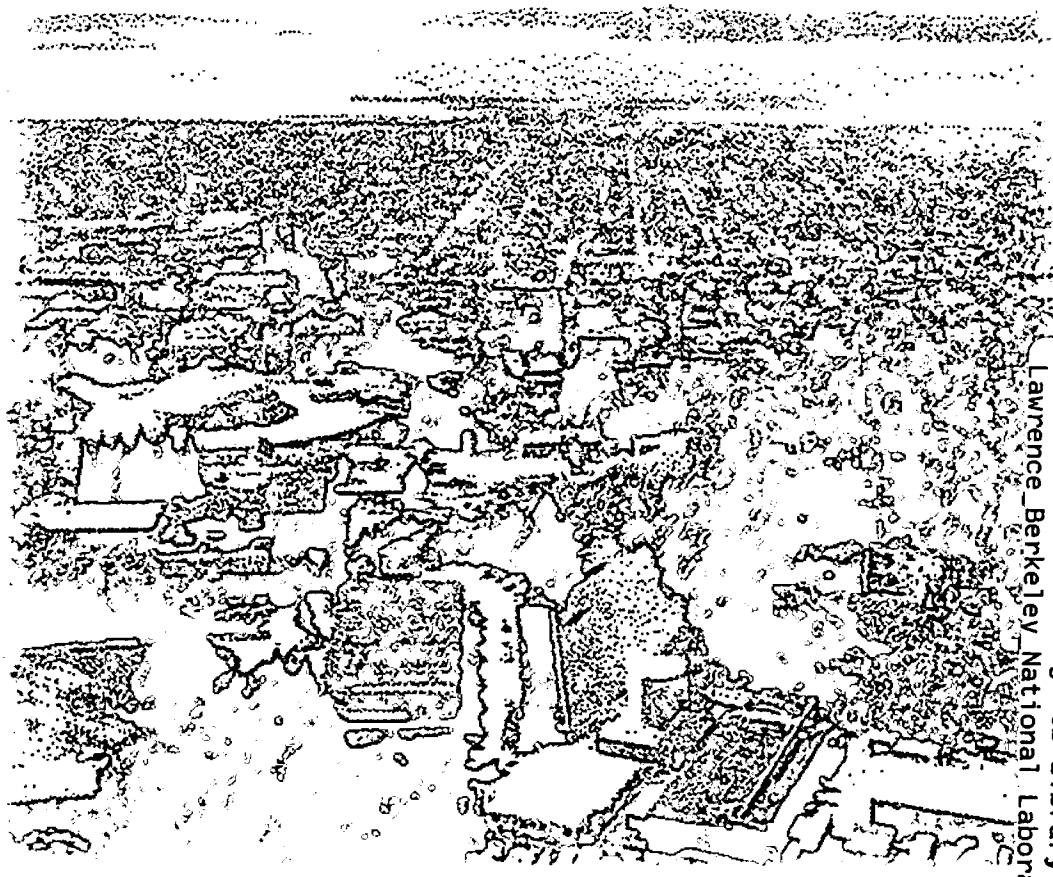

REFERENCE COPY
Does Not
Circulate

Bldg. 50 Library - Ref.
Lawrence Berkeley National Laboratory

LBNL-45379

Copy 1

## DISCLAIMER

This document was prepared as an account of work sponsored by the United States Government. While this document is believed to contain correct information, neither the United States Government nor any agency thereof, nor the Regents of the University of California, nor any of their employees, makes any warranty, express or implied, or assumes any legal responsibility for the accuracy, completeness, or usefulness of any information, apparatus, product, or process disclosed, or represents that its use would not infringe privately owned rights. Reference herein to any specific commercial product, process, or service by its trade name, trademark, manufacturer, or otherwise, does not necessarily constitute or imply its endorsement, recommendation, or favoring by the United States Government or any agency thereof, or the Regents of the University of California. The views and opinions of authors expressed herein do not necessarily state or reflect those of the United States Government or any agency thereof or the Regents of the University of California.

LBNL-45379

# Ultrafast Excited State Dynamics of Tris-(2,2'-Bipyridine) Ruthenium(II)

Alvin Tien-Wei Yeh
Ph.D. Thesis

Department of Chemistry
University of California, Berkeley

and

Materials Sciences Division
Ernest Orlando Lawrence Berkeley National Laboratory
University of California
Berkeley, CA 94720

March 2000

This work was supported by the Director, Office of Science, Office of Basic Energy Sciences, Materials Sciences Division, of the U.S. Department of Energy under Contract No. DE-AC03-76SF00098.

Abstract

Ultrafast Excited State Dynamics of Tris-(2,2'-Bipyridine) Ruthenium(II)

by

Alvin Tien-Wei Yeh

Doctor of Philosophy in Chemistry

University of California, Berkeley

Professor Charles V. Shank, Chair

Time resolved anisotropy measurements and time dependent transient absorption measurements are used to study the evolution of the photoexcited Franck-Condon state to the formation of the long-lived triplet metal-to-ligand charge-transfer ($^3$MLCT) state in tris-(2,2'-bipyridine) ruthenium(II). $[Ru(bpy)_3]^{2+}$ represents a large class of inorganic compounds with interesting and potentially applicable photophysical properties. These compounds have generated much interest in the inorganic chemistry community because their photophysical properties are easily manipulated by synthetic chemistry methods. However, little remains known about the processes which govern the evolution from initial photoexcitation to the formation of the long-lived excited state.

Metal to ligand charge transfer, when used to describe inorganic compounds, is a description of how the compound reacts to the absorption of light. Typically, these inorganic compounds are made of a transition metal with organic ligands, consisting of carbon, nitrogen and oxygen, coordinated in a highly symmetrical manner to the metal center. The highest occupied molecular orbitals (HOMO) in these compounds are isoenergetic with the frontier atomic orbitals of the metal and are localized to the metal

center. The lowest unoccupied molecular orbitals (LUMO) are isoenergetic with the coordinating ligand orbitals and are localized to the ligands. Upon absorption of light in which an electron is promoted from the HOMO to the LUMO, the electron is excited from the metal to the ligands.

Time dependent transient absorption measurements resolve the evolution of the initially excited state to the formation of the $^3$MLCT state. These measurements also reveal ultrafast dynamics which are characterized as intramolecular in nature and are associated with non-radiative relaxation processes. Symmetry argues the excited state should be delocalized among the bipyridine ligands. Rapid, solvent dependent depolarization of femtosecond anisotropy measurements indicate a change in symmetry of the excited state from a doubly degenerate delocalized state to a singly degenerate localized state. The anisotropy measurements also reveal that localization is facilitated through interactions with the solvent environment.

Two distinct processes have been resolved in the evolution of the $[Ru(bpy)_3]^{2+}$ Franck-Condon state to the formation of the $^3$MLCT state. Charge localization and ultrafast dynamics associated with non-radiative relaxation pathways are distinguished by their susceptibility to intermolecular interactions. These experiments represent the first measurements resolving these processes in the $[Ru(bpy)_3]^{2+}$ metal to ligand charge transfer complex.

# Table of Contents


**1. INTRODUCTION ..... 1**

1.1 METAL TO LIGAND CHARGE TRANSFER (MLCT) IN $[RU(BPY)_3]^{2+}$--ELECTRONIC STRUCTURE ..... 3
1.2 SINGLET TO TRIPLET INTERSYSTEM CROSSING ..... 11
1.3 LOCALIZATION OF CHARGE ..... 12

**2. SPECTRAL EVOLUTION OF THE $[RU(BPY)_3]^{2+}$ EXCITED STATE ..... 15**

2.1 DYNAMICS OF TRANSIENT ABSORPTION SPECTROSCOPY ..... 16
*2.1.1 Pump Perturbed Free Induction Decay ..... 21*
*2.1.2 Coherent Artifact ..... 23*
*2.1.3 Population Dynamics ..... 27*
2.2 EVOLUTION OF $[RU(BPY)_3]^{2+}$ TRANSIENT ABSORPTION SPECTRUM ..... 32

**3. BREAKING OF SYMMETRY—LOCALIZATION OF CHARGE ..... 37**

3.1 INTRODUCTION TO THE ANISOTROPY MEASUREMENT ..... 39
3.2 ANISOTROPY MEASUREMENT OF $[RU(BPY)_3]^{2+}$ ..... 47
3.3 SOLVENT DEPENDENCE OF LOCALIZATION ..... 53

**4. SINGLET TO TRIPLET TRANSITION ..... 57**

4.1 INTRAMOLECULAR PROCESSES IN $[RU(BPY)_3]^{2+}$ ..... 58
4.2 INTERACTION OF LIGHT WITH CHIRAL MOLECULES ..... 61
4.3 TIME RESOLVED CIRCULAR DICHROISM MEASUREMENT ..... 63

**5. CONCLUSIONS ..... 73**

5.1 LOCALIZATION OF CHARGE ..... 73
5.2 INTRAMOLECULAR PROCESSES ..... 75

**APPENDIX A. BLUE LASER SYSTEM ..... 77**

*A.1 Quad-detector piezo mount feedback beam stabilizer for Mach 500 Nd:YAG laser ..... 82*

**APPENDIX B. VIBRON C++ PROGRAM—COMPUTER SIMULATION OF FWM SIGNALS ..... 85**

B.1 CURRENT STATUS OF PROGRAM ..... 85
B.2 COMPILATION USING WATCOM C/C++ ..... 89
B.3 COMPILING ON THE CRAY ..... 90
*Vectorization and parallelization of code for the Cray ..... 90*
*Pros and cons of using the Cray ..... 91*
B.4 COMPILING ON SILICON GRAPHICS WORKSTATION ..... 93
B.5 RECOMMENDED ADDITIONAL FEATURES ..... 94
B.6 VIBRON.CPP ..... 94

**REFERENCES ..... 132**

## List of Figures

*Figure 1-1 Nonradiative relaxation processes. Illustrated are intramolecular vibrational relaxation (IVR), internal conversion (IC) and intersystem crossing (ISC).... 2*
*Figure 1-2 MLCT absorption band of $[Ru(bpy)_3]^{2+}$ in $CH_3CN$..... 4*
*Figure 1-3 Illustrates the splitting of metal d-orbitals due to symmetry of ligand field.... 5*
*Figure 1-4 The two-fold symmetry axis ($C_2$) in 2,2'-bipyridine..... 6*
*Figure 1-5 Mapping of symmetry constructed frontier orbitals of $[Ru(bpy)_3]^{2+}$ from octahedral symmetry to $D_3$ symmetry. The highest occupied molecular orbitals are metal centered and the lowest unoccupied molecular orbitals are localized on the ligands..... 7*
*Figure 1-6 Simplification of the basis set. The symmetry of $[Ru(bpy)_3]^{2+}$ is preserved in the simplified stick figure..... 10*
*Figure 1-7 The symmetry constructed E state using $\sigma$ bonds from the center to the three ligands as a basis. The sign denotes how the $\sigma$ bonds are combined to form the excited state..... 11*
*Figure 2-1 The effect of truncation of exponential decay functions at different points in time. This illustrates the effect of pump-perturbed free induction decay..... 22*
*Figure 2-2 Illustration of resonance Raman spectroscopy in the time domain. The Raman spectrum is the half Fourier transform of the time dependent overlap of the propagating wavepacket $|i(t)\rangle$ and the final state $|f\rangle$..... 25*
*Figure 2-3 Pictorial representation of third order Raman signals. The Raman signal is dependent on the overlap of the propagating wavepackets on the ground and excited state potential surfaces (see text)..... 26*
*Figure 2-4 Pictorial representation of linear absorption in the time domain. The absorption spectrum is the full Fourier transform of the time dependent overlap between the wavepacket $|i(t)\rangle$ and the ground state $|i(0)\rangle$ (see text)..... 28*
*Figure 2-5 Wavepacket dynamics in nonlinear absorption (see text)..... 29*
*Figure 2-6 Wavepacket dynamics in stimulated emission (see text)..... 31*
*Figure 2-7 Time resolved transient absorption spectra of $[Ru(bpy)_3]^{2+}$ in $CH_3CN$..... 32*
*Figure 2-8 Contributions to differential transmission spectra include bleaching of the absorption, excited state absorption of the probe and stimulated emission..... 33*
*Figure 2-9 Pictorial representation of wavepacket dynamics seen in the transient absorption spectra of $[Ru(bpy)_3]^{2+}$ (see text)..... 34*
*Figure 3-1 A delocalized electronic wavefunction preserves $D_3$ symmetry. A localized wavefunction reduces the $D_3$ symmetry to $C_2$ symmetry..... 38*
*Figure 3-2 Simple diagram of the experimental setup for an anisotropy measurement (see text)..... 40*
*Figure 3-3 Anisotropy as a function of angle for an isotropic distribution of singly degenerate transition moments..... 42*
*Figure 3-4 Chemical structure of 3,3'-diethyloxacarbocyanine iodide (DOCI)..... 43*
*Figure 3-5 Simultaneously collected pump-probe traces of DOCI with the probe polarization parallel and perpendicular to the pump polarization..... 44*
*Figure 3-6 Time dependent anisotropy of DOCI. DOCI was used to calibrate the anisotropy measurement..... 45*

*Figure 3-7 Energy level diagram of a system with a doubly degenerate excited state.* .. 46
*Figure 3-8 Simultaneously collected pump-probe traces of $[Ru(bpy)_3]^{2+}$ with probe polarization both parallel and perpendicular to the pump polarization.* ..... 48
*Figure 3-9 Time dependent anisotropy of $[Ru(bpy)_3]^{2+}$ in $CH_3CN$.* ..... 49
*Figure 3-10 Transient absorption spectra of $[Ru(bpy)_3]^{2+}$ in $CH_3CN$ with the probe polarization parallel to the pump polarization.* ..... 50
*Figure 3-11 Transient absorption spectra of $[Ru(bpy)_3]^{2+}$ in CH3CN with the probe polarization perpendicular to the pump polarization.* ..... 51
*Figure 3-12 Anisotropy spectra for different probe delays show there is no wavelength dependence to the anisotropy. The effect of the excited state absorption is seen at early times at 462 nm and 466 nm. The discontinuous anisotropy at 496 nm at 0 fs is in a spectral region of small pump-probe signal and is not seen for delays $\Delta t \geq 25$ fs where the signal is larger.* ..... 52
*Figure 3-13 Solvent dependent anisotropy of $[Ru(bpy)_3]^{2+}$.* ..... 54
*Figure 4-1 Transient absorption spectra of $[Ru(bpy)_3]^{2+}$ in $CH_3CN$ with the probe polarization at the magic angle relative to the pump polarization.* ..... 58
*Figure 4-2 Transient absorption spectra of $[Ru(bpy)_3]^{2+}$ in $CH_3CH_2CH_2CN$ with the probe polarization at the magic angle relative to the pump polarization.* ..... 60
*Figure 4-3 Circular dichroism spectra of $\Delta$- and $\Lambda$-enantiomers of $[Ru(bpy)_3]^{2+}$.* ..... 63
*Figure 4-4 Typical energy dispersion of semiconductor conduction and valence bands and the selection rules for circularly polarized light.* ..... 64
*Figure 4-5 Transient absorption spectra of $[Ru(bpy)_3]^{2+}$ with pump and probe of the same circular polarization.* ..... 66
*Figure 4-6 Transient absorption spectra of $[Ru(bpy)_3]^{2+}$ with pump and probe of opposite circular polarization.* ..... 66
*Figure 4-7 Time-resolved CD traces of $\Delta$-$[Ru(bpy)_3]^{2+}$ with pump and probe of the same ($\sigma+\sigma+$) and opposite ($\sigma+\sigma-$) circular polarizations. The inset is pump-probe of population dynamics with the pump polarization at the magic angle relative to the probe.* ..... 68
*Figure 4-8 Time-resolved CD traces of $\Lambda$-$[Ru(bpy)_3]^{2+}$ with pump and probe of the same ($\sigma+\sigma+$) and opposite ($\sigma+\sigma-$) circular polarizations.* ..... 69
*Figure A-1 Block diagram of the blue laser system.* ..... 77
*Figure A-2 The CPM ring dye laser.* ..... 78
*Figure A-3 Four-pass red amplifier using sulforhodamine 640 with preserving agent DABCO (shown) in ethylene glycol.* ..... 79
*Figure A-4 Two-pass blue amplifier shown with a series of coumarin dyes to amplify at different wavelengths.* ..... 80
*Figure A-5 Pulse compression using a single-mode optical fiber and gratings and prisms.* ..... 81
*Figure A-6 Simple diagram of placement of quad-detectors and piezo optical mounts in the blue laser system.* ..... 82
*Figure A-7 Second-order response to a unit step forcing function. The optimum response is the critically damped system.* ..... 83
*Figure B-1 Basic flowchart of vibron.* ..... 85
*Figure B-2 Four response functions for the third-order polarization of a two-level system.* ..... 86

## Acknowledgements

This dissertation is a testament to the power of persistence. It is the only trait in a person's character that can be attributed to achievement or to finishing a task. Intelligence alone won't do it. Berkeley and the world are filled with unmotivated, intelligent people. Talent alone won't do it. I've encountered many talented people without the work ethic to carry them to greatness. Education alone won't do it. Academic pedigree can be impressive, but at some point, one has to start producing outside the classroom. This dissertation encapsulates a very challenging graduate school experience which makes its completion that much greater of a personal accomplishment.

My graduate school career has been spent working with ultrafast laser systems based on technology my research advisor and co-workers developed. This pioneering work by Charles Shank spawned the growth of time-resolved studies with femtosecond resolution in various disciplines of scientific research. A testament to this can be found in the breadth of his group's research which can be associated with physics, chemistry and biology. It has been a privilege to be a member of his research group. Perhaps what I will remember most about my time in his group is his vision of new scientific frontiers to explore.

Sandy Rosenthal first taught me how to turn on a laser and to conduct my first pump-probe experiment. She and the Alivisatos group were of great help with the trials of the second year and my advancement to candidacy.

It was a real pleasure to be able to work with Giulio Cerullo for nearly a year studying quantum onions with Alf Mews and Uri Banin and $[Ru(bpy)_3]^{2+}$ in collaboration with Jim

McCusker and his research group. We spent many days and nights battling the lasers to make progress on the two research fronts. I think in our time together we learned much not only about science, but about people as well.

There have been two constants in my years with the Shank research group. Robert Schoenlein is one of the most technically knowledgeable experimentalists I know. Whenever I had a problem, Bob was my ace in the hole to whom I could turn to solve my problem. It was a real goal of mine in my later years with the group to be as technically savvy as Bob. My only regret is that we never worked together on any experiment so that I could learn first hand from him.

The other constant in my years with the group has been Ernie Glover. He has become one of my good friends. I owe much to him in helping me make it through the frustration of the moment to the next productive day. When I move on in my career, I will miss having him as a friend around the office or lab.

I have confined these acknowledgements to people directly involved with my research and the laboratory. However, there are many friends I did not mention who have made my time at Berkeley so enjoyable. As a final acknowledgement, I would like to thank my family, teachers and coaches whose contributions to my intellectual and personal development have helped me reach this academic and intellectual milestone.

A.T.Y.

March, 2000

# 1. Introduction

For the past few decades, metal to ligand charge transfer compounds have been one of the most studied inorganic compounds. The intense interest generated in these compounds comes from their interesting and potentially applicable photophysical properties which can be easily manipulated by synthetic chemistry techniques. It is generally true that the excited state of these molecules with these interesting photophysical properties is not the initially photoinduced excited state of these compounds.

Tris-(2,2'-bipyridine) ruthenium(II) or $[Ru(bpy)_3]^{2+}$ is the prototypical molecule for which to study the metal to ligand charge transfer complex. Fundamentally, the excited state of $[Ru(bpy)_3]^{2+}$ has broad appeal to a diversity of interests in physical and inorganic chemistry. $[Ru(bpy)_3]^{2+}$ has many electronic characteristics malleable for different applications and has spawned the growth of a variety of research interests. These characteristics have led to research into such uses as a light sensitizer for electron transfer reactions, a reduction-oxidation reagent, and a catalyst for a number of chemical reactions, for example, the conversion of simple molecules like $H_20$ to $H_2$ or $CO_2$ to $CH_4$[1].

Much of this work utilizes the very long lived excited state (lifetime ~ μs) of the molecule. However, it is generally believed the initially formed, photoinduced excited state evolves to form this long lived excited state. Despite the large amount of work done with $[Ru(bpy)_3]^{2+}$, little is known and understood about the photophysical processes which lead to and determine the properties of this long lived excited state.

How a molecule dissipates energy upon excitation is one of the main topics of physical chemistry. The radiationless relaxation pathways utilized by an excited molecule are divided into three distinct processes. These processes are illustrated in figure 1-1. A

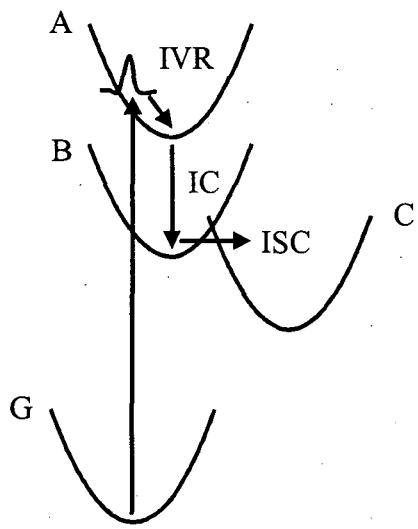


**Figure 1-1 Nonradiative relaxation processes. Illustrated are intramolecular vibrational relaxation (IVR), internal conversion (IC) and intersystem crossing (ISC).**

photon excites the system from the ground state G to the excited state A. For short pulse excitation, the laser pulse may couple to many vibrational levels of excited state A, creating a superposition of vibrational states in the excited state or a time-dependent wavepacket. Within the electronic state A, what is believed to be the most immediate process is intramolecular vibrational relaxation (IVR) or the relaxation of a nonequilibrium distribution of vibrational level populations to an equilibrium distribution of vibrational level populations. This equilibrium distribution is temperature dependent and commonly described by the Boltzmann distribution. The system may also undergo various electronic relaxation processes. "Spin allowed" relaxation processes are

associated with internal conversion (IC) between electronic states. Long lived excited states are generally associated with "spin forbidden" processes commonly referred to as intersystem crossing (ISC). ISC involves a change in multiplicity of the system or a spin "flip" which must coincide with a momentum conserving process (e.g. creation or destruction of phonons). These processes have been introduced in the absence of radiative relaxation processes and intermolecular interactions.

Upon photoexcitation, $[Ru(bpy)_3]^{2+}$ undergoes a spin allowed metal to ligand charge transfer ($^1$MLCT) and forms on some time scale a long lived triplet state ($^3$MLCT). The photophysical properties of this $^3$MLCT state have stimulated research in $[Ru(bpy)_3]^{2+}$ for various uses in chemistry. Much of this work has focused on chemically manipulating the properties of the $^3$MLCT state for various applications. Fundamental to the chemical understanding of this state is the understanding of the processes involved in the creation of this state. The experiments presented in this thesis are designed to observe and resolve the processes involved in the $^1$MLCT to $^3$MLCT conversion. These processes include intermolecular processes and IVR, IC, and ISC relaxation pathways to facilitate the conversion of the $^1$MLCT to the formation of the $^3$MLCT state.

### *1.1 Metal to ligand charge transfer (MLCT) in $[Ru(bpy)_3]^{2+}$--electronic structure*

The intense research interest in $[Ru(bpy)_3]^{2+}$ stems from its metal to ligand charge transfer upon excitation by blue light. A portion of the absorption spectrum is shown in

figure 1-2. The main absorptive feature with a maximum at 450 nm is the metal to ligand

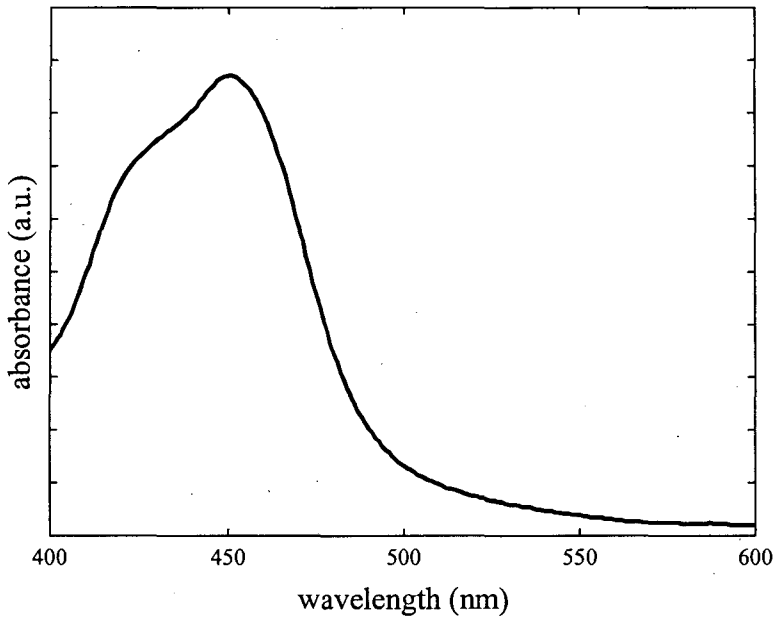


**Figure 1-2 MLCT absorption band of $[Ru(bpy)_3]^{2+}$ in $CH_3CN$.**

charge transfer absorption band. Upon the absorption of light within this band, an electron from the Ru d orbital is excited to the $\pi^*$ orbital of the bipyridine ligand. The MLCT absorption is the subject of this thesis, however, it should be noted that at higher energies of the absorption spectrum include metal-metal and ligand-ligand absorptions. The electronic configuration for assigning these absorptions, in particular the MLCT absorption, can be made to a first approximation using the symmetry of the molecule.

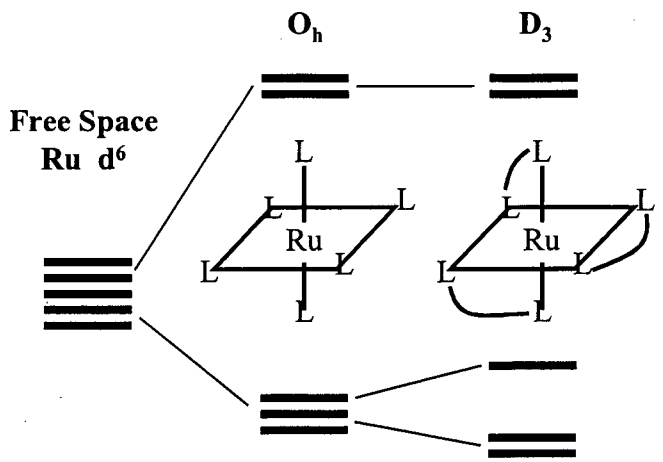


**Figure 1-3 Illustrates the splitting of metal d-orbitals due to symmetry of ligand field.**

In free space, the d orbitals of a metal are degenerate. There is no axis or orientation which can distinguish one orbital from the rest. However, in a six coordinate, octahedral environment, the d-orbital degeneracy is split into a doubly degenerate (E) and triply degenerate (T) d-orbital band. The breaking of degeneracy is based upon the orientation of the orbitals relative to the coordinating ligands. The E orbitals orient in the direction of coordinating ligands and are raised in energy as opposed to the T orbitals which do not orient toward coordinating ligands. In the symmetry of $[Ru(bpy)_3]^{2+}$, the T orbitals are further split in the ligand field into a singly degenerate ($A_1$) and doubly degenerate (E) orbitals. This split is based upon the orbitals orientations relative to the unique axis of the molecule, whether they lie in a plane of the $C_3$ axis or in the plane orthonormal to this axis.

The splitting of the d orbitals is caused by the symmetry of the ligand field and its strength varies with the electronegativity of the ligand and the size of the metal. The ligand field strength is defined by the energy separation in the metal d orbitals. Ru has six d electrons to fill the orbitals and the strength of the ligand field relative to electron-electron repulsion determines how the d-orbitals will fill and whether the metal will be high spin or low spin. For $[Ru(bpy)_3]^{2+}$, the complex is low spin meaning the ligand field strength is larger than the cost in energy of electron repulsion and the six electrons fill the lower three orbitals.

The bipyridine ligands have a two fold ($C_2$) axis of symmetry bisecting the pyridine rings. This is shown in figure 1-4. The $\pi$ orbitals of the bipyridine ligands are separated

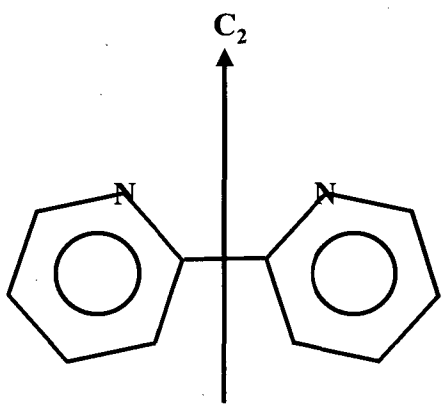


**Figure 1-4 The two-fold symmetry axis ($C_2$) in 2,2'-bipyridine.**

in energy with the $\pi$ bonding orbitals symmetric with respect to the $C_2$ axis ($\chi$) and the $\pi^*$ antibonding orbitals antisymmetric with respect to the $C_2$ axis ($\psi$). The unoccupied $\pi^*$

antibonding orbitals of the three bipyridine ligands are degenerate (T) in octahedral symmetry. In the reduced symmetry of $[Ru(bpy)_3]^{2+}$, the T orbitals of the bipyridine ligands are split into states of $A_2$ symmetry (singly degenerate) and E symmetry (doubly degenerate).

The mixing of the d metal orbitals with the $\pi^*$ antibonding orbitals of the ligand form the highest occupied molecular orbitals (HOMO) and the lowest unoccupied molecular orbitals (LUMO) as shown in figure 1-5. Because of the large difference in energy

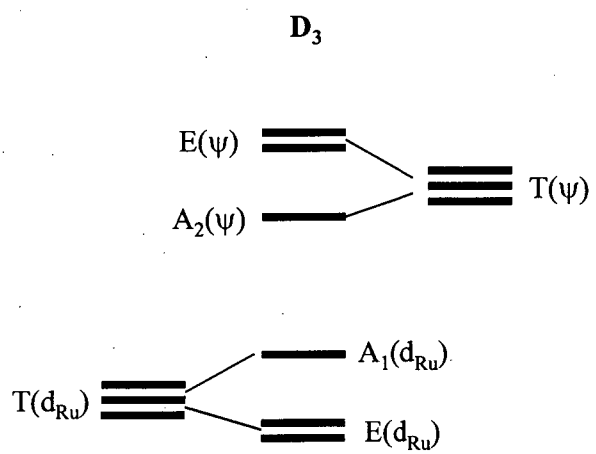


**Figure 1-5 Mapping of symmetry constructed frontier orbitals of $[Ru(bpy)_3]^{2+}$ from octahedral symmetry to $D_3$ symmetry. The highest occupied molecular orbitals are metal centered and the lowest unoccupied molecular orbitals are localized on the ligands.**

between the occupied metal orbitals and the antibonding orbitals of the ligands, the HOMO is nearly isoenergetic with the metal orbitals and therefore resides primarily on the metal. The LUMO, nearly isoenergetic with the antibonding orbitals of the ligand, resides primarily on the ligands. Therefore, upon excitation of an electron from the HOMO to the LUMO, the electron is said to be excited from the metal to the ligands.

The symmetry of inorganic complexes lends itself for the use of group theory to help solve the wave equation,

$$H\psi = E\psi,$$

for these compounds (for a good review of applications of group theory to chemistry, see reference [2]). The Hamiltonian contains all the physical quantities of the electrons and nuclei of the system. Here $\psi$ is the eigenfunction which describes the electronic and nuclear distribution in a molecule. Upon exchange of like particles of the system, the Hamiltonian and eigenfunction are unchanged. Similarly, an exchange of particles through a symmetry operation of the system will leave the system and the Hamiltonian unchanged. It is this symmetry property of the Hamiltonian which is exploited in the use of group theory.

The symmetry of $[Ru(bpy)_3]^{2+}$ is assigned to the point group $D_3$. This point group will only support electronic states of single degeneracy and double degeneracy. The molecular orbitals of $[Ru(bpy)_3]^{2+}$ will be eigenfunctions of the Hamiltonian for this molecule and the symmetry of these eigenfunctions can be assigned to the irreducible representations of the $D_3$ point group. To a first approximation, the molecular orbitals, $\psi$, may be constructed from the linear combination of atomic orbitals, $\phi_i$, of the system. Quantum mechanically, this becomes an exercise of forming the eigenfunctions for the Hamiltonian of $[Ru(bpy)_3]^{2+}$ from the basis set of atomic orbitals. In general, the eigenfunctions and eigenvalues of an operator may be found beginning with

$$\langle \phi_i | A | \psi \rangle = \lambda \langle \phi_i | \psi \rangle,$$

where $\lambda$ is the eigenvalue of the operator A. From this, all of the eigenvalues of the operator A may be found using the characteristic equation,

$$\sum_j (A_{ij} - \lambda\delta_{ij})c_i = 0.$$

For each eigenvalue $\lambda$, an eigenfunction(s) $\psi$ of A may be constructed from a linear combination of functions from the basis set $\{\phi\}$

$$\psi = \sum_i c_i\phi_i ,$$

where

$$c_i = \langle \phi_i | \psi \rangle ,$$

given the degeneracy of $\lambda$, g=1 (g>1). This exercise reduces to finding the coefficients $c_i$ to all the functions in the basis $\{\phi\}$ for each eigenvalue $\lambda$. For molecules as large as $[Ru(bpy)_3]^{2+}$, constructing the molecular orbitals for each electronic energy level becomes an enormous task. However, by using group theory, the electronic states can be approximated with a more tractable basis (e.g. frontier atomic orbitals, bonding orbitals, etc.) while preserving the symmetry of the state.

The use of group theory begins to simplify the enormous task of constructing the molecular orbitals by shrinking the basis set. Instead of using a basis of the 206 electronic wavefunctions in $[Ru(bpy)_3]^{2+}$, the wavefunctions of each energy level may be approximated using, for example, the $\sigma$ bonding orbitals between the bipyridine ligands and the Ru metal. The $\sigma$ bonding orbitals form a basis from which the electronic states may be formed. This basis may be further simplified to three $\sigma$ bonding orbitals as

shown in figure 1-6 because the symmetry of the system is preserved. In the $D_3$ point

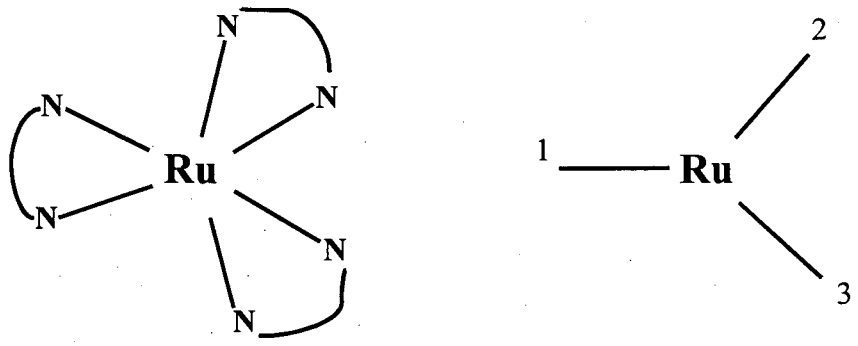


**Figure 1-6 Simplification of the basis set. The symmetry of $[Ru(bpy)_3]^{2+}$ is preserved in the simplified stick figure.**

group, this basis will combine to form the irreducible representations $A_1$ and E states. The projection of each bonding orbital on the symmetry operations of each state combine to form the irreducible representations from the $\sigma$ bonding orbital basis. The lowest state is the totally symmetric $A_1$ state, $\sigma_1+\sigma_2+\sigma_3$, which is symmetrically equivalent to the ground state. The first excited state or MLCT state is the doubly degenerate E state, $\sigma_1-\sigma_2-\sigma_3$ and $\sigma_2-\sigma_3$. The E state is illustrated in figure 1-7. This state is a superposition of the two electronic states which are orthonormal to each other.

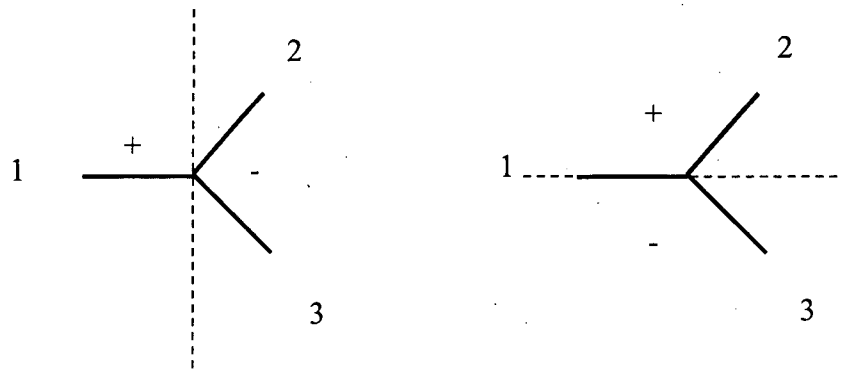


**Figure 1-7 The symmetry constructed E state using σ bonds from the center to the three ligands as a basis. The sign denotes how the σ bonds are combined to form the excited state.**

### *1.2 Singlet to triplet intersystem crossing*

There are a number of relaxation pathways through which a system may dissipate energy. A subset of radiationless transitions was illustrated previously. It is generally believed that ISC is one of the relaxation pathways through which the excited state of $[Ru(bpy)_3]^{2+}$ dissipates energy. Upon photoexcitation of the $[Ru(bpy)_3]^{2+}$ molecule into its MLCT absorption band, an electron is promoted from the metal d-orbitals to a $\pi^*$ orbital of the ligands. With an absorptivity of 14000 $M^{-1}cm^{-1}$, which is comparable to dye molecules, the MLCT absorption ($\lambda_{max}$ ~ 450 nm) is believed to be largely singlet in nature. The fluorescence is red shifted ($\lambda_{max}$ ~ 650 nm) and long lived (radiative lifetime ~ 10 μs). The spin multiplicity of the fluorescing state is widely accepted to be triplet in nature. Excitation dependent studies of the quantum yield of fluorescence indicate the quantum yield is independent of excitation wavelength[3, 4]. The independence of the

fluorescence quantum yield to excitation wavelength suggests the yield of conversion from the singlet manifold to the $^3$MLCT state is near unity.

The near unity quantum yield of the $^3$MLCT state is evidence that the ISC relaxation pathway factors largely in the dynamics of the $[Ru(bpy)_3]^{2+}$ excited state. It must dominate "spin allowed" processes including IC and fluorescence. With the $^1$MLCT absorptivity $\varepsilon \sim 10^4$ $M^{-1}cm^{-1}$, the rate of ISC can be estimated to be $k_{isc} = 10^{10}$-$10^{11}$ $sec^{-1}$. Temperature dependent quantum yield and lifetime luminescence measurements have determined this rate to be $k_{isc} = 10^{11}$-$10^{12}$ $sec^{-1}$[5]. Fundamentally, the formation of the $^3$MLCT state from the $^1$MLCT state cannot be understood without resolving the processes involved in ISC. The time scale of experiments designed to observe the ISC must be made on the subpicosecond time scale to resolve the excited state dynamics. A portion of this thesis will present a variety of femtosecond pump-probe experiments to resolve the excited state dynamics.

### *1.3 Localization of charge*

$[Ru(bpy)_3]^{2+}$ can be assigned to the $D_3$ point group. This assignment is supported by structure determination measurements via x-ray crystallography[6]. The major axis of the molecule is a three-fold axis ($C_3$) perpendicular to the plane of the bipyridine ligands. Bisecting each bipyridine ligand in the plane of the ligand is a two fold axis ($C_2$) of symmetry. The symmetry of the molecule dictates that there are two transition dipole moments of different symmetry. One transition dipole moment is singly degenerate (A) and lies parallel to the major three fold axis. The other dipole moment is doubly degenerate (E) and lies in the plane of the bipyridine ligands. This is the symmetry of the MLCT absorption dipole moment.

Upon photoexcitation, an electron from the Ru metal is transferred to the bipyridine ligands. The symmetry of the molecule does not differentiate one bipyridine from another so the excited state should be delocalized among the ligands. Various Raman and luminescence studies have supported a delocalized excited state of $[Ru(bpy)_3]^{2+}$ in solid environments[7-11]. Luminescence and Raman studies of $[Ru(bpy)_3]^{2+}$ through a solid to liquid phase transition, however, indicate electron localization due to intermolecular processes[9-11]. Furthermore, studies in various solutions have shown that on some very fast time scale, the electron localizes to one bipyridine ligand. Time resolved resonance Raman (TRRR) compared the bipyridine Raman spectrum of the excited $^*[Ru(bpy)_3]^{2+}$ with the ground state $[Ru^{III}(bpy)_3]^{3+}$ and a bipyridine radical Raman spectrum. It was found the excited $^*[Ru(bpy)_3]^{2+}$ Raman spectrum was the sum of the ground state $[Ru^{III}(bpy)_3]^{3+}$ and the bipyridine radical Raman spectra. This indicated that within the time resolution of this experiment (~2 ps) the electron had localized to a single bipyridine ligand[12, 13]. In addition, time resolved anisotropy experiments and TRRR on $[Ru(bpy)_3]^{2+}$ have observed electron hopping among the ligands[14, 15].

There is evidence which suggests the environment in which $[Ru(bpy)_3]^{2+}$ is placed influences the properties of its excited state. Our understanding of the photophysics of $[Ru(bpy)_3]^{2+}$ must include an understanding of these intermolecular interactions which manipulate the excited state. The time scale of localization may have profound consequences on our understanding of the excited state of $[Ru(bpy)_3]^{2+}$. For example, if the electron is initially localized upon excitation, this would conflict with the $D_3$ point group assignment to $[Ru(bpy)_3]^{2+}$ implying the solvent interaction is strong enough to

change the molecular symmetry. The experiments presented in this thesis will utilize symmetry to observe charge localization. These results are presented in chapter 3.

## 2. Spectral Evolution of the $[Ru(bpy)_3]^{2+}$ Excited State

The photophysical properties of metal to ligand charge transfer complexes have generated much interest. Their excited state properties are easily influenced chemically making these complexes an ideal candidate for uses in a variety of photoinitiated reactions including reduction-oxidation reactions, photosensitizing reactions, and photochemical reactions[1, 16-23]. It is generally true that the reactive excited state in these complexes is not the initially excited state. Pivotal to understanding and eventually controlling the properties of the reactive state hinge on understanding the processes involved in the formation of this state.

One of the most studied molecules of this class of inorganic complexes is tris-(2,2'-bipyridine) ruthenium(II) or $[Ru(bpy)_3]^{2+}$. It exhibits a strong absorption, on the order of 10000 $M^{-1}$ $cm^{-1}$ absorptivity, centered at 450 nm in the visible with a relatively long lived fluorescence (lifetime ~1 μs) centered at 650 nm. The strong absorption in the blue portion of the visible spectrum is a metal to ligand charge transfer (MLCT) absorption band. Upon excitation, an electron from the metal d-orbitals is promoted to the $\pi^*$ antibonding orbitals of the bipyridine ligands. From this initial excitation, the system undergoes an intersystem crossing to the formation of the reactive state from which the long lived fluorescence is seen. It is generally believed that the initial excitation is a singlet absorption ($^1$MLCT) which evolves to a $^3$MLCT state. Transient absorption spectroscopy is used to capture the evolution of the excited state from the $^1$MLCT state to the $^3$MLCT state and resolve the processes involved in the formation of the $^3$MLCT state.

The fluorescing state or the lowest excited state of $[Ru(bpy)_3]^{2+}$ in solution is believed to be a triplet state localized on one of the bipyridine ligands. The formation of a triplet

state must involve an intersystem crossing. The magnitude of spin-orbit coupling due to the metal center has been a matter of debate, but the spin quantum numbers remain on the labels of the excited state. The absorbing state has been calculated to be 90% singlet and the fluorescing state to be 90% triplet in nature[24-26]. The intersystem crossing may be facilitated by phonons, but it has been found that the Ru-N bond length shows little change upon excitation[27-30].

The symmetry of the molecule is such that one bipyridine ligand is not differentiable from the other two. Time resolved resonance Raman spectroscopy has shown that upon excitation, the electron localizes to a single bipyridine ligand in less than 2 ps[12, 13, 31]. The localization of charge to a single ligand may involve intramolecular processes or intermolecular interactions with the solvent. The symmetry of the molecule must be broken by some fluctuation whether solvent induced or through an intramolecular process which causes the electronic wavefunction in the excited state to localize to a single ligand.

### *2.1 Dynamics of transient absorption spectroscopy*

Transient absorption spectroscopy is used to track the evolution of the $[Ru(bpy)_3]^{2+}$ excited state from the Frank-Condon region to the lowest triplet excited state. Long time differential absorption spectra of $[Ru(bpy)_3]^{2+}$ have been previously measured[17, 32, 33]. This will provide a reference for the differential absorption spectrum of the lowest energy excited state of the molecule.

The experiment is similar to pump-probe spectroscopy in which a pump pulse and a probe pulse are spatially overlapped on the sample. In this case the sample is a solution of $[Ru(bpy)_3]^{2+}$ dissolved in acetonitrile in a 200 μm pathlength cell at a concentration

with an absorbance of 0.5 OD at 475 nm. The measurement is the difference in transmission of the probe through the sample with the pump on and pump off. Time dependence is attained by delaying the probe pulse relative to the pump pulse. Consequently, negative (positive) time delays signify the probe pulse arrives before (after) the pump pulse and the differential transmission is time integrated at each delay. The time resolution of the experiment is dependent upon the temporal width of the pump and probe pulses.

For positive probe delays, the pump pulse with intensity profile $I_1(t)$ induces a change in the absorption of the sample,

$$\Delta\alpha(t) = \int dt' \, A(t-t') I_1(t') \quad ,$$

where A(t) is the response function of the sample. The pump-probe signal is the change in intensity of the probe pulse $I_2(t) = aI_1(t)$, $a \ll 1$, due to the pump modulated absorption of the sample, $\Delta\alpha(t)$. For positive probe delays $\tau$ over some small sample pathlength d, the signal becomes,

$$\Delta I_2(\tau) = ad \int d\tau' \, A(\tau'+\tau) \int dt' \, I_1(\tau'+t') I_1(t') \, ,$$

which is the convolution of the system response function and the pump and probe pulse autocorrelation function.[34]

In transient absorption spectroscopy, the probe pulse is collected after the sample and dispersed spectrally on a diode array. In this way, the experiment provides both temporal and spectral information of the dynamics of the system. However, for finite pulses, there are contributions to the total transient absorption spectrum when the probe pulse precedes the pump and when the pump and probe pulses are overlapped which cannot be

accounted for in the previous theoretical treatment. These contributions have been studied previously and will be briefly reviewed[34-38].

The signal for transient absorption will be seen as a differential transmittance of the probe pulse due to the effects of the pump pulse. The field of the pulses at point r will be defined,

$$E(r,t) = E_{pu}(r,t)e^{-i\omega t + ik_{pu}\bullet r} + E_{pr}(r,t)e^{-i\omega t + ik_{pr}\bullet r} + c.c.,$$

where E(r,t) is a slowly varying field envelope, k is the wavevector and ω is the central frequency. The pulse field will induce a polarization P(r,t) in the sample which can act back upon the pulse field,

$$\left[\nabla^2 - \frac{1}{c^2}\frac{\partial^2}{\partial t^2}\right]E(r,t) = \frac{4\pi}{c^2}\frac{\partial^2}{\partial t^2}P(r,t).$$

The transmittance of the probe pulse traveling in the z direction will be spectrally resolved [ $E(\omega,r) = \int dt e^{-i\omega t}E(t,r)$ ] at the detector and defined,

$$T(\omega) = \frac{\left|E_{pr}(\omega,z)\right|^2}{\left|E_{pr}(\omega,0)\right|^2},$$

as the ratio of intensities of the probe pulse before and after the sample. The probe field after the sample will see contributions from linear absorption by the sample and a small change in this linear absorption by the pump pulse, $E_{pr}(\omega,z) = E_{pr}^{(1)}(\omega,z) + E_{pr}^{(3)}(\omega,z)$.

The differential transmittance of the probe field with the pump on and the pump off, $\left|E_{pr}(\omega,z)\right|^2 - \left|E_{pr}(\omega,z)\right|^2$, then becomes

$$\frac{\Delta T}{T} = 2\,\mathrm{Re}\frac{E_{pr}^{(3)}(\omega,z)}{E_{pr}^{(1)}(\omega,z)},$$

when normalized by the transmittance of the probe pulse. In the limit of slowly varying field envelopes compared with the central frequency, the normalized differential transmittance of the probe can be rewritten in terms of the induced polarization in the sample

$$\frac{\Delta T}{T} \propto \omega \operatorname{Im} \frac{P_{pr}^{(3)}(\omega)}{E_{pr}(\omega)}.$$

The polarization induced by the pulse fields is determined by the response of the sample. This response of the sample may be captured by use of the density matrix ρ(t) and the Liouville equation,

$$\frac{d\rho}{dt} = -\frac{i}{\hbar}[H(t), \rho(t)] - \Gamma(t)\rho(t),$$

where Γ(t) represents some relaxation function. In the density matrix, the diagonal terms represent populations and the off-diagonal terms represent polarizations or a superposition of states. In this way, a statistical mixture of states is characterized on the diagonal of the matrix and the off-diagonal terms represent a superposition of states. For a two level system, the dynamics of $P^{(3)}(t)$ is captured in the off-diagonal element of the density matrix, $\rho_{ba}^{(3)}(t)$. All terms which contribute to the pump-probe signal will be all orderings of the pulse fields in the phase-matched direction, k=kpu-kpu+kpr. The total polarization response for a two-level system with phenomenological decays will be

$$P_{ba}^{(3)}(t) = \left(\frac{i}{\hbar}\right)^3 \int_{-\infty}^{t} dt' \int_{-\infty}^{t'} dt'' \int_{-\infty}^{t''} dt''' e^{\frac{t'-t''}{T_1}} e^{\frac{t-t'+t''-t'''}{T_2}} [E_{pu}(t''')E_{pu}^*(t'')E_{pr}(t')R_1(t,t',t'',t''')$$

$$+ E_{pu}^*(t''')E_{pu}(t'')E_{pr}(t')R_2(t,t',t'',t''')$$

$$+ E_{pu}^*(t''')E_{pu}(t'')E_{pr}(t')R_3(t,t',t'',t''')$$

$$+ E_{pu}(t''')E^*_{pu}(t'')E_{pr}(t')R_4(t,t',t'',t''')$$

$$+ E^*_{pu}(t''')E_{pr}(t'')E_{pu}(t')R_2(t,t',t'',t''')$$

$$+ E^*_{pu}(t''')E_{pr}(t'')E_{pu}(t')R_3(t,t',t'',t''')$$

$$+ E_{pr}(t''')E^*_{pu}(t'')E_{pu}(t')R_1(t,t',t'',t''')$$

$$+ E_{pr}(t''')E^*_{pu}(t'')E_{pu}(t')R_4(t,t',t'',t''')]$$

where $T_1$ and $T_2$ are exponential decay time constants for population and polarization dephasing, respectively, and $R_i(t,t',t'',t''')$ are the third order response functions. The third order response functions contain the system response to the three fields. For a two level system,

$$R_1 = \langle U_{ba}(t-t')U_{bb}(t'-t'')U_{ba}(t''-t''')\rho_{aa}(0)\rangle,$$

$$R_2 = \langle U_{ba}(t-t')U_{bb}(t'-t'')U_{ab}(t''-t''')\rho_{aa}(0)\rangle,$$

$$R_3 = \langle U_{ba}(t-t')U_{aa}(t'-t'')U_{ab}(t''-t''')\rho_{aa}(0)\rangle,$$

$$R_4 = \langle U_{ba}(t-t')U_{aa}(t'-t'')U_{ba}(t''-t''')\rho_{aa}(0)\rangle,$$

where $U_{ij}$ is the propagator for the system[38]. For example, in $R_1$, the system begins in a relaxed state with $|a\rangle\langle a|$. The first field interaction is marked by $t'''$ and the system propagates in the superposition state $|b\rangle\langle a|$ until the second field interaction at $t''$ which creates a population state $|b\rangle\langle b|$. The third field at $t'$ creates a polarization state $|b\rangle\langle a|$ until the measurement of the probe field at time t. It becomes obvious that an odd number of field interactions will always create a polarization state and an even number of interactions creates a population state.

The first four terms in $P_{ba}^{(3)}(t)$ represent contributions to the signal which is usually associated with pump-probe. That is the pump pulse induces a change in the sample followed by an interrogation of the pump effect in the sample with a probe pulse. The following two terms are contributions when the pump and probe pulses are overlapped spatially and temporally in the sample. The effect arising from this situation has commonly been referred to as the "coherent artifact". The last two terms can only be seen in pump-probe when the probe is spectrally resolved. The contributions from these terms are collectively referred to as "pump-perturbed free induction decay" and occur when the probe precedes the pump.

### 2.1.1 Pump Perturbed Free Induction Decay

The terms in the total polarization $P_{ba}^{(3)}(t)$ which are due to pump-perturbed free induction decay are ones at negative probe delays or with the electric field orderings $E_{probe}$--$E_{pump}$--$E_{pump}$. The label of this effect implies the polarization induced in the sample by the preceding probe pulse is perturbed by the trailing pump pulse. This necessarily means this effect can only be seen at negative delays within the lifetime of the polarization. The pump perturbed signal appears as an oscillating signal in frequency space. This effect will not be seen when time integrating over all frequencies of the probe.

Assuming exponential dephasing of the polarization induced in the sample by the probe pulse, this will transform as a lorentzian in frequency space. For spectrally resolved pump-probe measurements, the polarization is sampled in the phase-matched direction ($k = k_{probe} \pm k_{pump} \mp k_{pump}$) of $P_{ba}^{(3)}(t)$ after three field interactions. For zero probe delay relative to the pump, the polarization is sampled as its dephasing begins and

transforms to a lorentzian in frequency space. For negative probe delays, the initial pulse (the probe pulse) induces a polarization in the sample and the following pump pulse perturbs this polarization dephasing. Frequency components are added in the transform of the polarization decay and the period of the oscillations decrease with increasing delay between pump and probe. This effect is illustrated in figure 2-1 and may be compared to

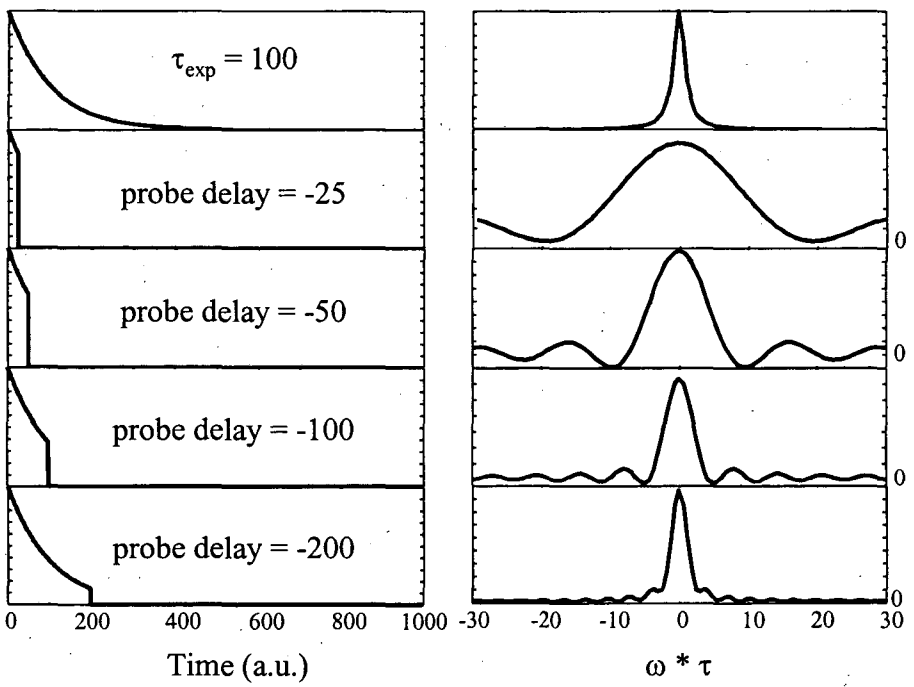


**Figure 2-1 The effect of truncation of exponential decay functions at different points in time. This illustrates the effect of pump-perturbed free induction decay.**

calculations for a two-level system in reference [37]. The left side of figure 2-1 are time domain traces of the exponential polarization decay. The exponential time constant for the decay is $\tau = 100$. For the series of probe delays, the perturbation of the pump is modeled simply as a truncation of the exponential decay. The right side of figure 2-1 is the Fourier transform of the corresponding time traces. For negative probe delays, where the pump perturbs the polarization decay, frequency components are added to account for the truncation of the exponential decay function. As the delay between the arrival times

of the pump and probe pulse shortens, the period of the oscillations in the Fourier transform increases.

### 2.1.2 Coherent Artifact

The coherent artifact arises from terms in which the field ordering is $E_{pump}$—$E_{probe}$—$E_{pump}$. This can only occur when the pump and probe pulses are overlapped spatially and temporally in the sample. This effect is seen in pump-probe signals when resolved spectrally and when the probe is integrated over all wavelengths.

The pump and probe fields interact in the sample and create a spatially varying excitation, $k = \pm k_{pump} + k_{probe}$. This is sometimes referred to as a "population grating". The third field interacts with this population grating and is scattered in the phase matched direction of $k = k_{probe}$. The coherent artifact is therefore an additional contribution to the pump-probe signal and does not reflect changes in the transmittance of the probe through the sample. The time resolution of the pump-probe experiment is determined by the temporal width of the pulses and the population dynamics of the system can only be reliably interpreted when the pulses are separated temporally.

When the pump-probe experiment is resolved spectrally, an enhancement to vibrational sidebands can be seen when the pulses are overlapped due to a Raman-like effect[39-43]. In describing this effect, it is instructional to first review the physics of Raman spectroscopy (for a good review see reference [44]).

The resonance Raman polarizability can be described as

$$\alpha_{i\to f} = M^2 \sum_{\nu} \frac{\langle f|\nu\rangle\langle\nu|i\rangle}{\varepsilon_\nu - \varepsilon_i + E_0 - E_L - i\Gamma},$$

where the Born-Oppenheimer and the Condon approximations are invoked; M is the magnitude of the electronic transition moment; i, ν, and f are the initial, intermediate and final vibrational states and $\varepsilon_i$ and $\varepsilon_\nu$ are their respective energies. $E_0$ is the energy separation between the lowest vibrational levels in the ground and excited state potentials and $E_L$ is the incident laser energy. The homogeneous linewidth is reflected in Γ. The resonance Raman cross section then becomes,

$$\sigma_{i\to f} \propto M^4 E_S^3 E_L \left| \sum_\nu \frac{\langle f|\nu\rangle\langle\nu|i\rangle}{\varepsilon_\nu - \varepsilon_i + E_0 - E_L - i\Gamma} \right|^2,$$

where $E_s$ is the energy of the scattered photons.

Resonance Raman can be described in the time domain by expressing the denominator of the Raman polarizability as a half-Fourier transform,

$$\alpha_{i\to f} = \frac{i}{\hbar}\int_0^\infty dt \sum_\nu \langle f|\nu\rangle\langle\nu|i\rangle e^{\frac{-i(\varepsilon_\nu - \varepsilon_i + E_0 - E_L - i\Gamma)t}{\hbar}}.$$

This can be put in a more descriptive form by bringing the excited state propagator ($e^{\frac{-i(\varepsilon_\nu + E_0)t}{\hbar}} = e^{\frac{-iHt}{\hbar}}$) inside the overlap integral and removing the sum over ν,

$$\alpha_{i\to f} = \frac{i}{\hbar}\int_0^\infty dt \langle f|i(t)\rangle e^{\frac{i(\varepsilon_i + E_L + i\Gamma)t}{\hbar}},$$

and the Raman cross section then becomes,

$$\sigma_{i\to f} \propto M^4 E_S^3 E_L \left| \int_0^\infty dt \langle f|i(t)\rangle e^{\frac{i(\varepsilon_i + E_L + i\Gamma)t}{\hbar}} \right|^2.$$

The Raman cross section is dependent upon the overlap of the propagating wavefunction on the excited state $|i(t)\rangle$ and the ground state wavefunction $|f\rangle$.

Resonance Raman in the time domain is illustrated in figure 2-2. The laser excites the

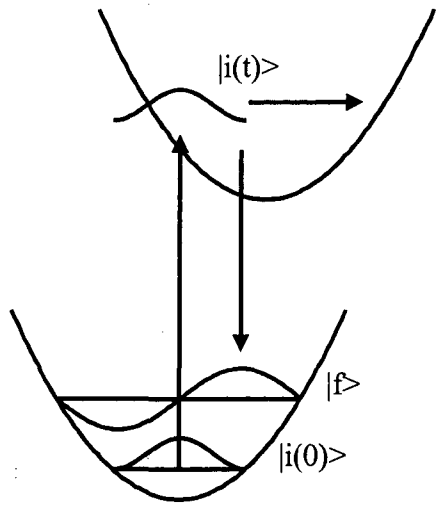


**Figure 2-2 Illustration of resonance Raman spectroscopy in the time domain. The Raman spectrum is the half Fourier transform of the time dependent overlap of the propagating wavepacket $|i(t)\rangle$ and the final state $|f\rangle$.**

ground state wavefunction to the excited state potential well. In this potential well, the wavefunction is time-dependent and is propagated by $e^{\frac{-iHt}{\hbar}}$. Initially, when $|i(t)\rangle = |i(0)\rangle$, there is no overlap between the orthonormal wavefunctions, but as $|i(t)\rangle$ propagates, the overlap increases through a maximum and recedes for the rest of the half of a vibrational period. In the last half of the vibrational period, the overlap builds to a maximum then recedes to zero at the end of the full period. The Raman spectrum is the square of the half Fourier transform of the time dependence of this overlap.

The term in the coherent artifact responsible for enhancement of vibrational sidebands in spectrally resolved pump-probe,

$$\int_{-\infty}^{t} dt' \int_{-\infty}^{t'} dt'' \int_{-\infty}^{t''} dt''' E_{pu}^{*}(t''')E_{pr}(t'')E_{pu}(t')R_3(t,t',t'',t''')e^{\frac{t'-t''}{T_1}} e^{\frac{t-t'+t''-t'''}{T_2}},$$

is illustrated in figure 2-3. The first pump field interaction creates a superposition state

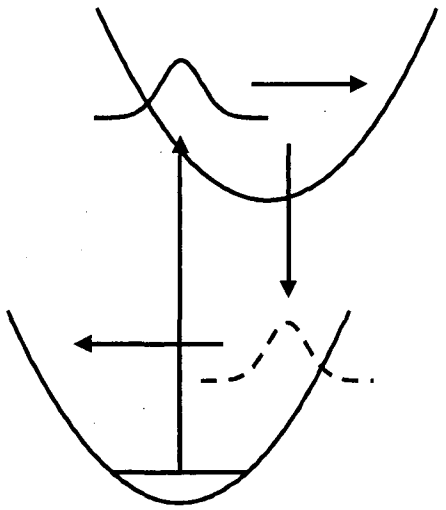

**Figure 2-3 Pictorial representation of third order Raman signals. The Raman signal is dependent on the overlap of the propagating wavepackets on the ground and excited state potential surfaces (see text).**

with the bra propagating on the excited state potential surface while the ket remains in its ground state. The interaction with the probe field places the propagating bra wavepacket on the ground state potential surface displaced from its origin. This creates a propagating bra wavepacket on the ground state. The propagating bra wavepacket is demarked as a dotted line in the figure. The assumption here is that the probe field arrives when the bra wavepacket is sufficiently displaced on the excited state potential surface from its hole in the ground state. The second pump field interacts with the system, promoting the ket to the excited state. The overlap of this ket wavepacket with the displaced bra wavepacket on the ground state contributes to the pump-probe signal when the pulses are temporally overlapped. In this sense, it leads to "Raman enhancement" of vibrational sidebands in spectrally resolved pump-probe signals.

### 2.1.3 Population Dynamics

For the field orderings $E_{pump}$—$E_{pump}$—$E_{probe}$, there are four terms in $P_{ba}^{(3)}(t)$ which capture the population dynamics of a two level system. These four terms are usually associated with pump-probe spectroscopy and can be related to stimulated emission, impulsive Raman, and nonlinear absorption. In addition, these terms reflect dynamics not only associated with the excited state, but with the ground state as well.

It is instructive to review linear absorption[44] in the time domain before reviewing the nonlinear signals arising from $P_{ba}^{(3)}(t)$. In frequency space, the absorption cross section can be described by

$$\sigma_{abs} \propto \sum_{\nu} \frac{\left|\langle \nu | i \rangle\right|^2}{(\varepsilon_\nu - \varepsilon_i + E_0 - E_L)^2 + \Gamma^2},$$

where the variables have the same meaning when describing Raman. This time, by taking the full Fourier transform of the denominator and employing the same simplifications as before, the absorption cross section in the time domain can be described by

$$\sigma_{i \to f} \propto M^2 E_L \int_{-\infty}^{\infty} dt \langle i | i(t) \rangle e^{\frac{i(\varepsilon_i + E_L + i\Gamma)t}{\hbar}}.$$

As opposed to Raman, the absorption cross section is determined by the time dependence of the overlap between the propagating wavepacket on the excited state $|i(t)\rangle$ with the

ground state hole it left behind $|i(0)\rangle$. This is illustrated in figure 2-4. The overlap is

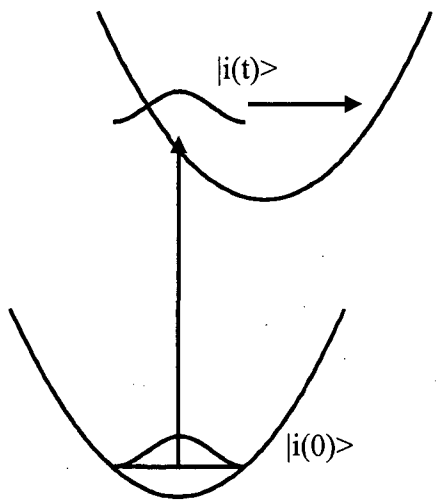


**Figure 2-4 Pictorial representation of linear absorption in the time domain. The absorption spectrum is the full Fourier transform of the time dependent overlap between the wavepacket $|i(t)\rangle$ and the ground state $|i(0)\rangle$ (see text).**

maximum at the time of the promotion of the ground state wavepacket to the excited state. The overlap will then recede and then recur at a vibrational period. The full Fourier transform of the time dependence of this overlap becomes the absorption spectrum.

The nonlinear absorption contribution to the signal terms of $P_{ba}^{(3)}(t)$ is described by

$$\int_{-\infty}^{t} dt' \int_{-\infty}^{t'} dt'' \int_{-\infty}^{t''} dt''' e^{\frac{t'-t''}{T_1}} e^{\frac{t-t'+t''-t'''}{T_2}} E_{pu}(t''')E_{pu}^{*}(t'')E_{pr}(t')R_4(t,t',t'',t'''),$$

and is illustrated in figure 2-5. In the figure, two field interactions with the pump pulse

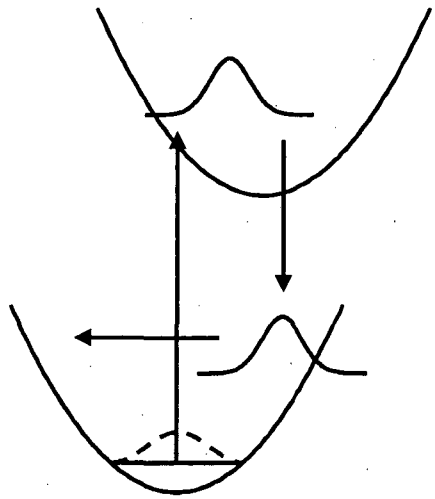

**Figure 2-5 Wavepacket dynamics in nonlinear absorption (see text).**

create a time dependent wavepacket on the ground state. The interaction with the probe field promotes this wavepacket to the excited state and the contribution from this term is dependent upon the overlap of this wavepacket with the ground state wavefunction. This term is analogous to linear absorption in the sense that the signal arises from the overlap of the wavepacket on the excited state with the ground state wavefunction.

The impulsive Raman contribution to the signal is described by

$$\int_{-\infty}^{t} dt' \int_{-\infty}^{t'} dt'' \int_{-\infty}^{t''} dt''' e^{\frac{t'-t''}{T_1}} e^{\frac{t-t'+t''-t'''}{T_2}} E_{pu}^{*}(t''')E_{pu}(t'')E_{pr}(t')R_3(t,t',t'',t'''),$$

and the wavepacket dynamics can be pictorally represented in the same way as the Raman term in the coherent artifact. That is, two field interactions with the pump places the bra wavefunction as a time dependent wavepacket on the ground state; the third field from the probe pulse promotes the ket wavefunction to the excited state and the

contribution from this term becomes the overlap of the ket wavepacket on the excited state with the bra wavepacket on the ground state.

In both nonlinear absorption and impulsive Raman, the pump pulse creates a propagating wavepacket on the ground state potential surface. The dynamics observed from these terms will therefore reflect dynamics of the ground state potential surface. In contrast, stimulated emission terms reflect dynamics on the excited state potential surface.

The stimulated emission terms in $P_{ba}^{(3)}(t)$ are described by

$$\int_{-\infty}^{t} dt' \int_{-\infty}^{t'} dt'' \int_{-\infty}^{t''} dt''' e^{\frac{t'-t''}{T_1}} e^{\frac{t-t'+t''-t'''}{T_2}} E_{pu}(t''')E_{pu}^{*}(t'')E_{pr}(t')R_1(t,t',t'',t'''),$$

and

$$\int_{-\infty}^{t} dt' \int_{-\infty}^{t'} dt'' \int_{-\infty}^{t''} dt''' e^{\frac{t'-t''}{T_1}} e^{\frac{t-t'+t''-t'''}{T_2}} E_{pu}^{*}(t''')E_{pu}(t'')E_{pr}(t')R_2(t,t',t'',t'''),$$

and are illustrated in figure 2-6. Interaction with the pump pulse promotes both the bra

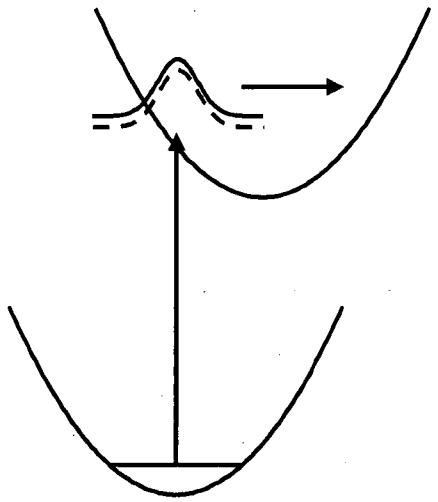

**Figure 2-6 Wavepacket dynamics in stimulated emission (see text).**

and ket to the excited state potential surface creating an excited state population wavepacket. The difference in the stimulated emission terms not depicted in the figure is whether the third field interacts with the bra or the ket wavefunction. The third field will create a propagating wavepacket on the ground state and the signal from these terms becomes the overlap between the bra and the ket on the ground and excited state surfaces.

### *2.2 Evolution of $[Ru(bpy)_3]^{2+}$ transient absorption spectrum*

Transient absorption spectra of $[Ru(bpy)_3]^{2+}$ are shown in figure 2-7 with the time

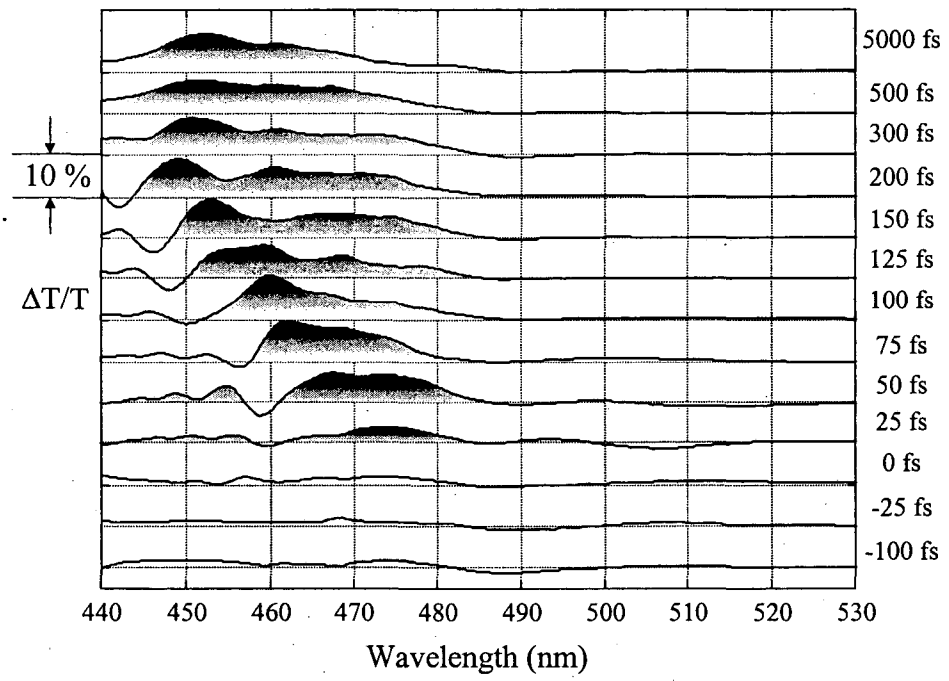


**Figure 2-7 Time resolved transient absorption spectra of $[Ru(bpy)_3]^{2+}$ in $CH_3CN$.**

delays, from -100 fs to 500 fs and an additional delay at 5 ps, offset from each other. The polarization orientation of the pump pulse relative to the probe pulse was set at the magic angle to eliminate the contribution of possible anisotropy to the signal. An increase in the differential transmission of the probe is seen to grow in beginning at 0 fs delay and evolve until 300 fs delay afterwhich the differential spectrum no longer appears to evolve. Comparison of the differential transmission spectra measured at 500 fs and 5 ps

delay in figure 2-7 with long time differential absorption spectra of the long lived excited state of $[Ru(bpy)_3]^{2+}$ shows the spectra are essentially superimposable[33].

There are three main contributions to the differential spectrum as shown in figure 2-8.

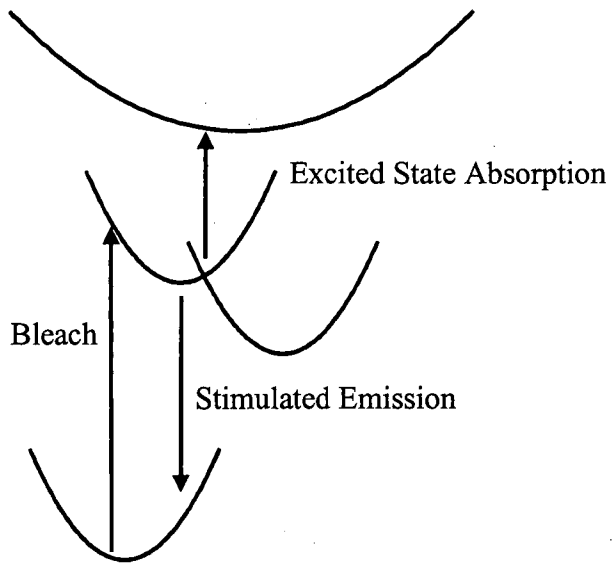


**Figure 2-8 Contributions to differential transmission spectra include bleaching of the absorption, excited state absorption of the probe and stimulated emission.**

Positive contributions to the differential transmission spectrum come from bleaching of the absorption by the pump pulse and stimulated emission from the excited state back down to the ground state. The bleach of the absorption and stimulated emission are described by terms in the previously reviewed theoretical treatment. The theoretical treatment for a two-level system, however, does not account for excited state absorption. This contribution is negative to the differential transmission spectrum and involves the absorption of the probe pulse to promote population to a higher excited state. All three photoprocesses can contribute to the differential spectrum which would reflect the sum of the contributions.

Prior to 300 fs, the spectra exhibit an excited state absorption to shorter wavelengths of the bleach which shifts further to shorter wavelengths with time. At 300 fs, the excited state absorption has shifted outside of the spectral window of the probe pulse. The differential absorption spectrum of the long lived excited state[17, 32, 33] shows an excited state absorption at wavelengths less than 400 nm and this is where the induced absorption is expected to evolve. From the time dependent spectra, the dynamics of the system are illustrated in figure 2-9. Upon excitation in the Frank-Condon region, the probe pulse experiences an

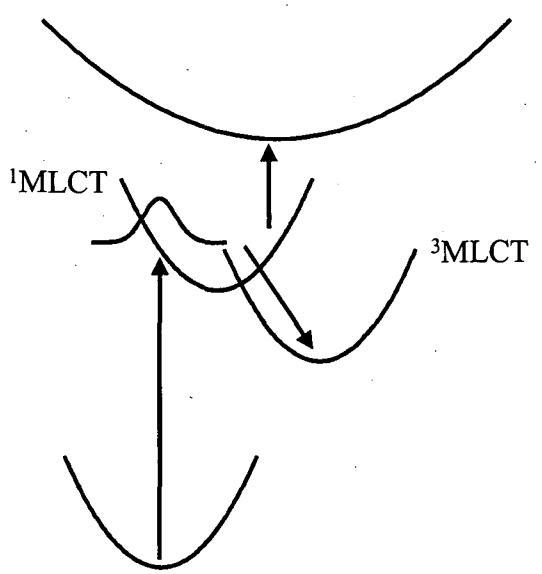


**Figure 2-9 Pictorial representation of wavepacket dynamics seen in the transient absorption spectra of $[Ru(bpy)_3]^{2+}$ (see text).**

increase in transmission from the bleach of the ground state. Contributing to this bleach signal is an absorption of the photoinduced wave-packet to a higher energy excited state. This manifests itself in the negative signal indicative of an excited state absorption to shorter wavelengths of the positive signal of the bleach. As the wavepacket evolves to

the lowest energy excited state potential well, the energy of the induced absorption shifts higher in energy until it is no longer in the spectral window of the probe pulse.

These measurements indicate the formation of the $[Ru(bpy)_3]^{2+}$ $^3$MLCT excited state occurs quickly, on the time scale of the experiment, and calls into question the typical model of excited state relaxation. The rate at which the differential transmission spectrum evolves calls into question the model of energy relaxation in which relaxation is accomplished in a sequence of cascading events from intramolecular vibrational relaxation (IVR) to internal conversion (IC) to intersystem crossing (ISC). IVR is widely believed to be the fastest simply because the system evolves on the same potential surface. IC is generally believed to be the faster of the remaining two processes because it relaxes within the spin-allowed manifold.

Previous work in measuring the quantum yield of formation of the lowest excited state or reactive state ($^3$MLCT) indicate a yield of near unity[3, 4, 16]. This is an interesting revelation in that it suggests the "spin forbidden" process of intersystem crossing dominates the relaxation of $[Ru(bpy)_3]^{2+}$ as opposed to "spin allowed" processes such as internal conversion and fluorescence. The transient absorption experiment is not sensitive to the spin multiplicity of the excited state. However, the wavepacket motion seen in the time-resolved differential spectra does not suggest a cascading event of relaxation processes in the formation of the $^3$MLCT.

The traditional models of IVR, IC, and ISC for energy relaxation need to be modified to explain the excited state dynamics resolved with this experiment. The wavepacket dynamics seen in the time-resolved differential spectra suggest a fast evolution of the $[Ru(bpy)_3]^{2+}$ excited state from the $^1$MLCT state to the formation of the $^3$MLCT state.

The implications of these results suggest that the processes which govern the formation of the excited state seen on the μs time scale (e.g. intersystem crossing, charge localization) occur on an ultrafast time scale in less than 300 fs.

## 3. Breaking of symmetry—localization of charge

The reactive excited state of $[Ru(bpy)_3]^{2+}$ has been well studied by inorganic chemists. It is commonly referred to as the $^3$MLCT, indicating the prevalent view that the spin quantum number is preserved and that the excited state undergoes an intersystem crossing. What is not indicated by the label of the reactive excited state but is commonly believed for the molecule in a liquid environment is that the electron in this excited state is localized on one bipyridine ligand following the work in reference[12, 45]. This work used time resolved resonance Raman spectroscopy and compared the vibrational spectra of ground state $[Ru^{III}(bpy)_3]^{3+}$, excited $^*[Ru(bpy)_3]^{2+}$ and a bipyridine ($bpy^-$) anion to show electron localization on one ligand. This study found that the Raman spectrum of $^*[Ru(bpy)_3]^{2+}$ was composed of two sets of Raman modes, one corresponding to $[Ru^{III}(bpy)_3]^{3+}$ modes and the other corresponding to $bpy^-$ modes. This was one indication the excited state should be described as $[Ru^{III}(bpy)_2(bpy^-)]^{2+}$, where the electron is promoted from the Ru metal and localizes to one bpy ligand[12].

A second comparison was made among the Raman spectra of $bpy^-$, $^*[Ru(bpy)_3]^{2+}$ and $^*[Ru(bpy)_2(en)]^{2+}$ (en = ethylenediamine). If charge was delocalized in the excited state, the Raman spectra should have different frequency shifts for resonances associated with the bpy ligand. These different frequency shifts would result from different electron densities with $e^-/3$ per bpy for $^*[Ru(bpy)_3]^{2+}$ and $e^-/2$ per bpy for $^*[Ru(bpy)_2(en)]^{2+}$. The frequency shifts were found to be nearly identical providing further evidence for a localized excited state[12]. This practice has since been extended to other metal to ligand charge transfer complexes to study the electronic structure of their excited states[13, 15, 46-53].

The three fold symmetry of $[Ru(bpy)_3]^{2+}$ dictates that the bipyridine ligands are indistinguishable from each other. In the three fold symmetry of the molecule, the MLCT excited state should be a doubly degenerate state delocalized among the bipyridine ligands. This delocalized MLCT state has yet to be observed experimentally for the molecule in a liquid environment. This has raised some questions about the effect of the solvent on the symmetry of the molecule[9, 11, 47, 54-58].

The work presented in this chapter utilizes the difference in symmetry of a delocalized state compared to a localized state. This difference is illustrated in figure 3-1. For a delocalized electron, the ligands remain indistinguishable from each other and the $D_3$ symmetry of the molecule is preserved. However, a localized electronic wavefunction breaks the three fold axis of symmetry and the molecular symmetry is reduced. The

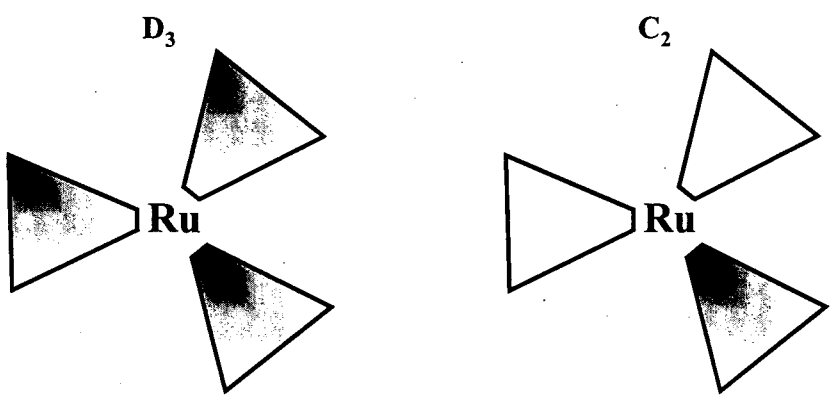


**Figure 3-1 A delocalized electronic wavefunction preserves $D_3$ symmetry. A localized wavefunction reduces the $D_3$ symmetry to $C_2$ symmetry.**

corresponding transition moments will also be different in symmetry. A delocalized state will have a corresponding transition moment which is doubly degenerate and a localized state will have a corresponding transition moment which is singly degenerate. The symmetry of the transition moment of the MLCT state may be probed by an anisotropy measurement.

### *3.1 Introduction to the anisotropy measurement*

The anisotropy measurement uses polarized light to measure the symmetry of the transition moment in a chromophore and its orientation. Typically, a sample is excited by polarized light and the absorption of light or the emission of light with polarizations parallel and perpendicular to the incident light are measured and compared. By using short, linearly polarized laser pulses, changes to the symmetry or orientation of the transition moment may be measured with time. This technique was extensively used with picosecond pulses to measure molecular rotations in solutions (for example see references[59, 60]).

The pulses used for the time resolved anisotropy measurements presented here are 25 fs in duration centered at 480 nm with a repetition rate of 540 Hz. A simple diagram of

the experimental setup is shown in figure 3-2. The experiment is similar to the setup for

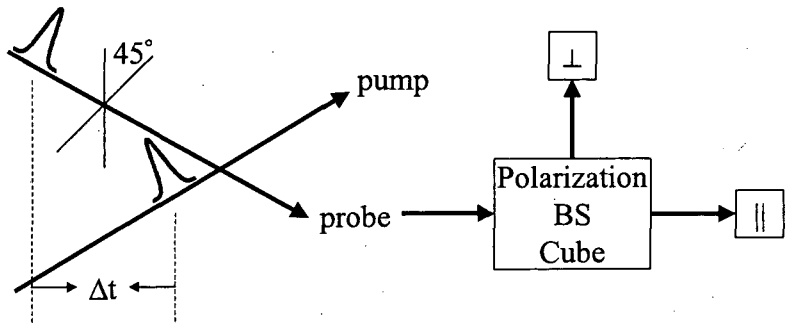


**Figure 3-2 Simple diagram of the experimental setup for an anisotropy measurement (see text).**

a pump-probe measurement with the polarization of the probe beam oriented 45° to the pump. After the beams are crossed in the sample, the probe is split by a polarization beam splitting cube to facilitate simultaneous detection of polarization components of the probe both parallel and perpendicular to the pump. By simultaneously detecting parallel and perpendicular components, errors caused by fluctuations in laser intensity are eliminated.

The theory for anisotropy experiments is well developed for fluorescence spectroscopy and is analogous to pump-probe measurements for positive probe delays following dephasing. For fluorescence anisotropy experiments, light emitted both parallel and perpendicular to the pump pulse are measured and compared as opposed to measuring the differential transmittance of the parallel and perpendicular components of the probe pulse

relative to the pump pulse in pump-probe. The theory for fluorescence anisotropy[59, 61, 62] necessarily implies no excited state absorption of the probe and is an additional condition, along with positive probe delays following dephasing, for it to apply to pump-probe anisotropy.

If $\varepsilon_i$ is the unit vector in the direction of the electric field of incident light and $\mu$ is the transition moment of absorption, the intensity of the fluorescence parallel to the pump polarization is

$$I_{\parallel} \approx \int_0^{\infty} \left\langle [\varepsilon_i \bullet \mu(0)]^2 [\varepsilon_i \bullet \mu(t)]^2 \right\rangle \exp(-\frac{t}{\tau}) dt ,$$

where $\tau$ is the lifetime of the excitation. The first dot product represents the absorption of polarized light and the second dot product represents the emission of light polarized parallel to the pump polarization. Similarly, the intensity of the fluorescence perpendicular to the pump polarization is

$$I_{\perp} \approx \int_0^{\infty} \left\langle [\varepsilon_i \bullet \mu(0)]^2 [\varepsilon_i \times \mu(t)]^2 \right\rangle \exp(-\frac{t}{\tau}) dt .$$

Anisotropy is defined[61]

$$r = \frac{I_{\parallel} - I_{\perp}}{I_{\parallel} + 2I_{\perp}} .$$

In an isotropic distribution of singly degenerate transition dipole moments,

$$I_{\parallel} - I_{\perp} = \frac{1}{15} \int_0^{\infty} \left\langle 3[\mu(0) \bullet \mu(t)]^2 - \mu^2(0)\mu^2(t) \right\rangle \exp(-\frac{t}{\tau}) dt ,$$

is the anisotropic term which is dependent upon the projection of the transition moment at time t upon the transition moment initially excited. This is normalized by

$$I_{\parallel} + 2I_{\perp} = \frac{1}{3} \int_0^{\infty} \left\langle \mu^2(0)\mu^2(t) \right\rangle \exp(-\frac{t}{\tau}) dt ,$$

which has no polarization dependence and represents the population kinetics of the system. The anisotropy of the system

$$r = \frac{2}{5}\int_0^\infty \langle P_2[\mu(0)\bullet\mu(t)]\rangle \exp(-\frac{t}{\tau})d(\frac{t}{\tau}),$$

follows a second order Legendre polynomial as shown in figure 3-3. As can be seen, the

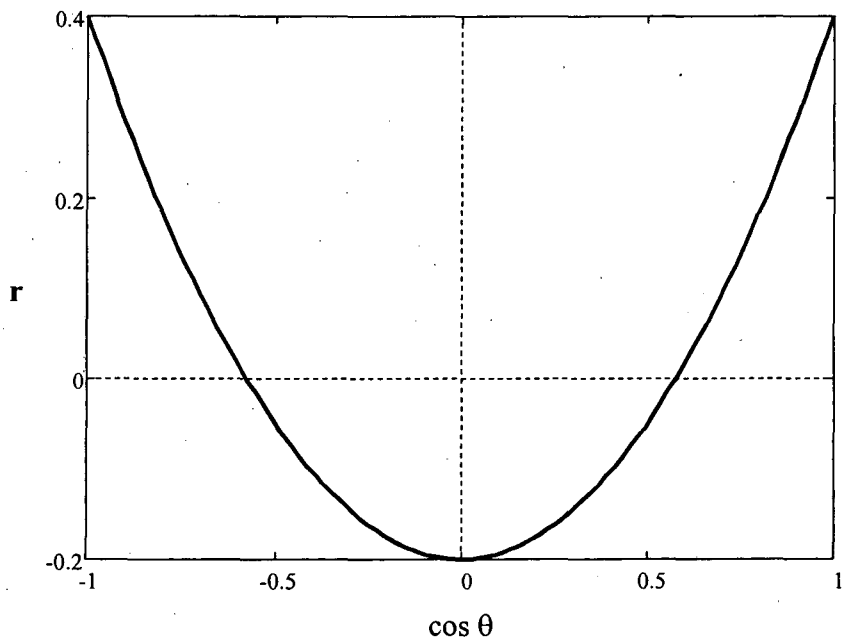


**Figure 3-3 Anisotropy as a function of angle for an isotropic distribution of singly degenerate transition moments.**

maximum value for the anisotropy of a singly degenerate transition moment is r = 0.4. This occurs when μ(t) remains aligned with the initial transition moment μ(0). The minimum value is -0.2 and occurs when μ(t) is normal to μ(0). There are two points on the graph in which r = 0. There is no anisotropy or orientational dependence at these points and the angle for these points θ = 54.7° is commonly referred to as the magic angle.

The maximum value for the anisotropy can be realized for molecules with a singly degenerate transition moment and can be described by a two level system. An example of one such molecule is the laser dye 3,3'-diethyloxacarbocyanine iodide or DOCI. As seen in figure 3-4, DOCI has a two fold axis of symmetry which will only support singly

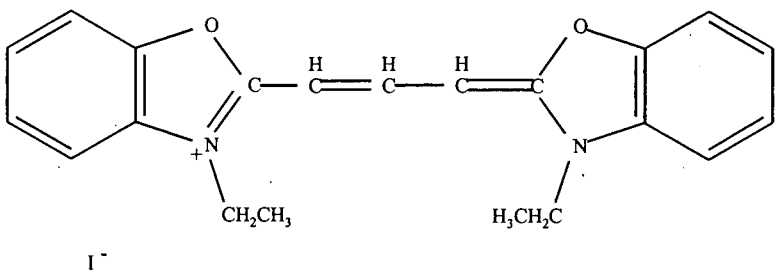


**Figure 3-4 Chemical structure of 3,3'-diethyloxacarbocyanine iodide (DOCI).**

degenerate transition moments.

The time dependent anisotropy is constructed from the pump-probe signals with the probe polarization parallel and perpendicular to the pump polarization. Simultaneously collected signals for DOCI with parallel and perpendicular probe polarizations to the

pump polarization are shown in figure 3-5. A reference is subtracted from the parallel

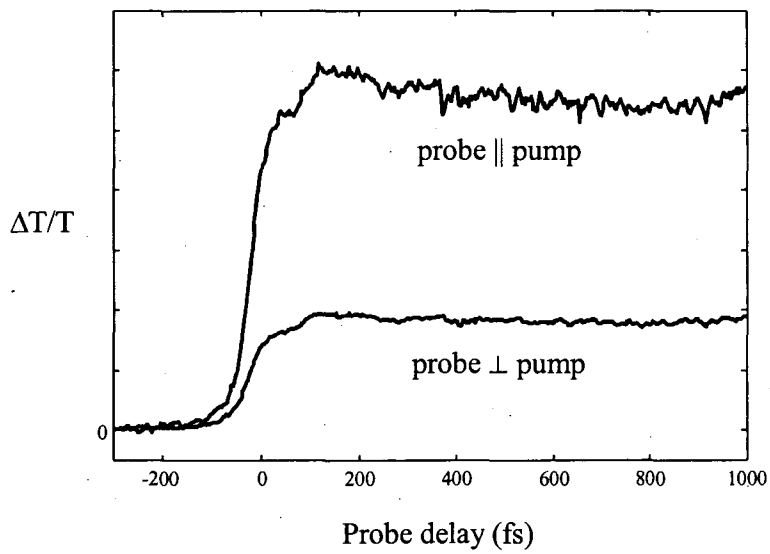


**Figure 3-5 Simultaneously collected pump-probe traces of DOCI with the probe polarization parallel and perpendicular to the pump polarization.**

and perpendicular signals in differential preamplifiers. The parallel and perpendicular signals are input to lockin amplifiers locked to the frequency of a chopper in the path of the pump beam. Other than the signal levels, there is very little difference seen in the dynamics of the parallel and perpendicular pump-probe traces. From these pump-probe traces, the constructed time dependent anisotropy is shown in figure 3-6. In figure 3-6 anisotropy is plotted versus probe delay. As can be seen, there is no time dependence to the anisotropy of DOCI, which has a constant value of r = 0.4 for all time shown in figure 3-6. There is no depolarization of the anisotropy due to rotation. These measurements

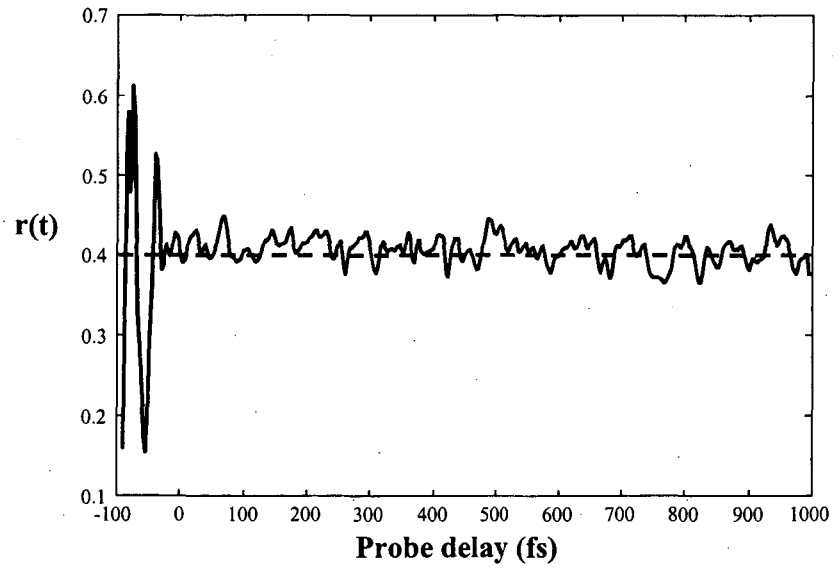


**Figure 3-6 Time dependent anisotropy of DOCI. DOCI was used to calibrate the anisotropy measurement.**

are performed on a time scale much less than the molecule's rotation time.

Anisotropy values larger than r = 0.4 can only be seen from transition moments with higher symmetry than single degeneracy and then only in pump-probe differential transmission experiments. These signals are derived from coherences induced in the molecules by the pump pulse. As such, some work has been done to use anisotropy to measure dephasing times of molecules (for example, see reference[63]). Anisotropy values larger than r = 0.4 can not be seen by fluorescence.

The theory for pump-probe anisotropy experiments on doubly degenerate transitions moments is well developed and will only be briefly reviewed here[63, 64]. An energy

level diagram for a doubly degenerate system is shown in figure 3-7. The ground state is

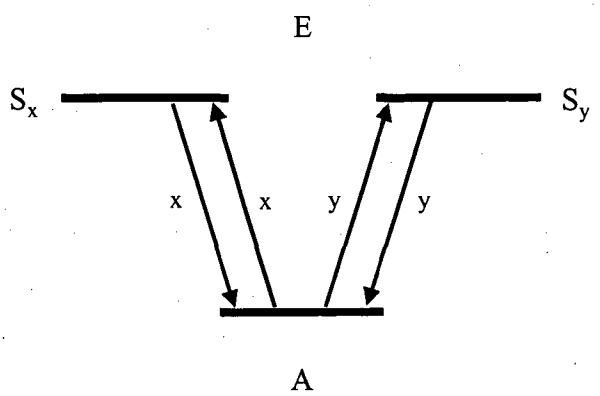


**Figure 3-7 Energy level diagram of a system with a doubly degenerate excited state.**

a totally symmetric A state and the excited state is a doubly degenerate E state. The E state is composed of two degenerate, orthonormal states labeled $S_x$ and $S_y$ with corresponding transition moments aligned along the x and y axis of the molecule.

Initially, the pump pulse will create a fully coherent state or Raman state in which the state is a superposition of A, $S_x$ and $S_y$. The ratio of perpendicular to parallel pump-probe signals for this state is equivalent to the resonance Raman depolarization ratio $\rho = 1/8$. Following the geometric arguments of reference [63, 64], the parallel and perpendicular . signals are an orientational average over a combination of four cosine functions

$$I_{\parallel} \propto \left\langle Z_x^4 + Z_y^4 + 2Z_x^2 Z_y^2 \right\rangle,$$

$$I_{\perp} \propto \left\langle Z_x^2 X_x^2 + Z_y^2 X_y^2 + 2Z_x Z_y X_x X_y \right\rangle,$$

where $L_m$ represents cos $\theta_{Lm}$ where $\theta$ is the angle between the polarization of light and the molecular axis. The last terms in the averages represent contributions from the interfering superpositions of $A \leftarrow S_x$ and $A \leftarrow S_y$ transitions. The anisotropy expected from this Raman state is r = 0.7.

The system may partially dephase in which there is no coherence between $S_x$ and $S_y$ but coherence between A and $S_x$ and A and $S_y$ remains. The parallel and perpendicular signals then become

$$I_{\parallel} \propto \left\langle Z_x^4 + Z_y^4 \right\rangle,$$

$$I_{\perp} \propto \left\langle Z_x^2 X_x^2 + Z_y^2 X_y^2 \right\rangle,$$

and the anisotropy is r = 0.4. After complete dephasing in which the system is composed of a statistical mixture of $S_x$ and $S_y$ of equal proportions, the signals become

$$I_{\parallel} \propto \left\langle \tfrac{1}{2} Z_x^2 \left(Z_x^2 + Z_y^2\right) + \tfrac{1}{2} Z_y^2 \left(Z_x^2 + Z_y^2\right) \right\rangle,$$

$$I_{\perp} \propto \left\langle \tfrac{1}{2} Z_x^2 \left(X_x^2 + X_y^2\right) + \tfrac{1}{2} Z_y^2 \left(X_x^2 + X_y^2\right) \right\rangle,$$

and, as in fluorescence, the anisotropy is r = 0.1.

These same geometric arguments may be used to predict the anisotropy values for a system with a triply degenerate transition moment. The fully coherent Raman state has an anisotropy value of r = 1, which is equivalent to the resonance Raman depolarization ratio of $\rho = 0/1$. The partially dephased anisotropy is r = 0.4 and a statistical mixture of states would have no anisotropy or r = 0.[64]

### *3.2 Anisotropy measurement of $[Ru(bpy)_3]^{2+}$*

Time resolved anisotropy measurements will be used to track the evolution of the symmetry of the MLCT transition moment in $[Ru(bpy)_3]^{2+}$. Figure 3-8 shows

simultaneously acquired pump-probe traces of $[Ru(bpy)_3]^{2+}$ in $CH_3CN$ with the probe

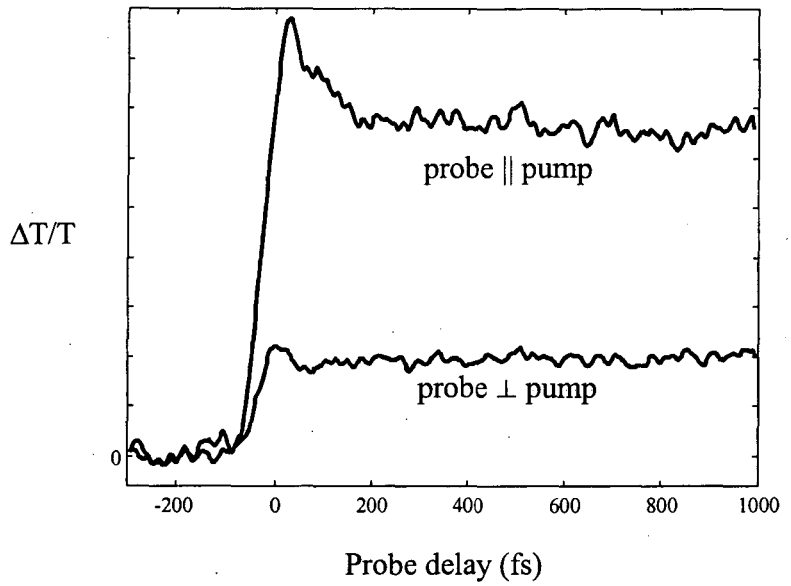


**Figure 3-8 Simultaneously collected pump-probe traces of $[Ru(bpy)_3]^{2+}$ with probe polarization both parallel and perpendicular to the pump polarization.**

polarization parallel and perpendicular to the pump polarization. The pump and probe pulses are 25 fs in duration centered at 480 nm. The sample solution is in a 200 μm pathlength cell with an O.D. ~ 0.4.

There are some obvious differences between the pump-probe traces with the probe polarization parallel to the pump polarization as opposed to the probe polarization perpendicular to the pump. The parallel pump-probe trace has a very fast decay within the first 200 fs which flattens to a long time signal level. In contrast, little dynamics are seen in the perpendicular pump-probe trace except perhaps a slow rise in the signal near probe delay $\Delta t \sim 70$ fs. The ratio between the perpendicular and parallel pump-probe traces at long times is $\rho \sim 1/3$.

Following the definition of anisotropy, the parallel and perpendicular traces are used to construct the time dependent anisotropy trace seen in figure 3-9. A very fast

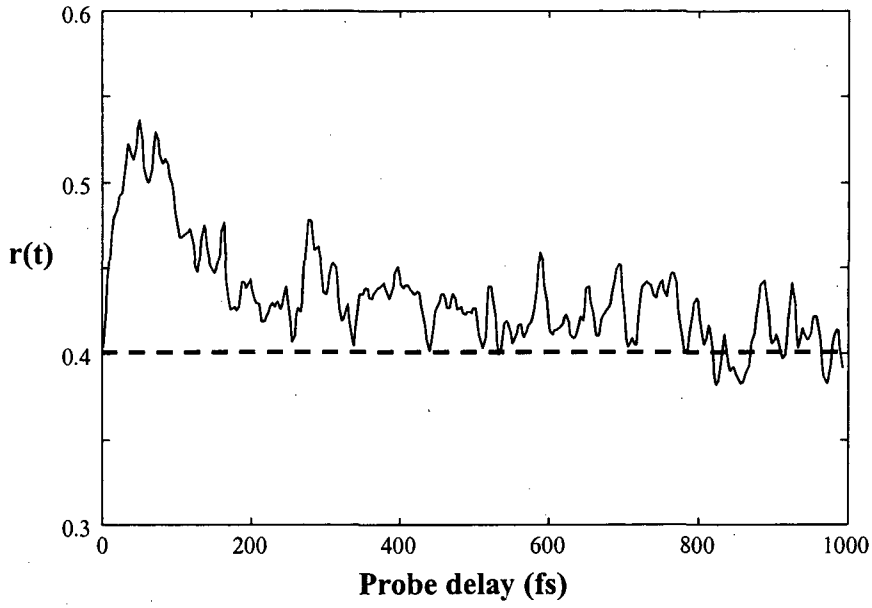


**Figure 3-9 Time dependent anisotropy of $[Ru(bpy)_3]^{2+}$ in $CH_3CN$.**

depolarization of the anisotropy is seen within the first 300 fs which decays to a long time anisotropy value. The time dependent anisotropy is initially at a value greater than 0.5 and quickly decays to a value of r = 0.4 in less than 300 fs. An initial anisotropy value greater than 0.4 is indicative of a transition moment which has a degeneracy greater than single degeneracy. The symmetry of $[Ru(bpy)_3]^{2+}$ in the ground state argues that the $^1$MLCT absorption pumped in our experiment is doubly degenerate. The initial anisotropy value expected for a doubly degenerate transition moment is r = 0.7. This experiment may not be able to resolve the fastest dynamics of the depolarization. The observed initial anisotropy of r = 0.55 is consistent with an initial transition moment of two-fold degeneracy.

On the same time scale as the depolarization of the anisotropy is the spectral shift of the transient absorption spectra seen in figure 2-7. Repeating the transient absorption experiment of figure 2-7 with the probe polarization parallel and perpendicular to the pump pulse, wavelength dependent anisotropy curves may be constructed for different probe delays. For these experiments, the probe polarizations parallel and perpendicular to the pump polarization signals are not simultaneously detected. Also, the pump polarization is rotated relative to the probe polarization to eliminate any anisotropic effects of the grating in the data collection scheme.

Transient absorption spectra for probe polarization parallel to the pump polarization is shown in figure 3-10. The differential transmission of the spectrally resolved probe for

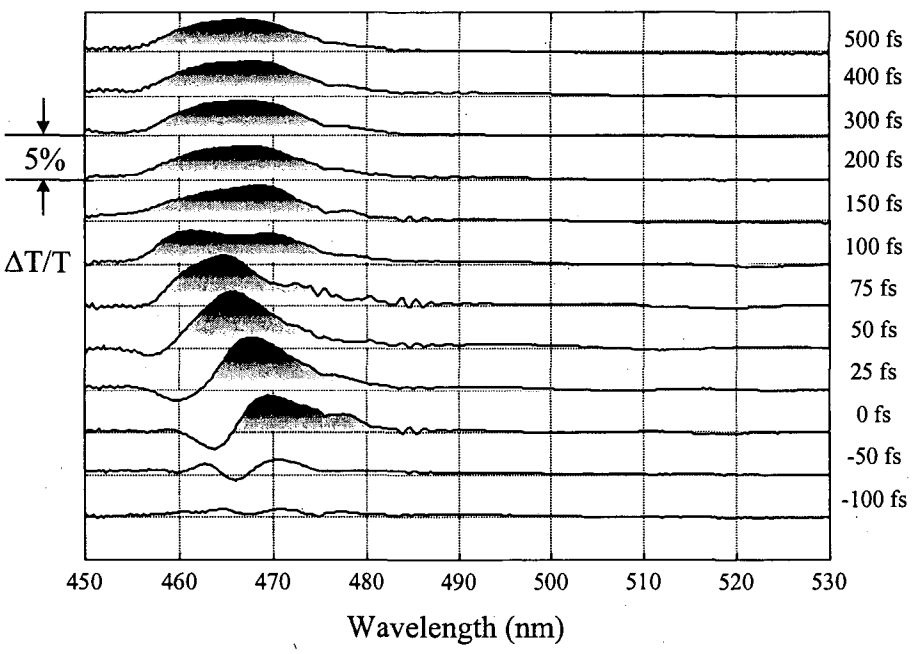


**Figure 3-10 Transient absorption spectra of $[Ru(bpy)_3]^{2+}$ in $CH_3CN$ with the probe polarization parallel to the pump polarization.**

each pump-probe delay is offset from each other as labeled. The intensity of the bleach signals is approximately 5% as shown by the scale on the graph. As previously seen,

there is a spectral shift of the bleach to shorter wavelengths as the probe delay is lengthened. The spectral dynamics appear to be complete in less than 300 fs as seen before. The spectral shift is from the dynamics of excited state absorption and is interpreted as wavepacket motion on the excited state surface(s).

Similar dynamics are seen in the transient absorption spectra for probe polarization perpendicular to the pump polarization as shown in figure 3-11. The spectra in this figure

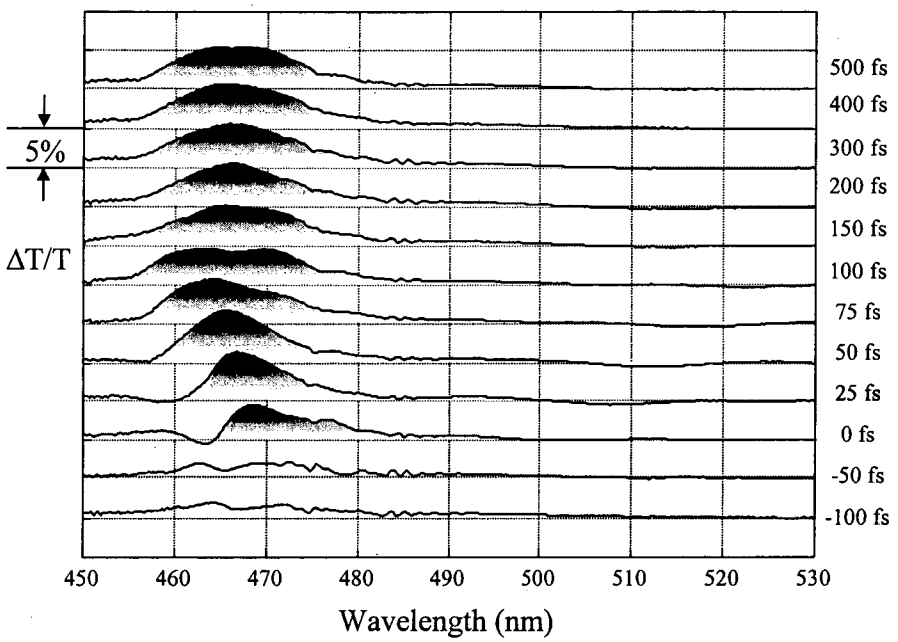


**Figure 3-11 Transient absorption spectra of $[Ru(bpy)_3]^{2+}$ in CH3CN with the probe polarization perpendicular to the pump polarization.**

were collected separately from the spectra of figure 3-10. The polarization of the pump was rotated normal to the probe polarization. The strength of the differential transmission is seen to be approximately 5%. The ratio of the signals seen in figure 3-10 and figure 3-11 cannot be compared to construct quantitative anisotropy curves. However, the wavelength dependence of the anisotropy may be constructed and these curves are shown in figure 3-12.

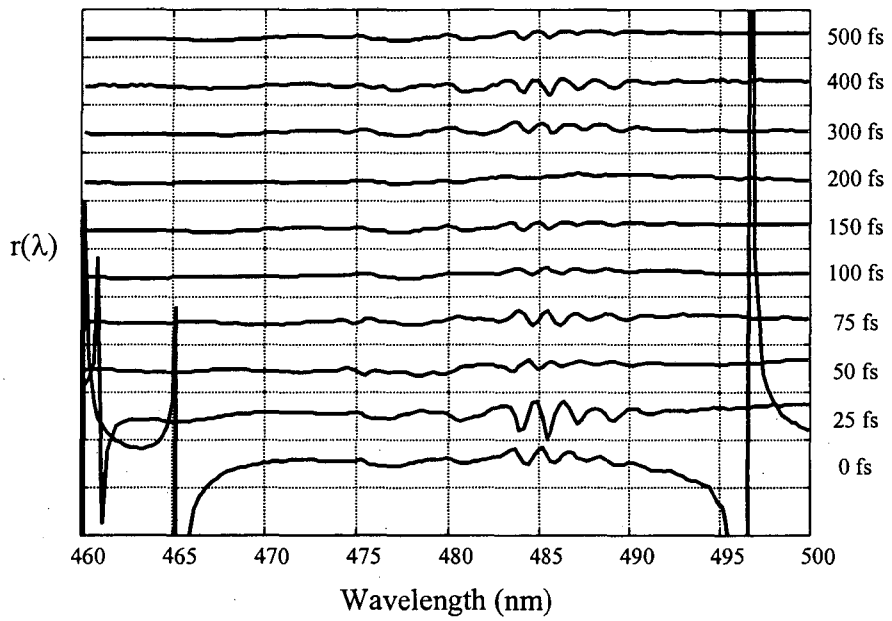


**Figure 3-12 Anisotropy spectra for different probe delays show there is no wavelength dependence to the anisotropy. The effect of the excited state absorption is seen at early times at 462 nm and 466 nm. The discontinuous anisotropy at 496 nm at 0 fs is in a spectral region of small pump-probe signal and is not seen for delays $\Delta t \geq 25$ fs where the signal is larger.**

In figure 3-12, the anisotropy spectra were constructed from the transient absorption spectra of figure 3-10 and figure 3-11 with the probe polarization parallel and perpendicular to the pump polarization, respectively. Each delay is offset as labeled in the figure. The effect of the excited state absorption in the transient absorption spectra is apparent for 0 fs probe delay at 466 nm and for 25 fs probe delay at 462 nm. The discontinuous anisotropy at 496 nm at 0 fs probe delay is in a spectral region of small pump-probe signal and is caused by the division of small numbers. For longer probe delays, the signal is larger in this spectral region and the discontinuous signal is not observed. It is seen for all anisotropy spectra between 470 nm and 490 nm that there is no wavelength dependence of the anisotropy and for probe delays of 50 fs and longer, there is no wavelength dependence from 460 nm to 500 nm.

The ultrafast depolarization of the anisotropy seen in figure 3-9 is due to an ultrafast change in symmetry of the $[Ru(bpy)_3]^{2+}$ transition moment. The initial value of the anisotropy of $r \sim 0.55$ indicates the initial excitation has a symmetry higher than single degeneracy. This is consistent with a doubly degenerate transition moment as predicted from symmetry arguments for the MLCT state. On a 300 fs time scale, the symmetry of the transition moment has changed as indicated by the depolarization in the anisotropy to $r = 0.4$. This anisotropy value is consistent with a transition moment reduced in symmetry to single degeneracy. This would be consistent with electron localization to a single bipyridine ligand as seen on much longer time scales.

The long time anisotropy value of $r = 0.4$ also gives some information about which of the three bipyridine ligands to which the electron localizes. The final anisotropy indicates the transition moment of the localized MLCT state is aligned with the pump polarization. Upon creation of the delocalized MLCT state, the electron wavefunction does not localize randomly to one the of the bipyridine ligands, but localizes to the bipyridine ligand aligned along the electric field of the pump pulse. This is an indication that localization of the electron is largely driven by intermolecular forces as opposed to an intramolecular process.

### *3.3 Solvent dependence of localization*

The simplest way to systematically vary the intermolecular forces on $[Ru(bpy)_3]^{2+}$ is to systematically vary the solvent. The effect of the environment on localization in this system has generated considerable interest[8-11, 16, 52-57, 65-67]. A nitrile solvent series is chosen beginning with acetonitrile ($CH_3CN$, $CH_3(CH_2)_nCN$, n=1,2). Here, the

inertial properties of the solvent are varied without dramatically changing other physical properties.

Time dependent anisotropy of $[Ru(bpy)_3]^{2+}$ in the nitrile solvent series is shown in figure 3-13 with the traces offset from each other. Similar to what was seen in

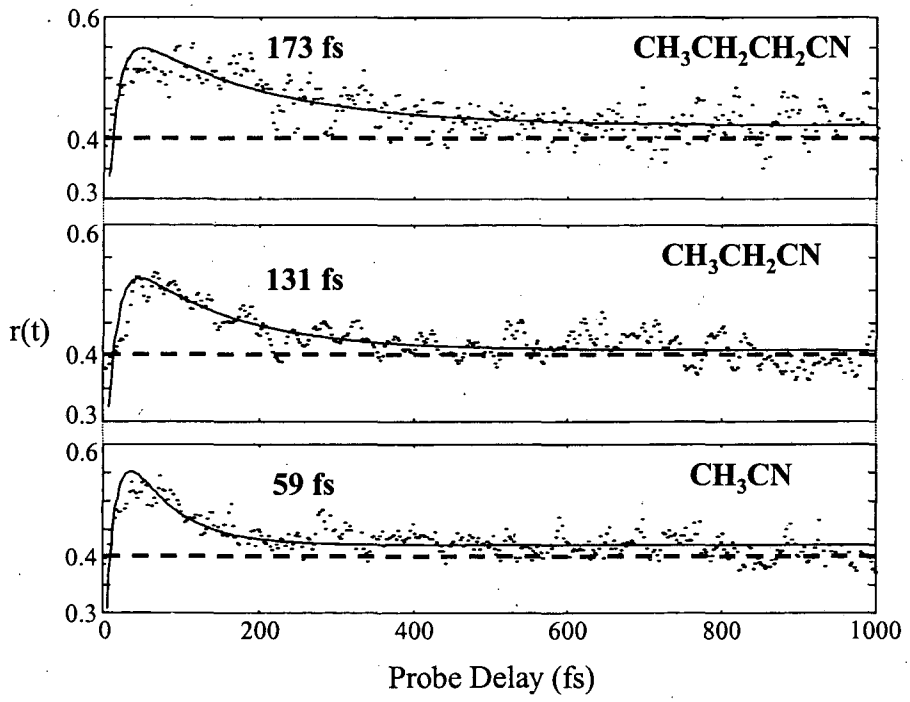


**Figure 3-13 Solvent dependent anisotropy of $[Ru(bpy)_3]^{2+}$.**

acetonitrile, the anisotropy traces in propionitrile and butyronitrile begin with an initial anisotropy value of r ~ 0.55 and depolarizes on a fast time scale to a value of r = 0.4. The decay of the anisotropy is dependent on solvent and quantified with a single exponential fit as shown in figure 3-13. The depolarization decay times become longer with the length and mass of the solvent.

Shown in the table are the depolarization times in each solvent normalized to the

**Table 1 Comparison of depolarization times with inertial moments of the solvent series.**

| Solvent | $\tau_{exp}$ (fs) | $\tau_d/\tau_{CH3CN}$ | $I/I_{CH3CN}$ | I (amu $A^2$) |
|---|---|---|---|---|
| $CH_3CN$ | 59 | **1** | **1** | 44.4 |
| $CH_3CH_2CN$ | 131 | **2.2** | **1.8** | 78.6 |
| $CH_3CH_2CH_2CN$ | 173 | **2.9** | **3.2** | 142 |

depolarization time of $CH_3CN$ compared with the inertial moment of the solvents normalized to the inertial moment of $CH_3CN$. The inertial moments were calculated from the Carbon and Nitrogen backbone atoms and bond distances and angles were used from the literature[68]. The inertial moment for butyronitrile is an average over the degrees of freedom of the molecule. As can be seen, the ratio of the depolarization times scale with the ratio of the inertial moment of the solvents.

This data reveal the localization process is mediated by the solvation of charge by the solvent[69-72]. The localization times are determined by the inertial solvent response to the new charge distribution of the excited molecule. This indicates that localization of charge in $[Ru(bpy)_3]^{2+}$ is driven by intermolecular forces and not by any intramolecular process.

The experiments in this chapter have resolved the charge localization process in $[Ru(bpy)_3]^{2+}$. The time resolved anisotropy measurements have resolved an ultrafast depolarization indicating an ultrafast change in symmetry of the MLCT transition moment. The initial anisotropy value of r = 0.55 is indicative of a transition moment with a degeneracy higher than single degeneracy. This is consistent with the predicted doubly degenerate MLCT transition moment from the $D_3$ ground state symmetry of the molecule. The initial anisotropy of the system quickly depolarizes to a long time value of r = 0.4. This long time anisotropy indicates the symmetry of the MLCT transition moment has changed to single degeneracy. This is indicative of a localized charge.

The solvent dependence of the charge localization process indicates the process is intermolecular in nature. The localization times in the different solvents scale with their inertial moments. This indicates that localization is limited by the polar solvent's ability to solvate the localized charge. Put in another way, localization of charge is dependent upon the dielectric response of the solvent.

The high anisotropy at long times also indicates the localization process is not random. Given an initial delocalized electronic wavefunction among the three bipyridine ligands, the electron does not randomly localize to one of the three ligands. If this were the case, the anisotropy value at long times would be less than $r = 0.4$. Instead, the electron localizes to the bipyridine ligand aligned with the electric field of the pump pulse.

This work represents the first observation of the evolution of charge in the MLCT excited state from a delocalized state to the localized state of $[Ru(bpy)_3]^{2+}$ in solution. However, it remains unclear whether this localized state is the same electronic state as the $^3$MLCT state. Given the spin quantum number remains valid for this system, a "spin flip" should mark the intersystem crossing from the singlet manifold to the triplet manifold.

## 4. Singlet to Triplet transition

The photophysics of $[Ru(bpy)_3]^{2+}$ when exciting the metal to ligand charge transfer band is commonly described as an absorption of light which promotes an electron from the metal center to the $^1$MLCT state on the ligands. As shown in the previous chapter, the initial excitation is delocalized among the bipyridine ligands. The reactive state of $[Ru(bpy)_3]^{2+}$ is labeled the $^3$MLCT and, in solution, is a localized electronic state on one bipyridine ligand. The results of chapter 3 are the first experiments to time resolve the localization process.

In describing the initial photoexcited state as a $^1$MLCT state and the final reactive state as a $^3$MLCT state, the assumption is made that spin is a good quantum number and that the system undergoes an intersystem crossing. A number of arguments have been made which question the validity of the spin quantum number in this system[73, 74], including the simple fact that ruthenium is a heavy metal and spin-orbit coupling strength scales as $\sim Z^4$.

The dynamics seen in the transient absorption spectra are not well understood. The spectral shift seen in the spectra has been explained by the excited state absorption of the photoinduced wavepacket on the excited state surfaces. However, the transient absorption spectra provide no information on the momentum states of the system which would relate the spectral shift to an intersystem crossing from the singlet manifold to the triplet manifold. This chapter will investigate this as well as any intermolecular dependencies of the spectral shift.

An intersystem crossing or "spin flip" involves a change in the angular momentum of the system. Similar processes have been observed in novel solid state systems. The spin

dynamics of these semiconductor systems have been studied using circularly polarized light with and without a magnetic field[75-79]. In this chapter, the spin dynamics of $[Ru(bpy)_3]^{2+}$ will be similarly studied using circularly polarized light.

### *4.1 Intramolecular processes in $[Ru(bpy)_3]^{2+}$*

Transient absorption spectra of $[Ru(bpy)_3]^{2+}$ under a number of different conditions have shown the same spectral dynamics. In $CH_3CN$, these same dynamics have been seen when the probe polarization is parallel to the pump, perpendicular to the pump and at the magic angle. Shown in figure 4-1 is the time resolved transient absorption spectra

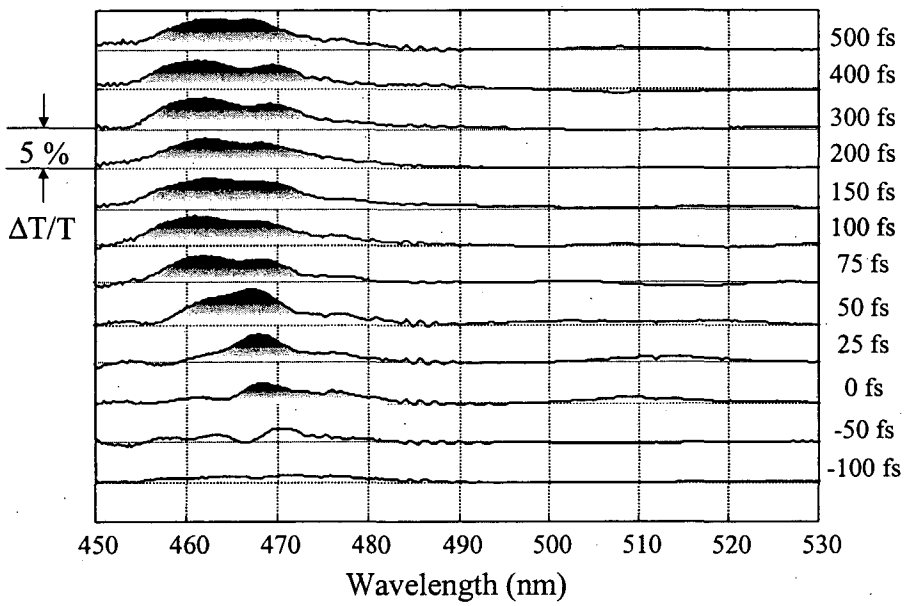


**Figure 4-1 Transient absorption spectra of $[Ru(bpy)_3]^{2+}$ in $CH_3CN$ with the probe polarization at the magic angle relative to the pump polarization.**

of $[Ru(bpy)_3]^{2+}$ in $CH_3CN$ with the probe polarization at the magic angle relative to the pump polarization. The spectra at different probe delays are offset as labeled and the maximum signal levels of the bleach for longer probe delays is $\Delta T/T \leq 5$ %. As seen previously, the differential spectra evolve out to 300 fs at which point the differential

spectra match nanosecond excited state absorption spectra[33]. The differential spectra at early times are combinations of bleach of the ground state absorption and excited state absorption of the probe. The time dependent spectral shift of the differential spectra to shorter wavelengths is the excited state absorption shifting to the blue leaving the ground state bleach.

In figure 3-13, the depolarization of the anisotropy was seen to be solvent dependent. For the solvent series, the fastest depolarization of the anisotropy in the nitrile solvent series was seen in acetonitrile and the slowest depolarization was seen in butyronitrile. Comparison of transient absorption spectra with pump and probe polarizations parallel and perpendicular to each other reveal the depolarization in the anisotropy is unrelated to the spectral dynamics of the excited state. However, it has not been shown that the spectral dynamics is independent of solvent effects.

The time resolved transient absorption of $[Ru(bpy)_3]^{2+}$ in $CH_3CH_2CH_2CN$ is shown in figure 4-2. The depolarization of the anisotropy was the slowest in butyronitrile for the

solvent series. Again, the spectra at different probe delays are offset from each other as

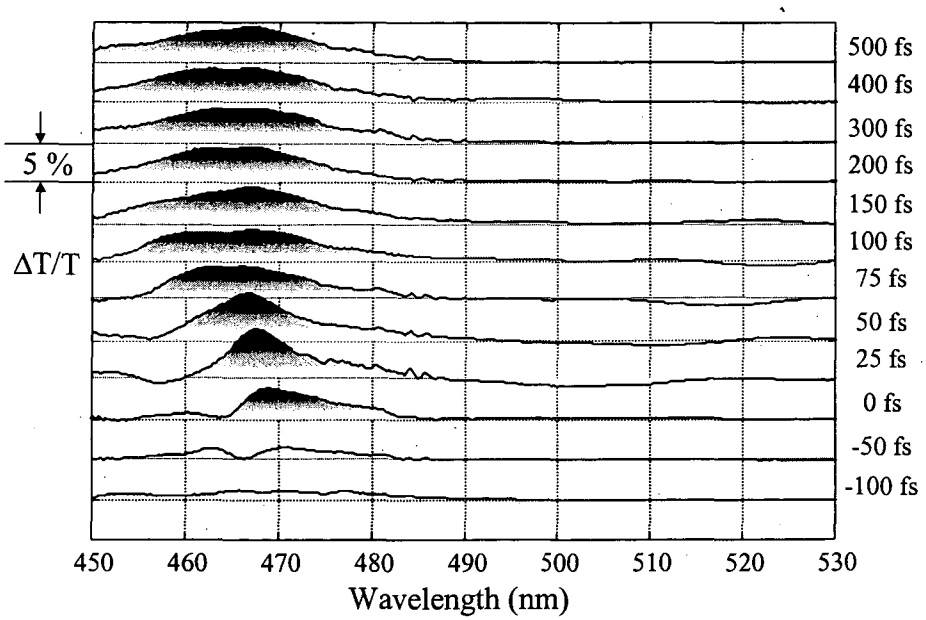


**Figure 4-2 Transient absorption spectra of $[Ru(bpy)_3]^{2+}$ in $CH_3CH_2CH_2CN$ with the probe polarization at the magic angle relative to the pump polarization.**

labeled. The signal levels of the bleach for longer probe delays is $\Delta T/T \sim 5$ %. As can be seen, the rate of the spectral shift of the excited state absorption to shorter wavelengths in butyronitrile appears to be the same as in acetonitrile. The wavepacket motion on the excited state appears to be independent of solvent or intramolecular in nature.

Thus far, two distinct processes have been observed in the evolution of the $^1$MLCT state to the $^3$MLCT. One process is localization which is seen to be facilitated by the solvation of charge and dependent upon the inertial response of the polar solvent. The other process which was revealed in figure 4-1 and figure 4-2 is intramolecular in nature and may be related to molecularly driven processes such as intersystem crossing.

### *4.2 Interaction of light with chiral molecules*

A chiral molecule does not possess an improper axis of rotation. An improper axis of rotation is commonly referred to as $S_n$ where the molecule is rotated about the axis $2\pi/n$ followed by a reflection through a plane perpendicular to the axis. The simplest improper axis of rotation is $S_1$. This simply defines a mirror plane perpendicular to the improper axis of rotation. $S_2$ is another operation of interest. In this operation, the molecule is rotated 180° and then reflected through a mirror plane perpendicular to its axis of rotation. This defines an inversion operation. These operations are two important tests to predict the optical activity of the molecule.

A chiral molecule is optically active. Optically active molecules will rotate the polarization of linearly polarized light. The optical activity of a sample can be quantified by its specific rotation $[\alpha]_\lambda$ of polarized light at wavelength $\lambda$ defined[80]

$$[\alpha]_\lambda \equiv \frac{\alpha_\lambda}{\rho_B \ell},$$

where $\rho_B$ is the mass concentration of B in the sample and $\ell$ is the pathlength of the linearly polarized light through the sample. A plot of specific rotation $[\alpha]_\lambda$ versus wavelength $\lambda$ gives the optical rotatory dispersion. The specific rotation $[\alpha]_\lambda$ is positive when the polarization of light is rotated clockwise as viewed looking into the oncoming beam and the sample is termed *dextrorotatory*. For counterclockwise rotation of light, the sample is termed *levorotatory*. Optical activity is contained in the real part of the linear susceptibility of the sample.

A chiral molecule may also exhibit properties of circular dichroism (CD). The transition moment of chiral molecules may have a net electric and magnetic dipole moment. This information is contained in the imaginary part of the molecule's

susceptibility. The probability of such a transition is the scalar product of the electric dipole μ and magnetic dipole **m** transition matrices given by the Rosenfeld equation[81]

$$R_{ge} = \mathrm{Im}\left\{\langle g|\vec{\mu}|e\rangle \bullet \langle e|\vec{m}|g\rangle\right\},$$

$$= -\tfrac{e^2\hbar}{2mc}\langle g|\sum_j \vec{r}_j|e\rangle \bullet \langle e|\sum_j \left(\vec{r}_j \times \vec{\nabla}_j\right)|g\rangle,$$

where g and e are the ground and excited electronic states of the molecule.

A typical CD experiment measures the difference in absorption of right- and left-circularly polarized light of an enantiomer of the chiral molecule. The difference in absorption of right- and left-circularly polarized light of the enantiomer comes from the interaction of the enantiomer's magnetic moment **m** with the magnetic moment of the circularly polarized light. Assuming an isotropic solution of enantiomers, the CD spectrum $\Delta\varepsilon(\nu)$ can be calculated for transitions into all excited states from the transition probability $R_{ge}$ from above,

$$\Delta\varepsilon(\nu) \propto \sum_a \frac{R_{ge}\nu_a e^{-\left(\frac{\nu-\nu_a}{2\sigma_a^2}\right)^2}}{\sigma_a},$$

where a Gaussian distribution with a standard deviation $\sigma_a$ of transition energies has been assumed.

The CD spectra for Δ- and Λ-$[Ru(bpy)_3]^{2+}$ are shown in figure 4-3. The CD spectra

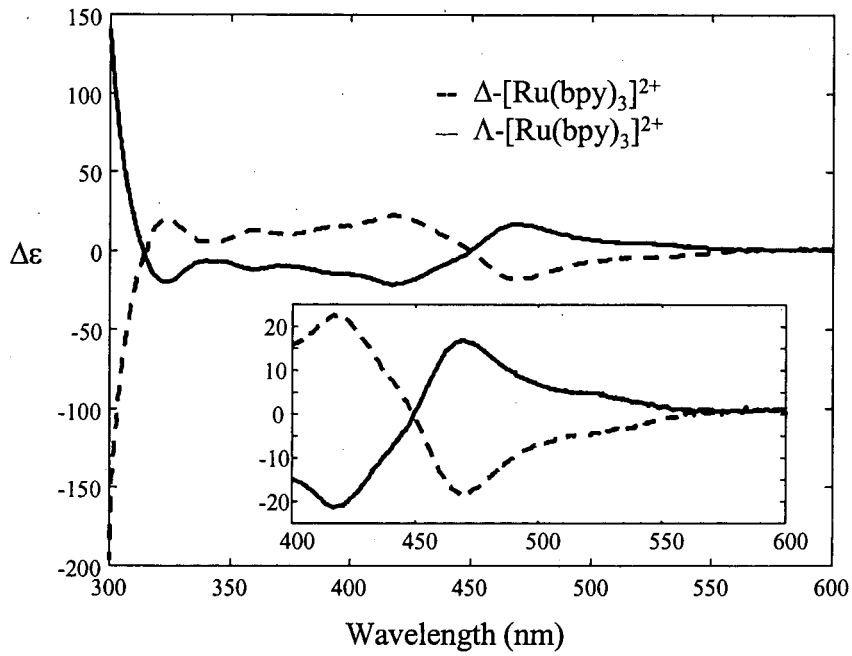


**Figure 4-3 Circular dichroism spectra of Δ- and Λ-enantiomers of $[Ru(bpy)_3]^{2+}$.**

for the two enantiomers in the wavelength region of the MLCT absorption are shown in the inset. The two spectra for Δ- and Λ-enantiomers are measured separately. The CD spectrometer measures the difference in absorption of right- and left-circularly polarized light by quickly toggling between the two light polarizations during the measurement. At $\lambda = 480$ nm, the CD for an enantiomer is $\Delta\varepsilon = |14\ M^{-1}cm^{-1}|$. As can be seen, this is near the maximum CD for the MLCT absorption. The CD compared to the total absorption at $\lambda = 480$ nm is $\Delta\varepsilon/\varepsilon \leq 1$ %.

### *4.3 Time resolved circular dichroism measurement*

The intersystem crossing involves a "spin flip" or a change in the magnetic moment of the molecule. Circularly polarized light has been used to study changes in momentum

states of semiconductor heterostructures, in particular GaAs quantum wells[75, 76, 79]. It is instructive to review the physics fundamental to these experiments.

The frontier orbitals of Gallium and Arsenic combine to form the conduction band and valence band of the semiconductor. In the model of ionic bonding, combinations of 4p atomic orbitals of As will make up the valence band and combinations of 5s orbitals of Ga will make up the conduction band. The heavy atoms of Ga and As will have strong spin-orbit coupling mixing the orbital and spin states. The momentum states of the conduction band will be m = ±1/2 and the valence band will be composed of m = ±3/2, ±1/2 and a split-off band. The energy dispersion of these bands in k-space in one dimension is illustrated in figure 4-4. The point of infinite wavelength or k = 0 is

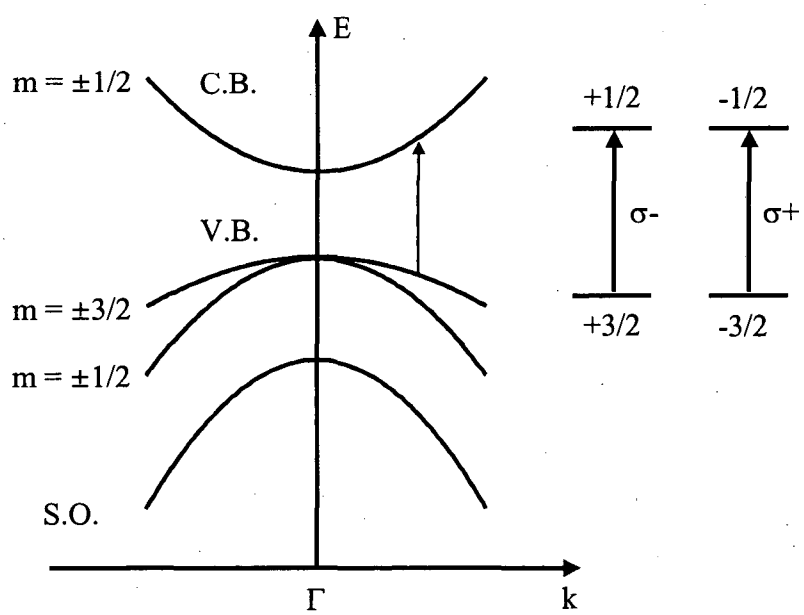


**Figure 4-4 Typical energy dispersion of semiconductor conduction and valence bands and the selection rules for circularly polarized light.**

demarked by the Γ point. This is the point in k-space at which the combination of all atomic orbitals are in phase. The energy dipsersion of a band in a particular dimension is dependent upon the crystal field of the semiconductor in that direction.

For GaAs quantum wells, the spatial extent of the semiconductor in one dimension is comparable or smaller than the de Broglie wavelength for an electron. This leads to quantum confinement of the electronic wavefunctions and causes the semiconducting bands in one dimension to collapse into discrete states. For these structures, the Γ point no longer exists and the lowest energy transitions occur for $k > 0$ as demarked by a vertical arrow on the band diagram in figure 4-4.

For points away from the Γ point, the valence band is split in energy into its momentum states. From here it is possible to selectively excite transitions from the $m = \pm 3/2$ momentum state of the valence band to the $m = \pm 1/2$ state of the conduction band. Spin relaxation processes may be studied in these systems using circularly polarized light[75, 79]. The selection rules for circularly polarized light are illustrated to the right of the band diagram in figure 4-4 where $\Delta m = 1$ for $\sigma+$ and $\Delta m = -1$ for $\sigma-$ polarized light.

Circularly polarized light will be used to differentiate between the $^1$MLCT state and the $^3$MLCT state and resolve the intersystem crossing in $[Ru(bpy)_3]^{2+}$. The spectral dynamics of the excited state absorption will be studied using a broadband $\lambda/4$ waveplate to circularly polarize the pulses. The dynamics of the excited state absorption was found to be intramolecular in nature and associated with internal processes such as intersystem crossing. A $\lambda/2$ waveplate in the pump beam is used to toggle the circular polarization of the pump pulse relative to the probe pulse.

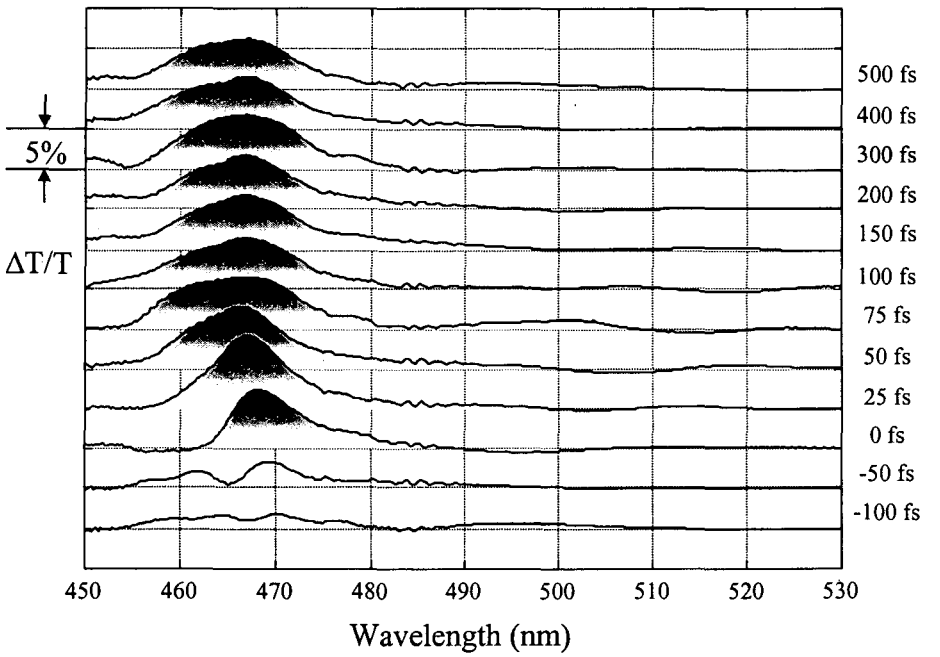


**Figure 4-5 Transient absorption spectra of $[Ru(bpy)_3]^{2+}$ with pump and probe of the same circular polarization.**

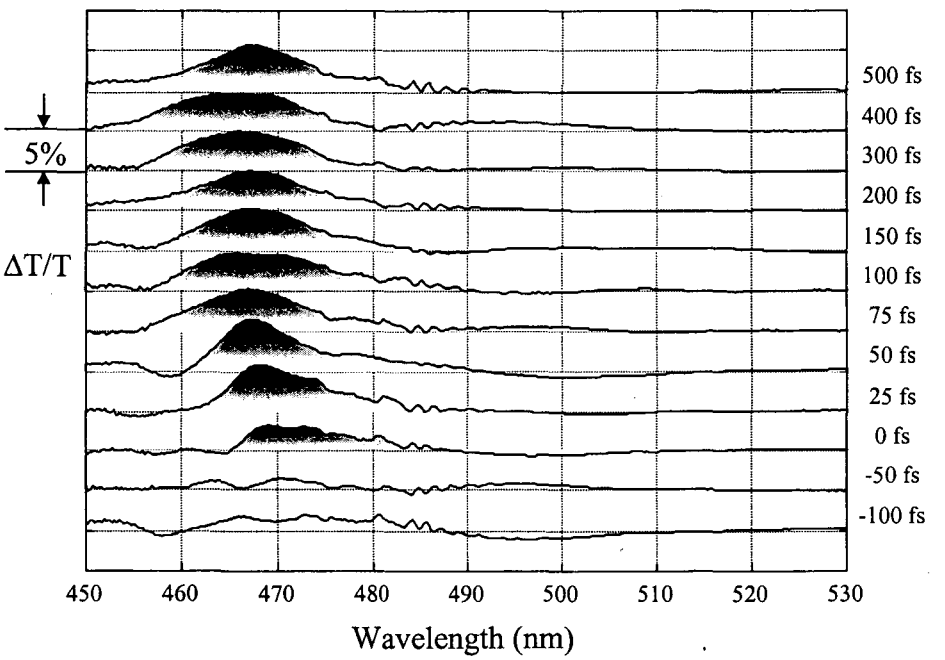


**Figure 4-6 Transient absorption spectra of $[Ru(bpy)_3]^{2+}$ with pump and probe of opposite circular polarization.**

Transient absorption spectra with pump and probe pulses of the same circular polarization are shown in figure 4-5. The transient absorption spectra for each delay are offset from each other as labeled. The signal level for longer probe delays is $\Delta T/T \sim 5\%$ as seen by the scale on the graph. The spectral evolution seen in these spectra is consistent with the spectral dynamics seen previously[33]. For comparison, the transient absorption spectra with pump and probe of opposite circular polarization are shown in figure 4-6. Again, the delays are offset and $\Delta T/T \sim 5\%$ signal is seen for longer probe delays. As can be seen, the dynamics of the spectral evolution is independent of the polarization of the pump and probe pulses. The spectra of figure 4-5 and figure 4-6 can be compared for each delay and no wavelength dependence can be seen.

Further selectivity may be attained by studying the Δ- and Λ-enantiomers of $[Ru(bpy)_3]^{2+}$ separately. The resolution of the enantiomers of $[Ru(bpy)_3]^{2+}$ begins with a racemic solution of *cis*-$[Ru(bpy)_2(py)_2]Cl_2$ (py = pyridine). An enantiomer may be selectively crystallized from this solution with use of the appropriate resolving agent. The Δ-enantiomer is crystallized in the form of Δ-$[Ru(bpy)_2(py)_2]$[(+)-*O,O'*-dibenzoyl-D-tartrate] where (+)-*O,O'*dibenzoyl-D-tartrate is used as the resolving agent. The Λ-enantiomer is crystallized in the form of Λ-$[Ru(bpy)_2(py)_2]$[(-)-*O,O'*-dibenzoyl-L-tartrate].[82] The two crystallized enantiomers are precursors to the Δ- or Λ-enantiomer of $[Ru(bpy)_3]^{2+}$. The Δ- or Λ-enantiomer of $[Ru(bpy)_3]^{2+}$ is synthesized by heating the appropriate precursor in solution with the mole equivalent of bipyridine. These enantiomers can be purified through recrystallization.[83]

As seen in figure 4-3, the difference in the steady-state absorption of right- and left-circularly polarized light of the enantiomers is $\Delta\varepsilon \sim 15\ M^{-1}cm^{-1}$ at 480 nm. This

difference is indicative of a steady-state difference in the magnetic moments of the $^3$MLCT state of the two enantiomers. The dynamics of the magnetic moment of the excited state of $[Ru(bpy)_3]^{2+}$ from the $^1$MLCT to the $^3$MLCT will be measured by time-resolving the CD spectra using circularly polarized pulses. For these experiments, a pump-probe configuration will be used with circularly polarized pulses of 25 fs in duration centered at 480 nm.

Shown in figure 4-7 are the time-resolved CD traces of $\Delta$-$[Ru(bpy)_3]^{2+}$ with pump and

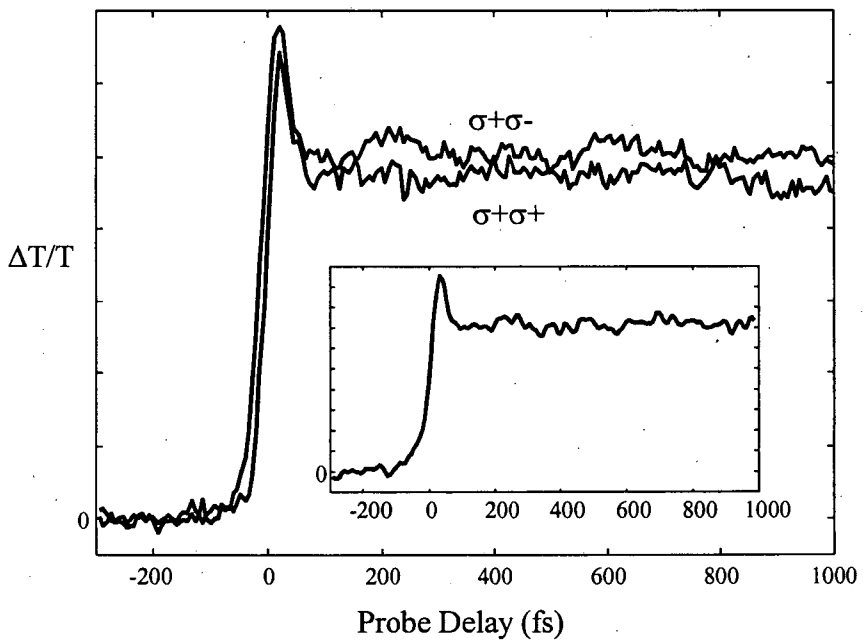


**Figure 4-7 Time-resolved CD traces of $\Delta$-$[Ru(bpy)_3]^{2+}$ with pump and probe of the same (σ+σ+) and opposite (σ+σ-) circular polarizations. The inset is pump-probe of population dynamics with the pump polarization at the magic angle relative to the probe.**

probe of the opposite and the same circular polarization. These polarizations are labeled σ+σ- and σ+σ+, respectively. The time-resolved CD traces of the two polarizations are taken separately with the pump polarization toggled between circular polarizations of the opposite and the same sense as the probe polarization. The two traces are averaged over the same experimental run where the pump polarization is rotated after each scan. The

signal of the two traces is from bleaching of the ground state. A very fast transient is seen in the two traces near zero probe delay which quickly reaches a near constant signal level for the remainder of the scan. The magnitude of the initial transient relative to the signal value at long times is wavelength dependent. The center wavelength of the pump and probe in these scans are on the red edge of the MLCT absorption. Scans with the pump and probe at 460 nm, in which the pulses are tuned higher into the absorption, do not have the initial transient.

After the initial spike, the pump-probe signal does not change for the duration of the two scans. The inset of figure 4-7 shows pump-probe scans with the pump polarization at the magic angle relative to the probe polarization. At the magic angle, the pump-probe scan is free of anisotropic effects and reflects the population dynamics of the system. At 480 nm, the signal is dominated by the ground state bleach. The magic angle pump-

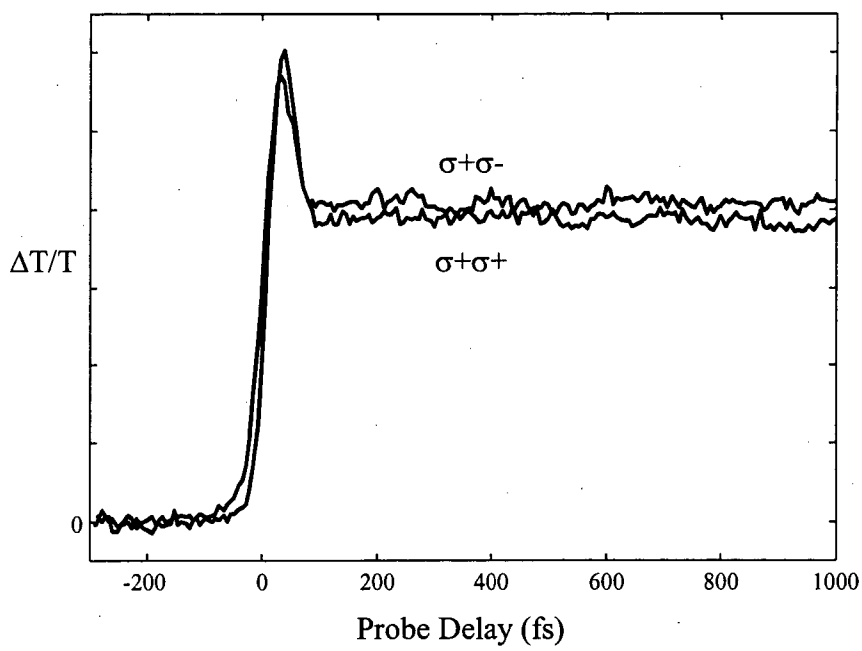


**Figure 4-8 Time-resolved CD traces of Λ-$[Ru(bpy)_3]^{2+}$ with pump and probe of the same (σ+σ+) and opposite (σ+σ-) circular polarizations.**

probe scan reflects the long lifetime of the excited state ($\tau \sim 1$ μs).

Time-resolved CD traces of Λ-$[Ru(bpy)_3]^{2+}$ are shown in figure 4-8. Pump and probe polarizations of the opposite and the same circular polarization are labeled the same as before. Scans from the same experimental run are shown in figure 4-8. After the initial very fast transient near zero probe delay, the CD traces are dominated by ground state bleach. The dynamics of the CD traces in figure 4-8 reflect what was seen in the magic angle pump-probe traces.

It is evident that the pump-probe scans with circularly polarized pulses do not detect any difference when performing the experiment with pulses with polarizations of the same sense as opposed to the opposite sense. A change in the magnetic moment of the excited state is not seen which would be indicative of an intersystem crossing. In fact, the time-resolved CD experiments exhibit the same dynamics as what was seen when exciting with linearly polarized pulses oriented at the magic angle relative to one another. That is, the dynamics reflect a bleach of the ground state which persists for the duration of the experiment.

One reason the time-resolved CD experiments are not measuring a change in the momentum of the system may be the sensitivity of the experiment. The CD of the enantiomers is on the order of $\Delta\varepsilon/\varepsilon \leq 1\%$. The pump-probe signal for the time-resolved CD experiments at 480 nm is on the order of $\Delta T/T \sim 2\%$. The time-resolved CD experiments comparing σ+σ+ and σ+σ- scans should measure a signal difference on the order of $\Delta T/T \sim 0.02\%$ for the steady-state CD. It should be noted that the difference in the signal levels seen in the σ+σ+ and σ+σ- scans for the Δ- and Λ-isomers in figure 4-7 and figure 4-8 is on the same order as the steady state CD (~1%) for one enantiomer.

This difference in signal level is not a result of long term drift of the laser power because the traces are averaged over the same experimental runs with the pump polarization changed after each scan. However, errors due to power fluctuations and other systematic errors may result because the traces are not recorded simultaneously.

Changes in the time-resolved CD indicative of an intersystem crossing may not have been measured because of the large spin-orbit coupling due to the metal center of $[Ru(bpy)_3]^{2+}$[73]. Spin-orbit coupling for Ruthenium is high ($\zeta \sim 878$ cm$^{-1}$) and may result in multiple allowed $^1$MLCT momentum state transitions for a given circular polarization. The MLCT states have Ru 4d and bipyridine $\pi^*$ orbital character. Large coupling between the spin and orbital angular momentum of the metal d atomic orbitals results in two total angular momentum states J = 5/2, 3/2. Each of these states have (2J+1) degeneracy. For the bipyridine $\pi^*$ molecular orbital, spin-orbit coupling results in total momentum states of J = 3/2, 1/2. Mixing of three $\pi^*$ molecular orbitals of the bipyridine ligands gives total angular momentum states of J = 9/2, 7/2, 5/2, 3/2, 1/2 for a total of 216 momentum states. The selection rules for the MLCT transition may not allow for selective excitation of individual momentum states such as in the case of GaAs quantum wells (see figure 4-4).

In this chapter, a series of experiments has resolved intramolecular processes in the evolution of the $^1$MLCT state to the $^3$MLCT state independent of charge localization which was presented in chapter 3. The dynamics associated with the spectral shift to shorter wavelengths seen in the transient absorption spectra is indicative of wavepacket motion on the excited state surfaces. These dynamics were found to be independent of

solvent forces and may be attributed to intramolecular processes such as intramolecular vibrational relaxation, internal conversion or intersystem crossing.

Time-resolved CD experiments did not resolve dynamics which could be attributed to an intersystem crossing from the $^1$MLCT state to the $^3$MLCT state. It is problematic to explain a non-result, but the validity of the spin quantum number in these systems may be questionable. It has been shown that spin-orbit coupling in the MLCT excited states relaxes the selection rules to allow for multiple transitions to individual momentum states. The mapping of the energy level structure of $[Ru(bpy)_3]^{2+}$ is still an active area of research[4, 5, 7, 8, 24-26, 32, 73, 74, 84-93].

# 5. Conclusions

This thesis addresses some fundamental issues concerning photoinduced processes in the evolution of the excited state of tris-(2,2'-bipyridine) ruthenium(II) from the $^1$MLCT to the $^3$MLCT reactive state. The time scale of this evolution challenges the traditional conventions used to describe excited state relaxation processes including intramolecular vibrational relaxation, internal conversion and intersystem crossing. The experiments presented in this thesis represent the first application of ultrafast spectroscopy (~20 fs resolution) to investigate the excited state dynamics of this metal-to-ligand charge transfer system.

The experiments presented probe the initial events upon excitation into the $^1$MLCT excited state. These events determine the evolution of the excited state to the $^3$MLCT state. By studying and understanding these initial events, the processes which govern the excited state evolution may be characterized relative to the conventional relaxation pathways. This knowledge may also further the ability to control the excited state evolution and to manipulate the properties of the final excited state.

Two distinct processes have been resolved in the evolution of the excited state. One is intermolecular in nature in which solvent forces have been shown to influence the symmetry of the final excited state. Another is intramolecular in nature and can be associated with wavepacket dynamics on the excited state surface(s).

## *5.1 Localization of charge*

The ground state symmetry of $[Ru(bpy)_3]^{2+}$ is such that one bipyridine ligand is indistinguishable from the other two. It follows from this symmetry that an electron promoted from the metal to the ligands would be delocalized among the three bipyridine

ligands. This is found to be the case for molecules in solid matrices[9, 11, 54]. However, prior to the experiments presented in this thesis, a delocalized excited state was not resolved for molecules in a liquid evironment. In fact, the electronic wavefunction was found to be localized to one bipyridine ligand[12]. It is this discontinuous behavior of the symmetry of the excited state wavefunction from the solid matrix to the liquid state which the experiments presented in chapter 3 sought to understand.

Ultrafast anisotropy measurements were presented in chapter 3. These measurements are sensitive to the symmetry of the transition dipole moment. Characterization of the symmetry of the excited state electronic wavefunction utilized the difference in symmetry of the transition moment of a delocalized state compared to a localized state.

The results of the anisotropy measurements resolved the evolution of the symmetry of the MLCT transition moment from one of at least two-fold degeneracy to a singly degenerate transition moment. This is indicative of an initially delocalized state which localizes on some time scale to one ligand. The time scale of this localization is dependent upon the inertial moment of the solvent. The final distribution of singly degenerate transition moments indicates the ligand to which charge is localized is aligned along the electric field of the pump pulse.

Charge localization to one ligand is predominantly driven by solvent forces. The propensity for charge to localize is the savings in energy to solvate charge localized to one ligand as opposed to the screening of charge delocalized among the three ligands. For the polar solvent environments, the rate of charge localization is determined by the inertial moment of the solvent. From the solid matrix to the liquid environment, it is the savings in energy in screening a localized charge relative to a delocalized charge and the

ability of the environment to solvate this localized charge which drives the charge localization process.

### *5.2 Intramolecular Processes*

The description of the evolution of a photoinduced charge transfer in an inorganic complex such as $[Ru(bpy)_3]^{2+}$ invariably begins with a dipole allowed, singlet transition which evolves in some manner through an intersystem crossing to a "spin forbidden" excited state. The dipole allowed, singlet transition is to the $^1$MLCT state which evolves to the "spin forbidden" $^3$MLCT state. The first evidence of this evolution was seen in the transient absorption spectra in figure 2-7 of chapter 2. A spectral evolution was resolved in which an excited state absorption shifted to shorter wavelengths. The excited state absorption was observed for less than 300 fs at which point it shifted outside the spectral window of the probe pulse. Spectra at probe delays $\Delta t > 300$ fs were compared to nanosecond excited state absorption spectra and the spectra were found to be superimposable[33]. The spectral evolution of the transient absorption spectra is indicative of the $^1$MLCT to $^3$MLCT "intersystem crossing" and is attributed to wavepacket dynamics on the excited state surfaces.

Subsequent experiments in chapter 4 found that these wavepacket dynamics are independent of solvent. These dynamics are largely unaffected by solvent forces and can be attributed to intramolecular processes. Previous work has assigned these processes to internal conversion in the singlet manifold, intersystem crossing and internal conversion in the triplet manifold[3-5]. The ultrafast evolution of the excited state absorption spectrum challenges the conventional definition of these processes.

Time-resolved CD experiments were performed to resolve the change in momentum which would accompany an intersystem crossing. Spectral CD experiments of racemic samples and single wavelength CD experiments of the Δ- and Λ-enantiomers did not resolve any dynamics indicative of a change in momentum states. In fact, the dynamics resolved in the CD experiments were similar to the population dynamics of the same experiments with the pump and probe polarizations at the magic angle relative to each other. A simple quantum-mechanical treatment of the system for spin-orbit coupling revealed the selection rules for circularly polarized pulses may allow multiple transitions to individual momentum states. The CD experiments may not be sensitive to changes in momentum due to spin-orbit coupling in the MLCT states.

The evolution of the excited state of tris-(2,2'-bipyridine) ruthenium(II) from the initially excited $^1$MLCT state to the $^3$MLCT state has been resolved. Two distinct processes have been observed in this evolution which can be characterized as intermolecular and intramolecular in nature. Solvent forces have been shown to dramatically affect the excited state wavefunction. The rate of charge localization has been found to be dependent upon the inertial moment of the solvent. Spectral dynamics in the excited state absorption spectrum are attributed to wavepacket motion on the excited state surfaces. These dynamics were found to be largely unsusceptible to intermolecular interactions. The wavepacket motion is indicative of the internal potential of the molecule. These results indicate that the excited state dynamics in charge transfer complexes have at least two distinct processes, one which is sensitive to the environment of the molecule and one which may only be influenced by the chemistry of the complex.

## Appendix A. Blue laser system

The focus of this thesis has been the ultrafast excited state dynamics of $[Ru(bpy)_3]^{2+}$. However, with ultrafast experiments using dye lasers, invariably, a significant amount of time is spent maintaining the laser system. The blue laser system is designed to generate short pulses in the blue-green region of the spectrum. This appendix is devoted to reviewing the blue laser system and some of its new components which were added recently.

A block diagram of the blue laser system is illustrated in figure A-1. It begins with the

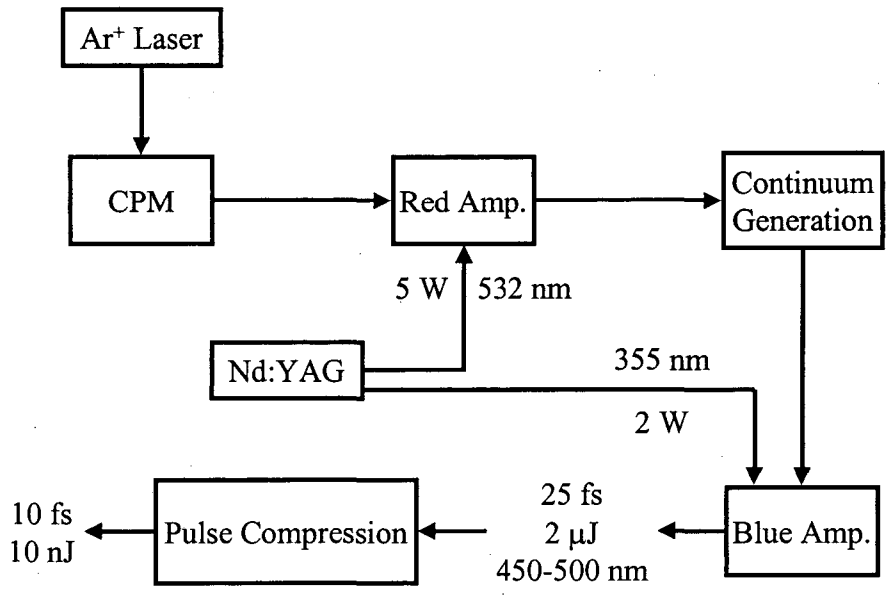


**Figure A-1 Block diagram of the blue laser system.**

colliding pulse modelocked (CPM) ring dye laser pumped by all lines of an Argon ion laser. The CPM generates 60 fs pulses at 620 nm at a repetition rate of 100 MHz. These pulses are amplified in the red amplifier pumped by the second harmonic of a high repetition rate Nd:YAG laser from tens of picojoules to a couple of microjoules at 540

Hz. These amplified pulses are focused into an ethylene glycol jet to generate continuum. This continuum is sent into a second amplifier pumped by the third harmonic of the Nd:YAG laser, a portion of which is amplified and compressed to generate short pulses in the blue-green region of the spectrum. The second amplifier is essentially tunable throughout the whole visible depending on the dye selected for gain. Further pulse compression is attained by coupling a portion of the amplified blue pulses into a short, single-mode, polarization preserving optical fiber broadening the pulse spectrum and compression to 10 fs using gratings and prism pairs.

The CPM is a passively modelocked ring dye laser and is illustrated in figure A-2.

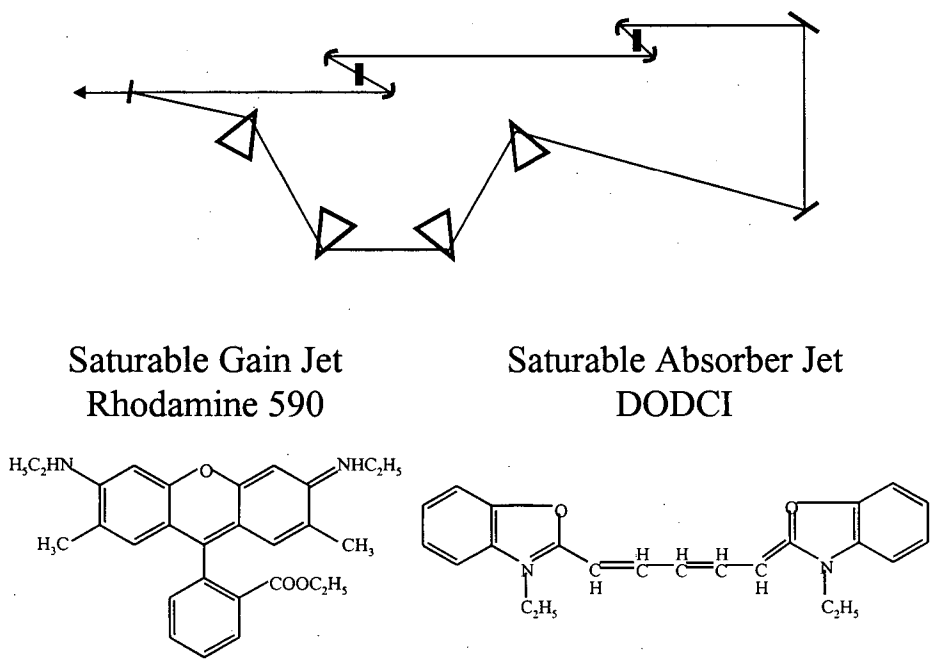


**Figure A-2 The CPM ring dye laser.**

The saturable gain is pumped by 3-4 W of all lines of an Ar+ laser. The combination of rhodamine 590 in the gain jet and DODCI in the saturable absorber reliably generates 60 fs pulses at 620 nm. Without the saturable absorber, the ring cavity will lase continuously. The intensity of this lasing will be noisy in which the noise spikes are

constructive interference of wavelengths supported by the gain and cavity. The generation of femtosecond pulses from a continuous wave source can be thought of intuitively. The saturable absorber concentration is set to absorb the continuous lasing but allow the noise spikes to pass through. These noise spikes interact with the saturable gain which amplifies the front end of the pulse effectively truncating the back end and the saturable absorber which absorbs the front end of the pulse shortening the pulse with each pass.

To generate blue-green pulses from the red pulses from the CPM, the laser system is designed to generate continuum, a portion of which is amplified and recompressed. Pulses directly from the CPM are not intense enough to generate continuum. These pulses are amplified in a four-pass amplifier shown in figure A-3. The gain dye is

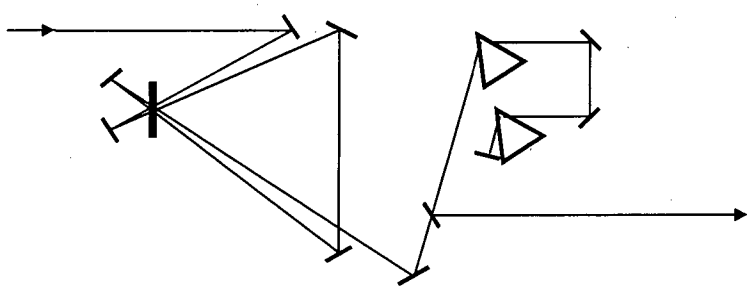

Sulforhodamine 640 1,4-Diaza-bicyclo[2.2.2]octane

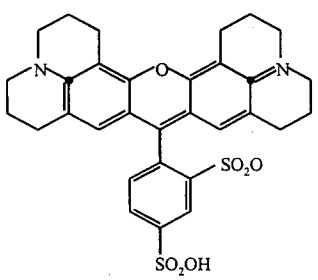


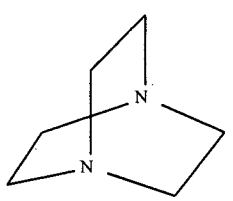


**Figure A-3 Four-pass red amplifier using sulforhodamine 640 with preserving agent DABCO (shown) in ethylene glycol.**

sulforhodamine 640 in ethylene glycol in which a preserving agent (DABCO) is used to extend the life of the dye. The 1 mm pathlength gain flow cell is pumped at 540 Hz by the second harmonic of a high repetition rate Nd:YAG laser at 532 nm. The alignment of the amplifier uses a longitudinal pump geometry. Amplified spontaneous emission from the gain cell may be attenuated by offsetting the height of the red pulse from mirror to mirror in the amplifier. The amplified red pulse is recompressed with a prism pair and focused into an ethylene glycol jet to generate continuum. The continuum is sent to the blue amplifier.

The two-pass blue amplifier is shown in figure A-4. This amplifier is tunable over the

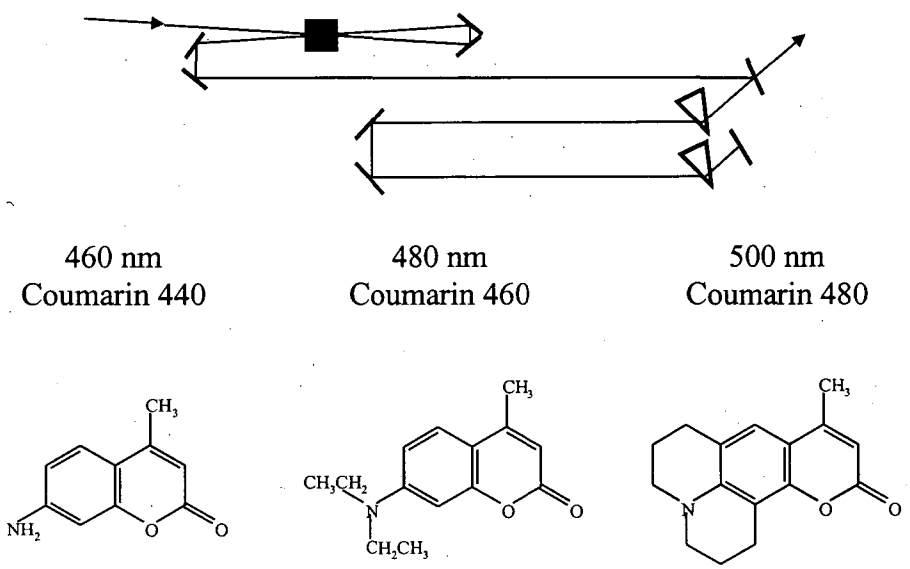


**Figure A-4 Two-pass blue amplifier shown with a series of coumarin dyes to amplify at different wavelengths.**

continuum input depending on the gain dye used. Shown in figure A-4 is a series of coumarin dyes used to amplify in the blue-green region of the spectrum. The amplifier is pumped by the third harmonic of the Nd:YAG at 355 nm in the transverse geometry. The

UV pump beam is focused into a line onto the cell and the passes are aligned collinear to the pump. This pump geometry is used to minimize the loss of gain due to excited state absorption of the short wavelength pump beam. After amplification, the blue pulses are recompressed using a prism pair and now may be used for experiments or further pulse compression.

Further pulse compression to 10 fs may be attained by using a single-mode optical fiber to generate bandwidth and recompression using gratings and prisms. This setup is shown in figure A-5. A portion of the amplified blue pulse may be coupled into a single-

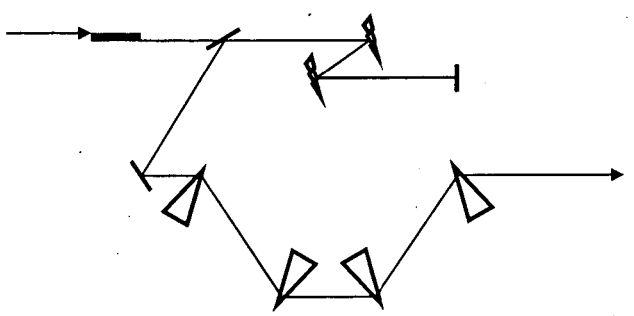

**Figure A-5 Pulse compression using a single-mode optical fiber and gratings and prisms.**

mode optical fiber. The same nonlinear effect which generates continuum in the ethylene glycol jet generates continuum in the optical fiber. Self-phase modulation of the pulse due to the nonlinear index induces a change in the phase of the pulse. The change in phase is proportional to the amplitude of the electric field of the pulse and the change in

frequency is proportional to the time derivative of the amplitude of the electric field of the pulse. The front end of the pulse contributes shorter wavelengths to the pulse spectrum and the back end contributes longer wavelengths to the pulse spectrum. Compression of the continuum is possible over the portion of the spectrum with a linear phase relationship. Pulse compression is accomplished with gratings and prisms to compensate for quadratic and third-order dispersion.

## A.1 Quad-detector piezo mount feedback beam stabilizer for Mach 500 Nd:YAG laser

One source of instability in the blue laser system is the pointing instability of the Nd:YAG pump laser. Two new optics were added to the laser system to alleviate this problem. A simplified setup is shown in figure A-6. One optical mount for a turning

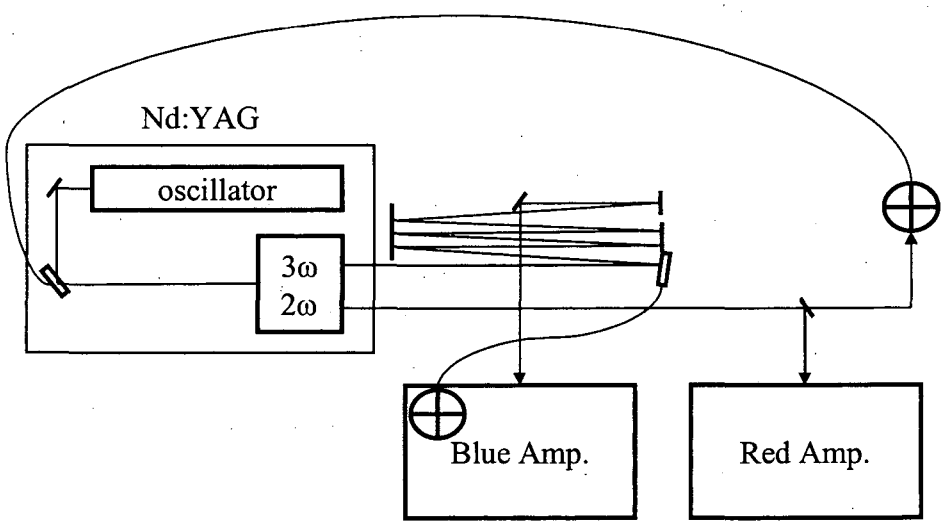


**Figure A-6 Simple diagram of placement of quad-detectors and piezo optical mounts in the blue laser system.**

mirror just outside the Nd:YAG cavity and one mount for a turning mirror on the third harmonic were replaced by piezo optical mounts which had feedback from quad-

detectors placed further downstream. One quad-detector was placed to monitor the second harmonic and feed back to the mount just outside the Nd:YAG cavity. One detector was placed to monitor the third harmonic in the blue amplifier and feed back to the turning mirror on the third harmonic.

In actuality, the signal from the quad-detectors are sent to the piezo drivers to control the two transverse (x, y) directions of the mounts. This signal is processed through control circuits home-built in the commercial piezo drivers. The time-constant of the 2nd-order response of the control circuit is set by components of the circuit. The damping of the response may be manually adjusted for the x, y directions by resistors on the front panel of the piezo drivers. The response of a 2nd-order system to a unit step forcing function is shown in figure A-7. An underdamped system will produce an oscillatory

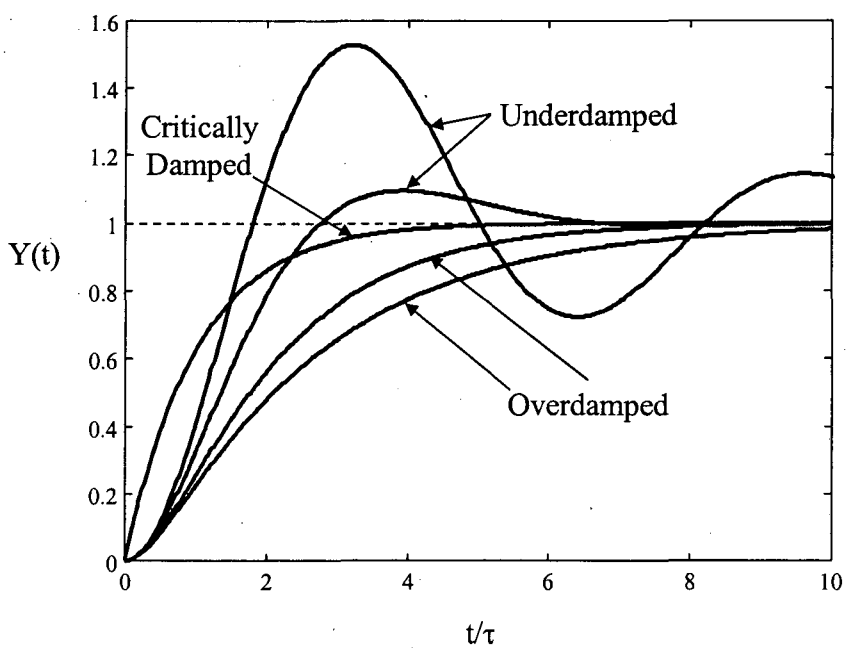


**Figure A-7 Second-order response to a unit step forcing function. The optimum response is the critically damped system.**

response to the forcing function. An overdamped system will produce a sluggish response to the forcing function. The optimal damping is a critically damped system and produces the fastest response to the forcing function.

# Appendix B. Vibron C++ program—computer simulation of FWM signals

Vibron is a computer program written in C++ to calculate four-wave mixing signals. This program is modeled after MDH written in Fortran 77 by W. Tom Pollard during his graduate work at UC Berkeley. Our group's version of MDH was lost in the decommissioning of one of the Cray computers at NERSC. Fortran 77 was scheduled to be phased out and was no longer supported by NERSC. This presented the need to rewrite the program in a different language. I chose C++ because it was new, widely used, and I wanted to learn about object oriented programming. Object oriented programming is not necessary for these calculations and C++ is not the optimal language to use for these intensive calculations.

## *B.1 Current status of program*

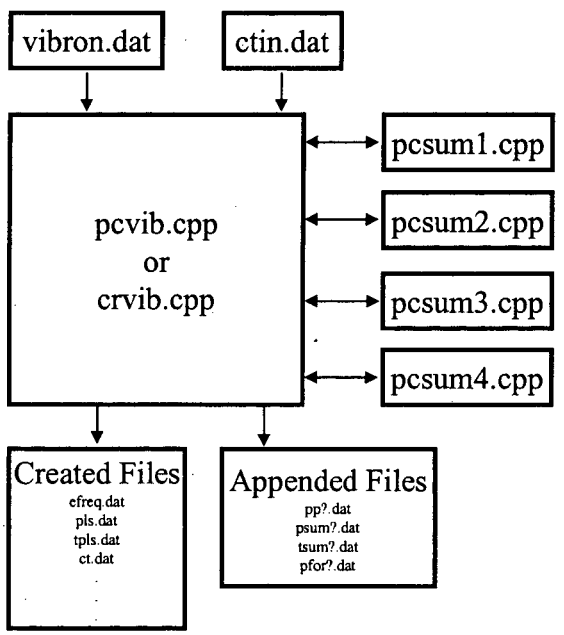


**Figure B-1 Basic flowchart of vibron.**

A general overview of the vibron program is illustrated in figure B-1. The main

program is contained in pcvib.cpp or crvib.cpp. It can take up to two input files. Vibron.dat contains information on the experiment and the system. Ctin.dat is an optional input file to enter the linear response function of the system. The main program will process this information, calculate a nonlinear response from four separate programs and generate files containing information on the four-wave mixing signals. Due to the architecture of the program, there are two kinds of generated files. One set of files is created every run and the other set of files is appended.

As reviewed in chapter 2, the third-order polarization of a two-level system can be

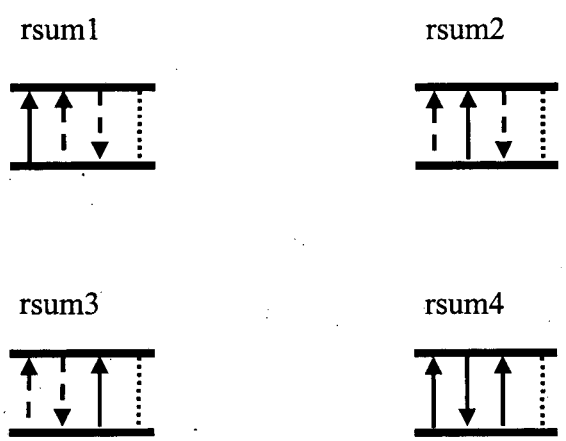


**Figure B-2 Four response functions for the third-order polarization of a two-level system.**

broken down into four nonlinear response functions. The four functions are illustrated in figure B- 2 and their labels correspond to the functions in the program. Time is from left to right in the diagrams. Each field interaction is denoted by an arrow in which a solid (dashed) arrow is a field interaction with the ket (bra). Unless a linear response function

is input through ctin.dat, the linear response function used to calculate the four functions is

$$c(t) = \exp\{s[(\langle n\rangle + 1)(e^{-i\omega t} - 1) + \langle n\rangle(e^{i\omega t} - 1)] + i\omega_e t\},$$

where $s = \frac{\Delta^2}{2}$ ($\Delta$ is the dimensionless origin shift) and $\langle n\rangle = \frac{1}{e^{\beta\hbar\omega} - 1}$. If the linear response function is input through ctin.dat, vibron.dat asks for a rough $T_2$ time for calculation purposes. Below is a data sheet containing information on the input format and the generated output files.

3 February 1998
vibron.dat is the input file for pcvib.cpp and crvib.cpp.
ctin.dat is the input file containing C(t).

**Input format:**

0-0 vertical transition energy ($cm^{-1}$)
inhomogeneous standard deviation ($cm^{-1}$)
number of phonon modes (if no modes, enter 1 and zero for phonon frequency and $\Delta$)

For each mode:
phonon frequency ($cm^{-1}$)
$\Delta$, dimensionless origin shift between potential surfaces

[if C(t) is from a file, enter $-T_2$.]
$T_1$ (fs)
$T_2$ (fs)
Temperature (K)
Number of pulses

For each pulse: (First pulse should have the most delay points)
Pulse type [0: $\delta$-function, 1: Gaussian, 2: $Sech^2$ (default), 3: FT of flattened Gaussian]
Initial delay (fs)
Delay step size (fs)
Number of delay points
Center wavelength (nm)
FWHM (fs) (0 fs for $\delta$-function)

Time step for integration (fs)
Number of diagrams to calculate

For each diagram:
Diagram number (1-4)
$E_3(t''')$ (1-number of pulses)
$E_2(t'')$
$E_1(t')$

**Output files:**

Files created for each program run:

| | |
|---|---|
| efreq.dat | pulse $E(\omega)$ (real & imaginary parts) |
| pls.dat | pulse $E(t)$ (real & imaginary parts) |
| tpls.dat | time points for pls.dat (fs) |
| ct.dat | $C(t)$ (real & imaginary parts) |
| absor.dat | Fourier Transform of $C(t)*g(t)$ (real & imaginary parts) |
| tct.dat | time points for ct.dat and gt.dat (fs) |
| gt.dat | inhomogeneous distribution in time |
| delay.dat | time delay points for p3t.dat |
| p3t.dat | $\lvert P^3(t)\rvert^2$ |

Files appended for each program run:

| | |
|---|---|
| pp?.dat | $P^3(t)*E^*_{pr}(t)$, pump-probe, two pulse only, signal for diagram '?' |
| psum?.dat | $P^3(t)$, 3rd order polarization response in time for diagram '?' and given delay (real & imag parts) |
| tsum?.dat | time points for psum?.dat (fs) |
| pfor?.dat | $P^3(\omega)$, 3rd order polarization in frequency for diagram '?' and given delay (real & imag parts) |

For convenience, a sample input file is included below calculating a three-pulse photon echo signal for a system with no phonon modes.

```
16180
0
1
0
0
100000
100
300
3
2
120
0
1
618
10
2
-20
4
11
618
10
2
0
0
1
618
10
2
8
2
3
```

2
1
3
3
2
1
2
3
1
2
3
3
1
2
1
2
3
1
4
2
3
1
1
1
3
2
4
1
3
2

### *B.2 Compilation using Watcom C/C++*

The programming environment of Watcom C/C++ is in the Integrated Development Environment or IDE. Project files contain the relevant .cpp and .hpp files for each executable file. Watcom has its own editor to write and edit program files. A nice feature of the editor is to view the program files with colors highlighting command words, comments, quotations, etc. at the user's discretion. Watcom has folders of standard library files which the user's program can call upon. The environment is menu driven leading to compiling of the source code at a push of a button. Compilation errors are displayed and linked to the source code.

### *B.3 Compiling on the Cray*

Compiling source code on the Cray is a bit more complicated than in the user friendly environment of Watcom C/C++. The object files of programs which the main program calls are archived in a library file. This library file is called when compiling the main program. The commands for compiling crvib.cpp are shown below.

```
CC -O2 -c csum1.o -lm -l/U2/u10462/complex csum1.cpp
CC -O2 -c csum2.o -lm -l/U2/u10462/complex csum2.cpp
CC -O2 -c csum3.o -lm -l/U2/u10462/complex csum3.cpp
CC -O2 -c csum4.o -lm -l/U2/u10462/complex csum4.cpp
CC -O2 -c yehmath.o -lm yehmath.cpp
ar -r libvib.a complex.o csum1.o csum2.o csum3.o csum4.o yehmath.o
CC -O2 -o vibron -L/U2/u10462 -lm -lvib crvib.cpp
```

#### Vectorization and parallelization of code for the Cray

Calculation of four-wave mixing signals is an enormous computational task. The numerical integration of the four nested time integrals in the third-order polarization converts to four nested **for** loops in the code. For the most part, vectorization and parallelization of loops are handled by the compiler. In addition, there are compiler commands which can specifically multitask and vectorize particular **for** loops. An example is given below. These commands are well documented on the NERSC website.

```
void rsum1(complex *ef[], complex *efc[], complex pt1[], complex ct[], complex cc[],
        complex ci[], complex cic[], double xT1[], double xT2[], int num, double dly1,
        double dly2, int diag[], int lowr, int uppr, int dt, double g[])
{
   int t,t1,t2,t3,xx;
   int p[3], dly[3];
   complex cti, ctc, igl1, igl2, igl3;

   xx=num/2-1;
   for (int i=0; i<3; i++){
      p[i]=diag[i+1]-1;
      dly[i]=0;
      if (p[i]==0)
         dly[i]=dly1;
      if (p[i]==1)
         dly[i]=dly2;
   }
#pragma _CRI parallel private(t,t1,t2,t3,ctc,cti,igl1,igl2,igl3) \
```

```
  shared(lowr,uppr,cc,cic,ct,ci,xT1,xT2,g,ef,efc,dt,xx,p,dly,pt1)
#pragma _CRI taskloop
  for (t=lowr; t<uppr+1; t+=dt){
    for (t1=lowr; t1<t; t1+=dt){
      for (t2=lowr; t2<t1; t2+=dt){
#pragma _CRI ivdep
        for (t3=lowr; t3<t2; t3+=dt){
          ctc=cc[xx+t2-t3]*cc[xx+t-t3]*cic[xx+t1-t3];
        igl1+=xT2[xx+t-t1+t2-t3]*g[xx+t-t1+t2-t3]*ctc*efc[p[0]][t3-dly[0]];
        }
        cti=ct[xx+t1-t2]*ci[xx+t-t2];
        igl2+=xT1[xx+t1-t2]*dt*cti*ef[p[1]][t2-dly[1]]*igl1;
        igl1=complex(0,0);
      }
      igl3+=dt*ct[xx+t-t1]*efc[p[2]][t1-dly[2]]*igl2;
      igl2=complex(0,0);
    }
    pt1[t]=dt*igl3;
    igl3=complex(0,0);
  }
#pragma _CRI endloop
#pragma _CRI endparallel
} // rsum1
```

## Pros and cons of using the Cray

The Cray supercomputers are attractive to use for large computational tasks. However, I have found for complex numbers, the computational power of the Cray is no better than a 233 MHz Pentium computer. The problem stems from the C++ compiler and the complex.h header file for complex numbers. The compiler is unable to vectorize and multitask the nested loops. The computation uses essentially a single processor of the Cray reducing its computational power to a PC.

I submitted a simple test program to NERSC illustrating the problems of the C++ compiler. NERSC determined the problems stemmed from the compiler and forwarded it to Silicon Graphics, the parent company of the Cray. Recently, Silicon Graphics addressed this issue by modifying the Cray C++ complex.h header file. The test program and results are given below along with the modifications to the header file.

```
 // time.cpp
 // compare speed of PC vs. Cray with complex numbers

#ifdef NEW_COMPLEX       // added by geir
 #include "complex.h"    // added by geir
#else                    // added by geir
 #include <complex.h>
#endif                   // added by geir
 #include <math.h>
 #include <iostream.h>
 #include <stdlib.h>

 main()
 {
     const int limit=600;
     complex t1,t2,ans1,ans2;

     for (int i=0; i<limit; i++){
         for (int j=0; j<limit; j++){
             for (int k=1; k<limit; k++){
                 t1=(i,k); //complex.h
                 t2=(j,k); //complex.h
 //                ans1=t1*t2;
                 ans2=t1/t2;
             }
         }
     }
     cout << "\nAll done!" << endl;

     return EXIT_SUCCESS;
 }
```

```
$ CC time.cpp; timex ./a.out

All done!

        seconds          "clocks"
real    200.935012       (88411405189)
user    199.052416       (87583063252)
sys     1.265003         (556601307)
```

For $2*10^8$ iterations, the Cray took 200 seconds which was slightly longer than the time it took for a 233 MHz PC to perform the same number of iterations. The individual processors of the Cray are rated at a lower speed than the PC indicating the Cray only took advantage of a single processor.

Below are the modifications to the complex.h header file made by Silicon Graphics and the performance of the program run with this header file.

```
$ diff /opt/ctl/CC/CC/include/complex.h complex.h
230c230
<       const double s1 = (a1.re + a1.im)*(a2.re + a2.im);
---
>       //const double s1 = (a1.re + a1.im)*(a2.re + a2.im);
233c233,246
<       return complex(s2 - s3, s1 - s2 - s3);
---
>       const double s4 = a1.re * a2.im;
>       const double s5 = a1.im * a2.re;
>       //return complex(s2 - s3, s1 - s2 - s3);
>       return complex(s2 - s3, s4 + s5);
> }
>
> inline complex operator/(complex a1, complex a2)
> {
>       const double s1 = (a2.re * a2.re) + (a2.im * a2.im);
>       const double s2 = a1.re * a2.re;
>       const double s3 = a1.im * a2.im;
>       const double s4 = a1.im * a2.re;
>       const double s5 = a1.re * a2.im;
>       return complex((s2 + s3)/s1, (s4 - s5)/s1) ;
```

```
$ CC -DNEW_COMPLEX time.cpp; timex ./a.out

All done!

        seconds         "clocks"
real    0.067288        (29606701)
user    0.000368        (162138)
sys     0.003024        (1330700)
```

The improvement in performance is dramatic. Unfortunately, calculations using vibron.cpp with these modifications have not been tested. A request for time on the supercomputers needs to be submitted.

### *B.4 Compiling on Silicon Graphics workstation*

Compilation of source code on the Silicon Graphics workstation is similar to compiling on the Cray in that the programs the main program calls need to be compiled first into library files. These commands are given below.

```
CC -O2 -o libpcsum1.so -shared pcsum1.cpp
CC -O2 -o libpcsum2.so -shared pcsum2.cpp
CC -O2 -o libpcsum3.so -shared pcsum3.cpp
CC -O2 -o libpcsum4.so -shared pcsum4.cpp
CC -O2 -o libyehmath.so -shared yehmath.cpp
```

The compilation of the source code can then be done with one command statement. This is shown below.

```
CC -O2 -o vibron pcvib.cpp -L/home/bigal -L/home/bigal -L/home/bigal \
-L/home/bigal -L/home/bigal -rpath /home/bigal -rpath /home/bigal -rpath \
/home/bigal -rpath /home/bigal -rpath /home/bigal -lpcsum1 -lpcsum2 -lpcsum3 \
-lpcsum4 -lyehmath -lm -lcomplex
```

The Silicon Graphics workstation performs approximately 10 times faster than the PC.

### *B.5 Recommended additional features*

The current version of vibron.cpp is not able to use an experimental pulse and spectrum. The addition of this feature would probably be most easily accomplished through the getpls() function of the main program.

If there is further interest to use the Cray for these computations, further multitasking of the calculation is possible. The main program calls four programs to calculate the four nonlinear response functions. There is no reason why these calls cannot be done simultaneously. Incorporation of this into the main program may be complicated by the use of some common variables. However, this should not be too difficult to rectify and the rewards in performance could be well worth the trouble.

### *B.6 Vibron.cpp*

Below are the header files called by the main program.

```
// csum1.hpp
// function declarations to calculate one term (R1) of P3(t) in
// linear dipole response approximation.

#ifndef csum1_hpp
#define csum1_hpp
#include <complex.h>
//#include "complex.hpp"

int cfour(complex [], complex [], int, int, int, int, int);
void p3sum1(complex *[], complex *[], complex [], complex [], complex [], complex [],
```

```
        double [], double [], double [], int, double *[], int [], double [], int, int,
        int, int [], double [], complex *[]);
void rsum1(complex *[], complex *[], complex [], complex [], complex [], complex [],
        complex [], double [], double [], int, double, double, int [], int, int, int,
        double []);
void r1delta(complex *[], complex [], complex [], complex [], complex [], double [],
         double [], int, double [], int, int [], int, int, int, int, double []);

#endif


// csum2.hpp
// function declarations to calculate one term (R2) of P3(t) in
// linear dipole response approximation.

#ifndef csum2_hpp
#define csum2_hpp
#include <complex.h>
//#include "complex.hpp"

int cfour(complex [], complex [], int, int, int, int, int);
void p3sum2(complex *[], complex *[], complex [], complex [], complex [], complex [],
        double [], double [], double [], int, double *[], int [], double [], int, int,
        int, int [], double [], complex *[]);
void rsum2(complex *[], complex *[], complex [], complex [], complex [], complex [],
        complex [], double [], double [], int, double, double, int [], int, int, int,
        double []);
void r2delta(complex *[], complex [], complex[], complex [], complex [], double [],
         double [], int, double [], int, int [], int, int, int, int, double []);

#endif


// csum3.hpp
// function declarations to calculate one term (R3) of P3(t) in
// linear dipole response approximation.

#ifndef csum3_hpp
#define csum3_hpp
#include <complex.h>
//#include "complex.hpp"

int cfour(complex [], complex [], int, int, int, int, int);
void p3sum3(complex *[], complex *[], complex [], complex [], complex [], double [],
        double [], double [], int, double *[], int [], double [], int, int, int,
        int [], double [], complex *[]);
void rsum3(complex *[], complex *[], complex [], complex [], complex [], complex [],
        double [], double [], int, double, double, int [], int, int, int, double []);
void r3delta(complex *[], complex [], complex [], complex [], double [], double [], int,
         double [], int, int [], int, int, int, int, double []);

#endif


// csum4.hpp
```

```
// function declarations to calculate one term (R4) of P3(t) in
// linear dipole response approximation.

#ifndef csum4_hpp
#define csum4_hpp
#include <complex.h>
//#include "complex.hpp"

int cfour(complex [], complex [], int, int, int, int, int);
void p3sum4(complex *[], complex *[], complex [], complex [], double [], double [],
        double [], int, double *[], int [], double [], int, int, int, int [],
        double [], complex *[]);
void rsum4(complex *[], complex *[], complex [], complex [], complex [], double [],
       double [], int, double, double, int [], int, int, int, double []);
void r4delta(complex *[], complex [], complex [], double [], double [], int, double [], int,
        int [], int, int, int, int, double []);

#endif


// some important mathematical functions
// functions in yehmath.cpp

#ifndef yehmath_hpp
#define yehmath_hpp

//fourier transform double[] (real[1],imag[2],real[3],imag[4],etc.)
//return transform in double[]
void fcfour(double [], unsigned long, int);
void swblock(double [], int);

#endif


// yehmath.cpp
// important math functions
#include "yehmath.hpp"
#include <math.h>


//*******************************************************
//fourier transform double[] (real[1],imag[2],real[3],imag[4],etc.)
//return transform in double[]
//nn  number of real or imaginary numbers; not number of elements

#define SWAP(a,b) tempr=(a); (a)=(b); (b)=tempr
void fcfour(double data[], unsigned long nn, int isign)
{
      unsigned long n,mmax,m,j,istep,i;
      double wtemp,wr,wpr,wpi,wi,theta;
      double tempr,tempi;

      n=nn << 1;
      j=1;
      for (i=1;i<n;i+=2) {
```

```
        if (j > i) {
           SWAP(data[j],data[i]);
           SWAP(data[j+1],data[i+1]);
        }

        m=n >> 1;

        while (m >= 2 && j > m) {
           j -= m;
           m >>= 1;
        }
        j += m;
     }

     mmax=2;
     while (n > mmax) {
        istep=mmax << 1;
        theta=isign*(6.28318530717959/mmax);
        wtemp=sin(0.5*theta);
        wpr = -2.0*wtemp*wtemp;
        wpi=sin(theta);
        wr=1.0;
        wi=0.0;
        for (m=1;m<mmax;m+=2) {
           for (i=m;i<=n;i+=istep) {
              j=i+mmax;
              tempr=wr*(data[j])-wi*(data[j+1]);
              tempi=wr*(data[j+1])+wi*(data[j]);
              data[j]=data[i]-tempr;
              data[j+1]=data[i+1]-tempi;
              data[i] += tempr;
              data[i+1] += tempi;
           }
           wr=(wtemp=wr)*wpr-wi*wpi+wr;
           wi=wi*wpr+wtemp*wpi+wi;
        }
        mmax=istep;
     }
} // fcfour
#undef SWAP

void swblock(double data[], int ndat)
{
   double *temp=new double[ndat];

   for (int j=0; j<ndat/2; j++){
      temp[j]=data[j+ndat/2];
      temp[j+ndat/2]=data[j];
   }
   for (j=0; j<ndat; j++)
      data[j]=temp[j];

   delete [] temp;
} // swblock
```

```
// pcvib.cpp
// Calculates transient absorption spectra for two harmonic potentials in the
// perturbative limit.
#include "csum1.hpp"
#include "csum2.hpp"
#include "csum3.hpp"
#include "csum4.hpp"
#include "yehmath.hpp"

#include <assert.h>
#include <complex.h>
#include <fstream.h>
#include <iostream.h>
#include <math.h>
#include <stdlib.h>

#define kcm 0.695029    // boltzmann (cm*K)-1
#define pi 3.14159265358979
#define cmfs 2.99792458e-5      // speed of light (cm/fs)
#define hbar 5308.837458876     // (cm-1*fs)
#define NDEBUG

void taxis(double [], int, double, double);        // creates array (#pts, begin, end)
void inhomo(double [], double [], int, double);    // inhomogeneous distribution
void daxis(double [], int, int, int);
void getdamp(double [], double [], double [], int, int);  // damping functions
void getct(complex [], double [], int, double, double, int);      // (ct, t, pts)
complex cterm(double, double, complex, complex, complex); // called by getct
void getpls(complex [], double [], int, double, double, int);      // creates pulse
int cfour(complex [], complex [], int, int, int, int, int);
void getabs(complex [], complex [], double [], double [], int, int);      // absorption spectrum

int dt;
double wvert,   // vertical transition (0-0) energy (cm-1)
    T1, T2,
    ufact=4,
    Temp;   // Temperature (K)

//**************Declarations and input from file***************************
main()
{
   const int tsize=4096,       // number of time points in integration
          tfn=tsize/2, tin=tfn-(tsize-1),   // limits of integration (fs)
          cntr=-tin*(tsize-1)/(tfn-tin);
   int npls,   // number of pulses
      nmode,  // number of phonon modes
      ndia,   // number of diagrams
      diag,   // diagrams number
      limit, ul, ll,
      ppt, ipt, fpt=1, ifpt,
      ctn=100;        // test variable for c(t) input file

   double e00, sigma, floor=0, top=0;
   double *time=new double[tsize],
       *gt=new double[tsize], // inhomogeneous broadening
       *xT1=new double[tsize],// population decay
```

```
        *xT2=new double[tsize];// dephasing
    complex p3;
    complex *ct=new complex[tsize],     // linear dipole response (ldr) function
          *cc=new complex[tsize],     // complex conjugate of c(t)
          *ci=new complex[tsize],     // inverse of c(t)
          *cic=new complex[tsize],    // complex conjugate of inverse of c(t)
          *spec=new complex[tsize];   // absorption spectrum  fft of c(t)*g(t)*xT2(t)

    ifstream wrtin ("vibron.dat", ios::in);
    if (!wrtin)
       cerr << "vibron.dat could not be opened" << endl;

    wrtin >> wvert >> sigma >> nmode;

    double *phw=new double[nmode],        // phonon frequency
        *delta=new double[nmode];      // displacement

    for (int i=0; i<nmode; i++)
       wrtin >> phw[i] >> delta[i];
    wrtin >> T1 >> T2 >> Temp >> npls;
    if (T2 < 0){
       ctn=1;
       T2=-1*T2;
    }

    int *shp=new int[npls],     // pulse shape
       *din=new int[npls],     // initial delay (fs)
       *dydt=new int[npls],    // delay time step (fs)
       *dpt=new int[npls];     // # of delay points
    double *lam=new double[npls], *fwhm=new double[npls];

    for (i=0; i<npls; i++)
       wrtin >> shp[i] >> din[i] >> dydt[i] >> dpt[i] >> lam[i] >> fwhm[i];
    wrtin >> dt >> ndia;

    int **dia=new int*[ndia];   // response funct. & E field order
    for (i=0; i<ndia; i++)
       dia[i]=new int[4];

    for (i=0; i<ndia; i++){
       for (int j=0; j<4; j++)
          wrtin >> dia[i][j]; // diagram # then 3 fields
    }
    wrtin.close();

    e00=0.0;
    for (i=0; i<nmode; i++)
       e00+=0.5*delta[i]*delta[i]*phw[i];
    for (i=0; i<npls; i++)      // set lam as detuning
       lam[i]=cmfs*(1/(lam[i]*1e-7)-(wvert+e00));
    wvert=0.0;
//   wvert+=e00;

    double **dly=new double*[npls];       // time and delay axis
    complex **ep=new complex*[npls],    // pulse fields
          **epc=new complex*[npls],   // complex conjugate of pulse fields
```

```
        **ew=new complex*[npls];    // pulse spectrum

    for (i=0; i<npls; i++){
        dly[i]=new double[dpt[i]];
        ep[i]=new complex[tsize];
        epc[i]=new complex[tsize];
        ew[i]=new complex[tsize];
    }

//**************Prepare variables*********************************************
    taxis(time, tsize, tin, tfn);       // time axis
    inhomo(gt,time,tsize,sigma);

    ofstream wrtpls ("pls.dat", ios::out);
    ofstream wrtts2 ("tpls.dat", ios::out);
    wrtpls << npls << "\t 0" << endl;
    wrtts2 << npls << endl;
    for (i=0; i<npls; i++){
        daxis(dly[i], dpt[i], din[i], dydt[i]); // pulse delays
        getpls(ep[i], time, tsize, fwhm[i], lam[i], shp[i]);    // get pulses
        for (int k=0; k<tsize; k++)
            epc[i][k]=conj(ep[i][k]);   // complex conjugate of pulse
        ppt=6*fwhm[i]/dt+1;
        ipt=(-1*(ppt-1)*dt/2-tin)*(tsize-1)/(tfn-tin);
        wrtpls << ppt << "\t 0" << endl;
        wrtts2 << ppt << "\n" << time[ipt] << "\n" << dt << endl;
        for (int j=0; j<ppt; j++)
            wrtpls << real(ep[i][ipt+j*dt]) << "\t"
                << imag(ep[i][ipt+j*dt]) << endl;
        if (floor > (dly[i][0]-(2*fwhm[i]))){
            floor=dly[i][0];
            while (floor > dly[i][0]-2*fwhm[i])
                floor-=dt;
        }
        if (top < dly[i][dpt[i]-1])
            top=dly[i][dpt[i]-1];
    }
    wrtpls.close();
    wrtts2.close();
    delete [] din;
    delete [] dydt;
    delete [] lam;

    limit=top+T2*ufact;
    if (limit < tfn){
        ul=double((limit-tin)*(tsize-1)/(tfn-tin));
        ll=double((floor-tin)*(tsize-1)/(tfn-tin));
        ifpt=(ul-ll)/dt+1;
    }
    else{
        cout << "time axis not large enough for numeric integration"
            << endl;
        exit(0);
    }
    ofstream wrtews ("efreq.dat", ios::out);
    wrtews << npls << "\t 0" << endl;
```

```
    for (i=0; i<npls; i++){
        ppt=6*fwhm[i]/dt+1;
        ipt=(-1*(ppt-1)*dt/2-tin)*(tsize-1)/(tfn-tin);  // initial pt for fft (pt/fs)
        fpt=cfour(ew[i], ep[i], ppt, ipt, dt, ifpt, cntr);
        wrtews << fpt << "\t 0" << endl;
        for (int j=0; j<fpt; j++)
            wrtews << real(ew[i][j]) << "\t" << imag(ew[i][j]) << endl;
    }
    wrtews.close();
    delete [] ew;

    ofstream wrtfrq ("wpls.dat", ios::out);
    wrtfrq << "1" << "\n" << fpt << "\n" << -1/(2*dt*cmfs) << "\n" << 1/(fpt*dt*cmfs) << endl;
    wrtfrq.close();

    for (i=0; i<tsize; i++)
        ct[i]=complex(1.0,0.0);
    for (i=0; i<nmode; i++)
        getct(ct, time, tsize, phw[i], delta[i], ctn);
    delete [] phw;
    delete [] delta;

    getdamp(xT1,xT2,time,tsize,ctn);
    getabs(spec,ct,xT2,gt,tsize,cntr);

    ofstream wrtct ("ct.dat", ios::out);
    ofstream tout ("tct.dat", ios::out);
    ofstream wrtgt ("gt.dat", ios::out);
    ofstream wrtabs ("absor.dat", ios::out);
    for (int s=0; s<tsize; s++){
        wrtct << real(ct[s]) << "\t" << imag(ct[s]) << endl;
        cc[s]=conj(ct[s]);
        ci[s]=1/ct[s];
        cic[s]=conj(ci[s]);
        tout << time[s] << endl;
        wrtgt << gt[s] << endl;
        wrtabs << real(spec[s]) << "\t" << imag(spec[s]) << endl;
    }
    wrtct.close();
    tout.close();
    wrtgt.close();
    wrtabs.close();
    delete [] spec;
    ofstream wrtwab ("wabs.dat", ios::out);
    wrtwab << "1" << "\n" << tsize << "\n" << -1/(2*cmfs) << "\n"
          << 1/(tsize*cmfs) << endl;
    wrtwab.close();

//**************Begin Calculation*************************************
    ofstream dout ("delay.dat", ios::out);
    for (i=0; i<npls; i++){
        for (int j=0; j<dpt[i]; j++)
            dout << dly[i][j] << "\t";
        dout << endl;
    }
    int inum=1;
```

```
for (i=0; i<npls; i++)
   inum*=dpt[i];
complex **P3t=new complex*[inum];
for (i=0; i<inum; i++)
   P3t[i]=new complex[tsize];

for (i=0; i<ndia; i++){
   diag=dia[i][0];

   switch (diag){
      case 1:
         p3sum1(ep,epc,ct,cc,ci,cic,time,xT1,xT2,tsize,dly,dpt,fwhm,npls,
             ll,ul,dia[i],gt,P3t);
         cout << "psum1" << endl;
      break;

      case 2:
         p3sum2(ep,epc,ct,cc,ci,cic,time,xT1,xT2,tsize,dly,dpt,fwhm,npls,
             ll,ul,dia[i],gt,P3t);
         cout << "psum2" << endl;
      break;

      case 3:
         p3sum3(ep,epc,ct,cc,ci,time,xT1,xT2,tsize,dly,dpt,fwhm,npls,ll,ul,
             dia[i],gt,P3t);
         cout << "psum3" << endl;
      break;

      case 4:
         p3sum4(ep,epc,cc,cic,time,xT1,xT2,tsize,dly,dpt,fwhm,npls,ll,ul,
             dia[i],gt,P3t);
         cout << "psum4" << endl;
      break;

      default:
         cout << "invalid diagram for # " << i+1 << "\n"
             << "term not calculated" << "\n"
             << "check input file 'vibron.dat'" << endl;
         exit(0);
      break;
   }
}
ofstream wrtp3t("p3t.dat", ios::out);
for (i=0; i<inum; i++){
   p3=complex(0,0);
   for (int j=0; j<tsize; j++)
      p3+=P3t[i][j]*conj(P3t[i][j]);
   p3*=dt;
   wrtp3t << real(p3) << "\t" << imag(p3) << endl;
}
delete [] time;
delete [] dpt;
delete [] xT1;
delete [] xT2;
delete [] fwhm;
delete [] dia;
```

```
    delete [] dly;
    delete [] ct;
    delete [] cc;
    delete [] ci;
    delete [] cic;
    delete [] ep;
    delete [] epc;
    delete [] P3t;
    return EXIT_SUCCESS;
} // main

//**************Functions*****************************************
// Creates time axis for integration.
void taxis(double tm[], int num, double beg, double fin)
{
    if (num > 1){
        for (int i=0; i<num; i++)
            tm[i]=beg+i*(fin-beg)/(num-1);
    }
    else
        tm[0]=beg;
} // taxis

void inhomo(double g[], double t[], int pts, double sig)
{
    double sigma=sig/hbar;

    sigma=pow(sigma/2,2.0);
    if (sig==0){
        for (int i=0; i<pts; i++)
            g[i]=1.0;
    }
    else{
        for (int i=0; i<pts; i++)
            g[i]=exp(-pow(t[i],2.0)*sigma);
    }
} // inhomo

void daxis(double dlay[], int num, int d0, int dyt)
{
    for (int i=0; i<num; i++)
        dlay[i]=d0 + i*dyt;
} // daxis

void getdamp(double x1[], double x2[], double t[], int num, int tst)
{
    int i=0;

    switch (tst){
        case 1:
            for (i=0; i<num; i++){
                x1[i]=1;
                x2[i]=1;
            }
        break;
```

```
        default:
            while (t[i]<0){
                x1[i]=0;
                x2[i]=0;
                i++;
            }
            while (i<num){
                x1[i]=exp(-t[i]/T1);
                x2[i]=exp(-t[i]/T2);
                i++;
            }
        break;
    }
} // getdamp

void getct(complex cf[], double t[], int pts, double phw, double delta, int test)
{
    int i, j;
    double n, beta, s=delta*delta/2.0;
    complex phn, php, exc;

    ifstream wrtm("ctin.dat", ios::in);
    switch (test){
        case 1:
            if (!wrtm)
                cerr << "ctin.dat could not be opened!" << endl;
            i=pts/2-1;
            for (j=0; j<i; j++)
                cf[j]=complex(0.0,0.0);
            while (i<pts){
                wrtm >> n >> beta;
                cf[i]*=complex(n,beta);
                i++;
            }
            if (Temp == 0 || phw == 0 || phw/(Temp*kcm) > 709)
                n=0;
            else{
                beta=1.0/(Temp*kcm);
                n=1.0/(exp(beta*phw)-1.0);
            }
            for (i=0; i<pts; i++){
                phn=exp(complex(0,-2*pi*phw*cmfs*t[i]));
                php=exp(complex(0,2*pi*phw*cmfs*t[i]));
                exc=complex(0,2*pi*wvert*cmfs*t[i]);
                cf[i]*=cterm(s, n, phn, php, exc);
            }
        break;

        default:
            if (Temp == 0 || phw == 0 || phw/(Temp*kcm) > 709)
                n=0;
            else{
                beta=1.0/(Temp*kcm);
                n=1.0/(exp(beta*phw)-1.0);
            }
            for (i=0; i<pts; i++){
```

```
            phn=exp(complex(0,-2*pi*phw*cmfs*t[i]));
            php=exp(complex(0,2*pi*phw*cmfs*t[i]));
            exc=complex(0,2*pi*wvert*cmfs*t[i]);
            cf[i]*=cterm(s, n, phn, php, exc);
         }
      break;
   }
   wrtm.close();
} // getct

complex cterm(double s, double n, complex phn, complex php, complex exc)
{
   complex ct;

   ct=exp(s*((n+1.0)*(phn-1.0) + n*(php-1.0)) + exc);

   return ct;
} // cterm

void getpls(complex e[], double t[], int pts, double fw, double wc, int shape)
{
   int count=0;
   double env, sig, norm, test;
   complex ef;

   switch (shape){
      case 0:  // delta function
         count=pts/2-1;
         ef=exp(complex(0,-2*pi*wc*t[count]));
         env=1.0;
         e[count]=env*ef;
      break;

      case 1:  // gauss
         sig=fw/(2*sqrt(log(2)));
         norm=100/(sig*sqrt(pi));
         for (count=0; count<pts; count++){
            ef=exp(complex(0,-2*pi*wc*t[count]));
            env=exp(-1*pow(t[count]/sig,2.0));
            e[count]=norm*env*ef;
         }
      break;

      default:  // sech
         sig=fw/(2*1.316958);
         norm=200/(pi*sig);
         test=fabs(t[0]/sig);
         while (test>709 && count+1<pts){
            count++;
            test=fabs(t[count]/sig);
         }
         while (test<=709 && count+1<pts){
            ef=exp(complex(0,-2*pi*wc*t[count]));
            env=1.0/(exp(t[count]/sig)+exp(-t[count]/sig));
            e[count]=norm*env*ef;
            count++;
```

```
            test=fabs(t[count]/sig);
         }
         while (test>709 && count+1<pts){
            count++;
            test=fabs(t[count]/sig);
         }
      break;

      case 3:  // flattened gauss
         sig=fw/(2*1.244240);
         norm=50/(4*pow(sig,3.0)*sqrt(pi));
         for (count=0; count<pts; count++){
            ef=exp(complex(0,-2*pi*wc*t[count]));
            env=(6*sig*sig-pow(t[count],2.0))*exp(-pow(t[count]/(2*sig),2.0));
            e[count]=norm*env*ef;
         }
      break;

      case 4:  // sech2
         sig=fw/(2*0.884792);
         norm=200/sig;
         test=fabs(t[0]/sig);
         while (test>709 && count+1<pts){
            count++;
            test=fabs(t[count]/sig);
         }
         while (test<=709 && count+1<pts){
            ef=exp(complex(0,-2*pi*wc*t[count]));
            env=pow(exp(t[count]/sig)+exp(-t[count]/sig),-2.0);
            e[count]=norm*env*ef;
            count++;
            test=fabs(t[count]/sig);
         }
         while (test>709 && count+1<pts){
            count++;
            test=fabs(t[count]/sig);
         }
      break;
   }
   return;
} // getpls

int cfour(complex ft[], complex dat[], int pts, int lw, int dt, int tpt, int ctr)
{
   int max, num=1, lft=pts;
   double rmax;
   complex *fdat=new complex[pts];

   for (int i=0; i<pts; i++)
      fdat[i]=dat[lw+i*dt];

   if (lft < 512)
      lft=512;
   if (tpt > lft)
      lft=tpt;
   while (num<lft)
```

```
      num*=2;
   complex *dft=new complex[num];
   max=(ctr-lw)/dt;
   rmax=fmod(ctr-lw,dt);
   if (rmax != 0)
      max++;
   for (i=0; i<pts-max; i++)
      dft[i]=fdat[max+i];
   for (i=0; i<max; i++)
      dft[i+num-max]=fdat[i];

   max=2*num+1;
   double *sub = new double[max];

   sub[0]=0;

   for (i=0; i<num; i++){
      sub[2*i+1]=real(dft[i]);
      sub[2*i+2]=imag(dft[i]);
   }
   delete [] dft;

   fcfour(sub, num, -1);

   for (i=0; i<num; i++)
      ft[i]=complex(sub[2*i+1], sub[2*i+2]);

   delete [] sub;
   return num;
} // cfour

void getabs(complex abs[], complex ct[], double T2[], double gt[], int pts, int cnr)
{
   int fpt, limit=pts/2-1;
   double *damp=new double[pts];
   complex *c=new complex[pts];

   for (int i=0; i<limit; i++){
      damp[i]=T2[pts-1-i];
      damp[i+limit]=T2[i+limit];
   }
   for (i=0; i<pts; i++)
      c[i]=damp[i]*gt[i]*ct[i];
   //    c[i]=T2[i]*gt[i]*ct[i];
   fpt=cfour(abs,c,pts,0,1,0,cnr);

   delete [] damp;
   delete [] c;
   return;
} // getabs
```

```
// pcsum1.cpp
// functions to calculate one term (R1) of P3(t) in
// linear dipole response approximation.

#include "csum1.hpp"
#include "yehmath.hpp"

#include <complex.h>
#include <fstream.h>
#include <iostream.h>
#include <iomanip.h>
#include <math.h>
#include <stdlib.h>

#define kcm 0.695029    // boltzmann (cm*K)-1
#define pi 3.14159265358979
#define cmfs 2.99792458e-5      // speed of light (cm/fs)

void p3sum1(complex *ei[], complex *ec[], complex ldr[], complex ldrc[], complex ldri[],
        complex ldric[], double t[], double dT1[], double dT2[], int num, double *dlay[],
        int dpts[], double ewide[], int nplses, int low, int upp, int dgmn[],
        double gbrd[], complex *P3t[])
{
   extern int dt;
   extern double T2, ufact;
   int i,j,k,top,butt,npt,ind,dpt1=dpts[0],dpt2,pick=nplses,fpt,mpt,cft;
   double remain, test=0, dy1=0, dy2=0, hgh, lw;
   complex pp, pconj;
   complex **Pt=new complex*[dpt1],    // P3(t)
         **Pf=new complex*[dpt1];    // P3(w)
   for (i=0; i<dpt1; i++){
      Pt[i]=new complex[num];
      Pf[i]=new complex[num];
   }

   for (i=0; i<nplses; i++)
         test+=ewide[i];
   if (test==0){
      if (nplses==2)
         pick=101;
      else
         pick=102;
   }

   top=upp;
   butt=low;
   mpt=(top-butt)/dt+1;

   ofstream wrtp1("psum1.dat", ios::app);
   ofstream wrtt1("tsum1.dat", ios::app);
   ofstream wrtpf1("pfor1.dat", ios::app);
   ofstream wrtpp1("pp1.dat", ios::app);
   switch (pick){
      case 2:
         wrtp1 << dpt1 << "\t 0" << endl;
```

```
    wrtt1 << dpt1 << endl;
    wrtpf1 << dpt1 << "\t 0" << endl;
    for (i=0; i<dpt1; i++){
        if (dlay[0][i] > 0){
            upp=double((dlay[0][i]+T2*ufact-t[0])*(num-1)/(t[num-1]-t[0]));
            low=double((-2*ewide[1]-t[0])*(num-1)/(t[num-1]-t[0]));
            if ((dlay[0][i]-2*ewide[0]) < (-2*ewide[1]))
                low=double((dlay[0][i]-2*ewide[0]-t[0])*(num-1)/(t[num-1]-t[0]));
        }
        else{
            upp=double((T2*ufact-t[0])*(num-1)/(t[num-1]-t[0]));
            low=double((dlay[0][i]-2*ewide[0]-t[0])*(num-1)/(t[num-1]-t[0]));
            if ((dlay[0][i]-2*ewide[0]) > (-2*ewide[1]))
                low=double((-2*ewide[1]-t[0])*(num-1)/(t[num-1]-t[0]));
        }
        dy1=dlay[0][i];
        cft=(dy1-t[0])*(num-1)/(t[num-1]-t[0]);
        ind=dy1;
        remain=fmod(upp-low,dt);
        while (remain != 0){
            upp++;
            remain=fmod(upp-low,dt);
        }
        npt=(upp-low)/dt + 1;
        wrtt1 << npt << "\n" << t[low] << "\n" << dt << endl;
        rsum1(ei,ec,Pt[i],ldr,ldrc,ldri,ldric,dT1,dT2,num,dy1,dy2,dgmn,low,upp,dt,
            gbrd);
        fpt=cfour(Pf[i],Pt[i],npt,low,dt,mpt,cft);
        wrtp1 << npt << "\t 0 " << endl;
        wrtpf1 << fpt << "\t 0 " << endl;
        for (j=0; j<npt; j++){
            wrtp1 << real(Pt[i][low+j*dt]) << "\t"
                << imag(Pt[i][low+j*dt]) << endl;
            wrtpf1 << real(Pf[i][j]) << "\t"
                << imag(Pf[i][j]) << endl;
            P3t[i][low+j*dt]+=Pt[i][low+j*dt];
            pconj=conj(ei[0][low+j*dt-ind]);
            pp+=Pt[i][low+j*dt]*pconj;
        }
        wrtpp1 << real(pp) << "\t" << imag(pp) << endl;
        pp=complex(0,0);
        while (j<fpt){
            wrtpf1 << real(Pf[i][j]) << "\t"
                << imag(Pf[i][j]) << endl;
            j++;
        }
    }
break;

case 3:
    dpt2=dpts[1];
    wrtp1 << dpt1*dpt2 << "\t 0" << endl;
    wrtt1 << dpt1*dpt2 << endl;
    wrtpf1 << dpt1*dpt2 << "\t 0" << endl;
    for (i=0; i<dpt2; i++){
        ind=i*dpt1;
```

```
        dy2=dlay[1][i];
        hgh=T2*ufact;
        lw=-2*ewide[2];
        if (dy2+T2*ufact > hgh)
           hgh=dy2+T2*ufact;
        else if (dy2-2*ewide[1] < lw)
           lw=dy2 - 2*ewide[1];
        for (j=0; j<dpt1; j++){
           dy1=dlay[0][j];
           cft=(dy1-t[0])*(num-1)/(t[num-1]-t[0]);
           if (dy1+T2*ufact > hgh)
              hgh=dy1+T2*ufact;
           else if (dy1-2*ewide[0] < lw)
              lw=dy1 - 2*ewide[0];
           upp=double((hgh-t[0])*(num-1)/(t[num-1]-t[0]));
           low=double((lw-t[0])*(num-1)/(t[num-1]-t[0]));
           remain=fmod(upp-low,dt);
           while(remain != 0){
              upp++;
              remain=fmod(upp-low,dt);
           }
           npt=(upp-low)/dt + 1;
           wrtt1 << npt << "\n" << t[low] << "\n" << dt << endl;
           rsum1(ei,ec,Pt[j],ldr,ldrc,ldri,ldric,dT1,dT2,num,dy1,dy2,dgmn,low,upp,dt,
              gbrd);
           fpt=cfour(Pf[j],Pt[j],npt,low,dt,mpt,cft);
           wrtp1 << npt << endl;
           wrtpf1 << fpt << endl;
           for (k=0; k<npt; k++){
              wrtp1 << real(Pt[j][low+k*dt]) << "\t"
                   << imag(Pt[j][low+k*dt]) << endl;
              wrtpf1 << real(Pf[j][k]) << "\t"
                   << imag(Pf[j][k]) << endl;
              P3t[ind+j][low+k*dt]+=Pt[j][low+k*dt];
           }
           while (k<fpt){
              wrtpf1 << real(Pf[j][k]) << "\t"
                   << imag(Pf[j][k]) << endl;
              k++;
           }
        }
     }
break;

case 101:
   dy1=dlay[1][0];
   wrtt1 << "1" << endl;
   r1delta(Pt,ldr,ldrc,ldri,ldric,dT1,dT2,num,dlay[0],dpt1,dgmn,dy1,butt,top,dt,gbrd);
   npt=(top-butt)/dt+1;
   wrtt1 << npt << "\n" << t[butt] << "\n" << dt << endl;
   wrtp1 << dpt1 << "\t 0" << endl;
   wrtpf1 << dpt1 << "\t 0" << endl;
   for (i=0; i<dpt1; i++){
      cft=(dlay[0][i]-t[0])*(num-1)/(t[num-1]-t[0]);
      ind=num/2-1+dlay[0][i];
      pp=Pt[i][ind];
```

```
        wrtpp1 << real(pp) << "\t" << imag(pp) << endl;
        fpt=cfour(Pf[i],Pt[i],npt,butt,dt,mpt,cft);
        wrtp1 << npt << "\t 0" << endl;
        wrtpf1 << fpt << "\t 0" << endl;
        for (j=0; j<npt; j++){
           wrtp1 << real(Pt[i][butt+j*dt]) << "\t"
                << imag(Pt[i][butt+j*dt]) << endl;
           wrtpf1 << real(Pf[i][j]) << "\t"
                << imag(Pf[i][j]) << endl;
           P3t[i][butt+j*dt]+=Pt[i][butt+j*dt];
        }
        while (j<fpt){
           wrtpf1 << real(Pf[i][j]) << "\t"
                << imag(Pf[i][j]) << endl;
           j++;
        }
     }
  break;

  case 102:
     dpt2=dpts[1];
     wrtt1 << "1" << endl;
     npt=(top-butt)/dt+1;
     wrtt1 << npt << "\n" << t[butt] << "\n" << dt << endl;
     wrtp1 << dpt1*dpt2 << "\t 0" << endl;
     wrtpf1 << dpt1*dpt2 << "\t 0" << endl;
     for (i=0; i<dpt2; i++){
        ind=i*dpt1;
        dy1=dlay[1][i];
        r1delta(Pt,ldr,ldrc,ldri,ldric,dT1,dT2,num,dlay[0],dpt1,dgmn,dy1,butt,top,dt,
             gbrd);
        for (j=0; j<dpt1; j++){
           cft=(dlay[0][j]-t[0])*(num-1)/(t[num-1]-t[0]);
           fpt=cfour(Pf[j],Pt[j],npt,butt,dt,mpt,cft);
           wrtp1 << npt << "\t 0" << endl;
           wrtpf1 << fpt << "\t 0" << endl;
           for (k=0; k<npt; k++){
              wrtp1 << real(Pt[j][butt+k*dt]) << "\t"
                   << imag(Pt[j][butt+k*dt]) << endl;
              wrtpf1 << real(Pf[j][k]) << "\t"
                   << imag(Pf[j][k]) << endl;
              P3t[ind+j][butt+k*dt]+=Pt[j][butt+k*dt];
           }
           while (k<fpt){
              wrtpf1 << real(Pf[j][k]) << "\t"
                   << imag(Pf[j][k]) << endl;
              k++;
           }
        }
     }
  break;

  default:
     cout << "program calculates two and three pulse experiments only"
        << endl;
     exit(0);
```

```
        break;
    }
    wrtp1.close();
    wrtt1.close();
    wrtpf1.close();
    wrtpp1.close();
    ofstream wrtwf1("wfor1.dat", ios::out);
    wrtwf1 << "1" << "\n" << fpt << "\n" << -1/(2*dt*cmfs) << "\n" << 1/(fpt*dt*cmfs) << endl;
    wrtwf1.close();
    delete [] Pt;
    delete [] Pf;
} // p3sum1

void rsum1(complex *ef[], complex *efc[], complex pt1[], complex ct[], complex cc[],
        complex ci[], complex cic[], double xT1[], double xT2[], int num, double dly1,
        double dly2, int diag[], int lowr, int uppr, int dt, double g[])
{
    int t,t1,t2,t3,xx;
    int p[3], dly[3];
    complex cti, ctc, igl1, igl2, igl3;

    xx=num/2-1;
    for (int i=0; i<3; i++){
        p[i]=diag[i+1]-1;
        dly[i]=0;
        if (p[i]==0)
            dly[i]=dly1;
        if (p[i]==1)
            dly[i]=dly2;
    }
    for (t=lowr; t<uppr+1; t+=dt){
        for (t1=lowr; t1<t; t1+=dt){
            for (t2=lowr; t2<t1; t2+=dt){
                for (t3=lowr; t3<t2; t3+=dt){
                    ctc=cc[xx+t2-t3]*cc[xx+t-t3]*cic[xx+t1-t3];
                    igl1+=xT2[xx+t-t1+t2-t3]*g[xx+t-t1+t2-t3]*ctc*efc[p[0]][t3-dly[0]];
                }
                cti=ct[xx+t1-t2]*ci[xx+t-t2];
                igl2+=xT1[xx+t1-t2]*dt*cti*ef[p[1]][t2-dly[1]]*igl1;
                igl1=complex(0,0);
            }
            igl3+=dt*ct[xx+t-t1]*efc[p[2]][t1-dly[2]]*igl2;
            igl2=complex(0,0);
        }
        pt1[t]=dt*igl3;
        igl3=complex(0,0);
    }
} // rsum1

void r1delta(complex *pt1[], complex ct[], complex cc[], complex ci[], complex cic[],
        double xT1[], double xT2[], int num, double dly[], int dpts, int diag[],
        int dly2, int lowr, int uppr, int dt, double g[])
{
    int xx=num/2-1, t;
    int p[3], d[3];
    complex cti, ctc;
```

```
    for (int i=0; i<dpts; i++){
      for (int j=0; j<3; j++){
        p[j]=diag[j+1]-1;
        d[j]=0;
        if (p[j]==0)
          d[j]=dly[i];
        else if (p[j]==1)
          d[j]=dly2;
        d[j]+=xx;
      }
      if (d[2] >= d[1] && d[1] >= d[0]){
        for (t=lowr; t<uppr+1; t+=dt){
          if (t >= d[2]){
            cti=ct[xx+t-d[2]]*ct[xx+d[2]-d[1]]*ci[xx+t-d[1]];
            ctc=cc[xx+d[1]-d[0]]*cc[xx+t-d[0]]*cic[xx+d[2]-d[0]];
            pt1[i][t]=xT2[xx+t-d[2]+d[1]-d[0]]*xT1[xx+d[2]-d[1]]*g[xx+t-d[2]+d[1]-d[0]]
                  *cti*ctc;
          }
          else
            pt1[i][t]=complex(0.0,0.0);
        }
      }
      else{
        for (t=lowr; t<uppr+1; t+=dt)
          pt1[i][t]=complex(0.0,0.0);
      }
    }
  } // r1delta
```

```
// pcsum2.cpp
// functions to calculate one term (R2) of P3(t) in
// linear dipole response approximation.

#include "csum2.hpp"
#include "yehmath.hpp"

#include <complex.h>
#include <fstream.h>
#include <iostream.h>
#include <iomanip.h>
#include <math.h>
#include <stdlib.h>

#define kcm 0.695029    // boltzmann (cm*K)-1
#define pi 3.14159265358979
#define cmfs 2.99792458e-5    // speed of light (cm/fs)

void p3sum2(complex *ei[], complex *ec[], complex ldr[], complex ldrc[], complex ldri[],
        complex ldric[], double t[], double dT1[], double dT2[], int num, double *dlay[],
        int dpts[], double ewide[], int nplses, int low, int upp, int dgmn[],
        double gbrd[], complex *P3t[])
{
   extern int dt;
   extern double T2, ufact;
   int i,j,k,top,butt,npt,ind,dpt1=dpts[0],dpt2,pick=nplses,fpt,mpt,cft;
   double remain, test=0, dy1=0, dy2=0, hgh, lw;
   complex pp, pconj;
   complex **Pt=new complex*[dpt1],    // P3(t)
         **Pf=new complex*[dpt1];    // P3(w)
   for (i=0; i<dpt1; i++){
      Pt[i]=new complex[num];
      Pf[i]=new complex[num];
   }

   for (i=0; i<nplses; i++)
         test+=ewide[i];
   if (test==0){
      if (nplses==2)
         pick=101;
      else
         pick=102;
   }

   top=upp;
   butt=low;
   mpt=(top-butt)/dt+1;

   ofstream wrtp2("psum2.dat", ios::app);
   ofstream wrtt2("tsum2.dat", ios::app);
   ofstream wrtpf2("pfor2.dat", ios::app);
   ofstream wrtpp2("pp2.dat", ios::app);
   switch (pick){
      case 2:
         wrtp2 << dpt1 << "\t 0" << endl;
```

```
    wrtt2 << dpt1 << endl;
    wrtpf2 << dpt1 << "\t 0" << endl;
    for (i=0; i<dpt1; i++){
      if (dlay[0][i] > 0){
        upp=double((dlay[0][i]+T2*ufact-t[0])*(num-1)/(t[num-1]-t[0]));
        low=double((-2*ewide[1]-t[0])*(num-1)/(t[num-1]-t[0]));
        if ((dlay[0][i]-2*ewide[0]) < (-2*ewide[1]))
          low=double((dlay[0][i]-2*ewide[0]-t[0])*(num-1)/(t[num-1]-t[0]));
      }
      else{
        upp=double((T2*ufact-t[0])*(num-1)/(t[num-1]-t[0]));
        low=double((dlay[0][i]-2*ewide[0]-t[0])*(num-1)/(t[num-1]-t[0]));
        if ((dlay[0][i]-2*ewide[0]) > (-2*ewide[1]))
          low=double((-2*ewide[1]-t[0])*(num-1)/(t[num-1]-t[0]));
      }
      dy1=dlay[0][i];
      cft=(dy1-t[0])*(num-1)/(t[num-1]-t[0]);
      ind=dy1;
      remain=fmod(upp-low,dt);
      while (remain != 0){
        upp++;
        remain=fmod(upp-low,dt);
      }
      npt=(upp-low)/dt + 1;
      wrtt2 << npt << "\n" << t[low] << "\n" << dt << endl;
      rsum2(ei,ec,Pt[i],ldr,ldrc,ldri,ldric,dT1,dT2,num,dy1,dy2,dgmn,
         low,upp,dt,gbrd);
      fpt=cfour(Pf[i],Pt[i],npt,low,dt,mpt,cft);
      wrtp2 << npt << "\t 0" << endl;
      wrtpf2 << fpt << "\t 0" << endl;
      for (j=0; j<npt; j++){
        wrtp2 << real(Pt[i][low+j*dt]) << "\t"
             << imag(Pt[i][low+j*dt]) << endl;
        wrtpf2 << real(Pf[i][j]) << "\t"
             << imag(Pf[i][j]) << endl;
        P3t[i][low+j*dt]+=Pt[i][low+j*dt];
        pconj=conj(ei[0][low+j*dt-ind]);
        pp+=Pt[i][low+j*dt]*pconj;
      }
      wrtpp2 << real(pp) << "\t" << imag(pp) << endl;
      pp=complex(0,0);
      while (j<fpt){
        wrtpf2 << real(Pf[i][j]) << "\t"
             << imag(Pf[i][j]) << endl;
        j++;
      }
    }
  break;

  case 3:
    dpt2=dpts[1];
    wrtp2 << dpt1*dpt2 << "\t 0" << endl;
    wrtt2 << dpt1*dpt2 << endl;
    wrtpf2 << dpt1*dpt2 << "\t 0" << endl;
    for (i=0; i<dpt2; i++){
      ind=i*dpt1;
```

```
        dy2=dlay[1][i];
        hgh=T2*ufact;
        lw=-2*ewide[2];
        if (dy2+T2*ufact > hgh)
           hgh=dy2+T2*ufact;
        else if (dy2-2*ewide[1] < lw)
           lw=dy2 - 2*ewide[1];
        for (j=0; j<dpt1; j++){
           dy1=dlay[0][j];
           cft=(dy1-t[0])*(num-1)/(t[num-1]-t[0]);
           if (dy1+T2*ufact > hgh)
              hgh=dy1+T2*ufact;
           else if (dy1-2*ewide[0] < lw)
              lw=dy1 - 2*ewide[0];
           upp=double((hgh-t[0])*(num-1)/(t[num-1]-t[0]));
           low=double((lw-t[0])*(num-1)/(t[num-1]-t[0]));
           remain=fmod(upp-low,dt);
           while(remain != 0){
              upp++;
              remain=fmod(upp-low,dt);
           }
           npt=(upp-low)/dt + 1;
           wrtt2 << npt << "\n" << t[low] << "\n" << dt << endl;
           rsum2(ei,ec,Pt[j],ldr,ldrc,ldri,ldric,dT1,dT2,num,dy1,dy2,dgmn,
               low,upp,dt,gbrd);
           fpt=cfour(Pf[j],Pt[j],npt,low,dt,mpt,cft);
           wrtp2 << npt << "\t 0" << endl;
           wrtpf2 << fpt << "\t 0" << endl;
           for (k=0; k<npt; k++){
              wrtp2 << real(Pt[j][low+k*dt]) << "\t"
                   << imag(Pt[j][low+k*dt]) << endl;
              wrtpf2 << real(Pf[j][k]) << "\t"
                    << imag(Pf[j][k]) << endl;
              P3t[ind+j][low+k*dt]+=Pt[j][low+k*dt];
           }
           while (k<fpt){
              wrtpf2 << real(Pf[j][k]) << "\t"
                    << imag(Pf[j][k]) << endl;
              k++;
           }
        }
     }
break;

case 101:
   dy1=dlay[1][0];
   wrtt2 << "1" << endl;
   r2delta(Pt,ldr,ldrc,ldri,ldric,dT1,dT2,num,dlay[0],dpt1,dgmn,dy1,butt,top,dt,gbrd);
   npt=(top-butt)/dt+1;
   wrtt2 << npt << "\n" << t[butt] << "\n" << dt << endl;
   wrtp2 << dpt1 << "\t 0" << endl;
   wrtpf2 << dpt1 << "\t 0" << endl;
   for (i=0; i<dpt1; i++){
      cft=(dlay[0][i]-t[0])*(num-1)/(t[num-1]-t[0]);
      ind=num/2-1+dlay[0][i];
      pp=Pt[i][ind];
```

```
        wrtpp2 << real(pp) << "\t" << imag(pp) << endl;
        fpt=cfour(Pf[i],Pt[i],npt,butt,dt,mpt,cft);
        wrtp2 << npt << "\t 0" << endl;
        wrtpf2 << fpt << "\t 0" << endl;
        for (j=0; j<npt; j++){
           wrtp2 << real(Pt[i][butt+j*dt]) << "\t"
                << imag(Pt[i][butt+j*dt]) << endl;
           wrtpf2 << real(Pf[i][j]) << "\t"
                << imag(Pf[i][j]) << endl;
           P3t[i][butt+j*dt]+=Pt[i][butt+j*dt];
        }
        while (j<fpt){
           wrtpf2 << real(Pf[i][j]) << "\t"
                << imag(Pf[i][j]) << endl;
           j++;
        }
     }
  break;

  case 102:
     dpt2=dpts[1];
     wrtt2 << "1" << endl;
     npt=(top-butt)/dt+1;
     wrtt2 << npt << "\n" << t[butt] << "\n" << dt << endl;
     wrtp2 << dpt1*dpt2 << "\t 0" << endl;
     wrtpf2 << dpt1*dpt2 << "\t 0" << endl;
     for (i=0; i<dpt2; i++){
        ind=i*dpt1;
        dy1=dlay[1][i];
        r2delta(Pt,ldr,ldrc,ldri,ldric,dT1,dT2,num,dlay[0],dpt1,dgmn,dy1,butt,top,
              dt,gbrd);
        for (j=0; j<dpt1; j++){
           cft=(dlay[0][j]-t[0])*(num-1)/(t[num-1]-t[0]);
           fpt=cfour(Pf[j],Pt[j],npt,butt,dt,mpt,cft);
           wrtp2 << npt << "\t 0" << endl;
           wrtpf2 << fpt << "\t 0" << endl;
           for (k=0; k<npt; k++){
              wrtp2 << real(Pt[j][butt+k*dt]) << "\t"
                   << imag(Pt[j][butt+k*dt]) << endl;
              wrtpf2 << real(Pf[j][k]) << "\t"
                   << imag(Pf[j][k]) << endl;
              P3t[ind+j][butt+k*dt]+=Pt[j][butt+k*dt];
           }
           while (k<fpt){
              wrtpf2 << real(Pf[j][k]) << "\t"
                   << imag(Pf[j][k]) << endl;
              k++;
           }
        }
     }
  break;

  default:
     cout << "program calculates two and three pulse experiments only"
        << endl;
     exit(0);
```

```
        break;
    }
    wrtp2.close();
    wrtt2.close();
    wrtpf2.close();
    wrtpp2.close();
    ofstream wrtwf2("wfor2.dat", ios::out);
    wrtwf2 << "1" << "\n" << fpt << "\n" << -1/(2*dt*cmfs) << "\n"
          << 1/(fpt*dt*cmfs) << endl;
    wrtwf2.close();
    delete [] Pt;
    delete [] Pf;
} // p3sum2

void rsum2(complex *ef[], complex *efc[], complex pt1[], complex ct[], complex cc[],
        complex ci[], complex cic[], double xT1[], double xT2[], int num, double dly1,
        double dly2, int diag[], int lowr, int uppr, int dt, double g[])
{
    int xx=num/2-1;
    int p[3], dly[3];
    complex cti, ctc, igl1, igl2, igl3;

    for (int i=0; i<3; i++){
        p[i]=diag[i+1]-1;
        dly[i]=0;
        if (p[i]==0)
            dly[i]=dly1;
        if (p[i]==1)
            dly[i]=dly2;
    }
    for (int t=lowr; t<uppr+1; t+=dt){
        for (int t1=lowr; t1<t; t1+=dt){
            for (int t2=lowr; t2<t1; t2+=dt){
                for (int t3=lowr; t3<t2; t3+=dt){
                    cti=ct[xx+t2-t3]*ct[xx+t1-t3]*ci[xx+t-t3];
                    igl1+=xT2[xx+t-t1+t2-t3]*g[xx+t-t1-t2+t3]*cti*ef[p[0]][t3-dly[0]];
                }
                ctc=cc[xx+t-t2]*cic[xx+t1-t2]*efc[p[1]][t2-dly[1]];
                igl2+=xT1[xx+t1-t2]*dt*ctc*igl1;
                igl1=complex(0,0);
            }
            igl3+=dt*ct[xx+t-t1]*efc[p[2]][t1-dly[2]]*igl2;
            igl2=complex(0,0);
        }
        pt1[t]=dt*igl3;
        igl3=complex(0,0);
    }
} // rsum2

void r2delta(complex *pt1[], complex ct[], complex cc[], complex ci[], complex cic[],
        double xT1[], double xT2[], int num, double dly[], int dpts, int diag[],
        int dly2, int lowr, int uppr, int dt, double g[])
{
    int xx=num/2-1, t;
    int p[3], d[3];
    complex cti, ctc;
```

```
    for (int i=0; i<dpts; i++){
        for (int j=0; j<3; j++){
            p[j]=diag[j+1]-1;
            d[j]=0;
            if (p[j]==0)
                d[j]=dly[i];
            else if (p[j]==1)
                d[j]=dly2;
            d[j]+=xx;
        }
        if (d[2] >= d[1] && d[1] >= d[0]){
            for (t=lowr; t<uppr+1; t+=dt){
                if (t >= d[2]){
                    cti=ct[xx+t-d[2]]*ct[xx+d[1]-d[0]]*ct[xx+d[2]-d[0]]*ci[xx+t-d[0]];
                    ctc=cc[xx+t-d[1]]*cic[xx+d[2]-d[1]];
                    pt1[i][t]=xT2[xx+t-d[2]+d[1]-d[0]]*xT1[xx+d[2]-d[1]]*g[xx+t-d[2]-d[1]+d[0]]
                            *cti*ctc;
                }
                else
                    pt1[i][t]=complex(0.0,0.0);
            }
        }
        else{
            for (t=lowr; t<uppr+1; t+=dt)
                pt1[i][t]=complex(0.0,0.0);
        }
    }
} // r2delta
```

```
// pcsum3.cpp
// functions to calculate one term (R3) of P3(t) in
// linear dipole response approximation.

#include "csum3.hpp"
#include "yehmath.hpp"

#include <complex.h>
#include <fstream.h>
#include <iostream.h>
#include <iomanip.h>
#include <math.h>
#include <stdlib.h>

#define kcm 0.695029    // boltzmann (cm*K)-1
#define pi 3.14159265358979
#define cmfs 2.99792458e-5      // speed of light (cm/fs)

void p3sum3(complex *ei[], complex *ec[], complex ldr[], complex ldrc[], complex ldri[],
        double t[], double dT1[], double dT2[], int num, double *dlay[], int dpts[],
        double ewide[], int nplses, int low, int upp, int dgmn[], double gbrd[],
        complex *P3t[])
{
   extern int dt;
   extern double T2, ufact;
   int i,j,k,top,butt,npt,ind,dpt1=dpts[0],dpt2,pick=nplses,fpt,mpt,cft;
   double remain, test=0, dy1=0, dy2=0, hgh, lw;
   complex pp, pconj;
   complex **Pt=new complex*[dpt1],    // P3(t)
         **Pf=new complex*[dpt1];    // P3(w)
   for (i=0; i<dpt1; i++){
      Pt[i]=new complex[num];
      Pf[i]=new complex[num];
   }

   for (i=0; i<nplses; i++)
         test+=ewide[i];
   if (test==0){
      if (nplses==2)
         pick=101;
      else
         pick=102;
   }

   top=upp;
   butt=low;
   mpt=(top-butt)/dt+1;

   ofstream wrtp3("psum3.dat", ios::app);
   ofstream wrtt3("tsum3.dat", ios::app);
   ofstream wrtpf3("pfor3.dat", ios::app);
   ofstream wrtpp3("pp3.dat", ios::app);
   switch (pick){
      case 2:
         wrtp3 << dpt1 << "\t 0" << endl;
```

```
    wrtt3 << dpt1 << endl;
    wrtpf3 << dpt1 << "\t 0" << endl;
    for (i=0; i<dpt1; i++){
        if (dlay[0][i] > 0){
            upp=double((dlay[0][i]+T2*ufact-t[0])*(num-1)/(t[num-1]-t[0]));
            low=double((-2*ewide[1]-t[0])*(num-1)/(t[num-1]-t[0]));
            if ((dlay[0][i]-2*ewide[0]) < (-2*ewide[1]))
                low=double((dlay[0][i]-2*ewide[0]-t[0])*(num-1)/
                        (t[num-1]-t[0]));
        }
        else{
            upp=double((T2*ufact-t[0])*(num-1)/(t[num-1]-t[0]));
            low=double((dlay[0][i]-2*ewide[0]-t[0])*(num-1)/(t[num-1]-t[0]));
            if ((dlay[0][i]-2*ewide[0]) > (-2*ewide[1]))
                low=double((-2*ewide[1]-t[0])*(num-1)/(t[num-1]-t[0]));
        }
        dy1=dlay[0][i];
        cft=(dy1-t[0])*(num-1)/(t[num-1]-t[0]);
        ind=dy1;
        remain=fmod(upp-low,dt);
        while (remain != 0){
            upp++;
            remain=fmod(upp-low,dt);
        }
        npt=(upp-low)/dt + 1;
        wrtt3 << npt << "\n" << t[low] << "\n" << dt << endl;
        rsum3(ei,ec,Pt[i],ldr,ldrc,ldri,dT1,dT2,num,dy1,dy2,dgmn,low,upp,
            dt,gbrd);
        fpt=cfour(Pf[i],Pt[i],npt,low,dt,mpt,cft);
        wrtp3 << npt << "\t 0" << endl;
        wrtpf3 << fpt << "\t 0" << endl;
        for (j=0; j<npt; j++){
            wrtp3 << real(Pt[i][low+j*dt]) << "\t"
                << imag(Pt[i][low+j*dt]) << endl;
            wrtpf3 << real(Pf[i][j]) << "\t"
                << imag(Pf[i][j]) << endl;
            P3t[i][low+j*dt]+=Pt[i][low+j*dt];
            pconj=conj(ei[0][low+j*dt-ind]);
            pp+=Pt[i][low+j*dt]*pconj;
        }
        wrtpp3 << real(pp) << "\t" << imag(pp) << endl;
        pp=complex(0,0);
        while (j<fpt){
            wrtpf3 << real(Pf[i][j]) << "\t"
                << imag(Pf[i][j]) << endl;
            j++;
        }
    }
break;

case 3:
    dpt2=dpts[1];
    wrtp3 << dpt1*dpt2 << "\t 0" << endl;
    wrtt3 << dpt1*dpt2 << endl;
    wrtpf3 << dpt1*dpt2 << "\t 0" << endl;
    for (i=0; i<dpt2; i++){
```

```
        ind=i*dpt1;
        dy2=dlay[1][i];
        hgh=T2*ufact;
        lw=-2*ewide[2];
        if (dy2+T2*ufact > hgh)
           hgh=dy2+T2*ufact;
        else if (dy2-2*ewide[1] < lw)
           lw=dy2 - 2*ewide[1];
        for (j=0; j<dpt1; j++){
           dy1=dlay[0][j];
           cft=(dy1-t[0])*(num-1)/(t[num-1]-t[0]);
           if (dy1+T2*ufact > hgh)
              hgh=dy1+T2*ufact;
           else if (dy1-2*ewide[0] < lw)
              lw=dy1 - 2*ewide[0];
           upp=double((hgh-t[0])*(num-1)/(t[num-1]-t[0]));
           low=double((lw-t[0])*(num-1)/(t[num-1]-t[0]));
           remain=fmod(upp-low,dt);
           while(remain != 0){
              upp++;
              remain=fmod(upp-low,dt);
           }
           npt=(upp-low)/dt + 1;
           wrtt3 << npt << "\n" << t[low] << "\n" << dt << endl;
           rsum3(ei,ec,Pt[j],ldr,ldrc,ldri,dT1,dT2,num,dy1,dy2,dgmn,
              low,upp,dt,gbrd);
           fpt=cfour(Pf[j],Pt[j],npt,low,dt,mpt,cft);
           wrtp3 << npt << "\t 0" << endl;
           wrtpf3 << fpt << "\t 0" << endl;
           for (k=0; k<npt; k++){
              wrtp3 << real(Pt[j][low+k*dt]) << "\t"
                 << imag(Pt[j][low+k*dt]) << endl;
              wrtpf3 << real(Pf[j][k]) << "\t"
                 << imag(Pf[j][k]) << endl;
              P3t[ind+j][low+k*dt]+=Pt[j][low+k*dt];
           }
           while (k<fpt){
              wrtpf3 << real(Pf[j][k]) << "\t"
                 << imag(Pf[j][k]) << endl;
              k++;
           }
        }
     }
break;

case 101:
   dy1=dlay[1][0];
   wrtt3 << "1" << endl;
   r3delta(Pt,ldr,ldrc,ldri,dT1,dT2,num,dlay[0],dpt1,dgmn,dy1,butt,top,
      dt,gbrd);
   npt=(top-butt)/dt+1;
   wrtt3 << npt << "\n" << t[butt] << "\n" << dt << endl;
   wrtp3 << dpt1 << "\t 0" << endl;
   wrtpf3 << dpt1 << "\t 0" << endl;
   for (i=0; i<dpt1; i++){
      cft=(dlay[0][i]-t[0])*(num-1)/(t[num-1]-t[0]);
```

```
        ind=num/2-1+dlay[0][i];
        pp=Pt[i][ind];
        wrtpp3 << real(pp) << "\t" << imag(pp) << endl;
        fpt=cfour(Pf[i],Pt[i],npt,butt,dt,mpt,cft);
        wrtp3 << npt << "\t 0" << endl;
        wrtpf3 << fpt << "\t 0" << endl;
        for (j=0; j<npt; j++){
           wrtp3 << real(Pt[i][butt+j*dt]) << "\t"
                << imag(Pt[i][butt+j*dt]) << endl;
           wrtpf3 << real(Pf[i][j]) << "\t"
                << imag(Pf[i][j]) << endl;
           P3t[i][butt+j*dt]+=Pt[i][butt+j*dt];
        }
        while (j<fpt){
           wrtpf3 << real(Pf[i][j]) << "\t"
                << imag(Pf[i][j]) << endl;
           j++;
        }
     }
  break;

  case 102:
     dpt2=dpts[1];
     wrtt3 << "1" << endl;
     npt=(top-butt)/dt+1;
     wrtt3 << npt << "\n" << t[butt] << "\n" << dt << endl;
     wrtp3 << dpt1*dpt2 << "\t 0" << endl;
     wrtpf3 << dpt1*dpt2 << "\t 0" << endl;
     for (i=0; i<dpt2; i++){
        ind=i*dpt1;
        dy1=dlay[1][i];
        r3delta(Pt,ldr,ldrc,ldri,dT1,dT2,num,dlay[0],dpt1,dgmn,dy1,butt,top,dt,gbrd);
        for (j=0; j<dpt1; j++){
           cft=(dlay[0][j]-t[0])*(num-1)/(t[num-1]-t[0]);
           fpt=cfour(Pf[j],Pt[j],npt,butt,dt,mpt,cft);
           wrtp3 << npt << "\t 0" << endl;
           wrtpf3 << fpt << "\t 0" << endl;
           for (k=0; k<npt; k++){
              wrtp3 << real(Pt[j][butt+k*dt]) << "\t"
                   << imag(Pt[j][butt+k*dt]) << endl;
              wrtpf3 << real(Pf[j][k]) << "\t"
                   << imag(Pf[j][k]) << endl;
              P3t[ind+j][butt+k*dt]+=Pt[j][butt+k*dt];
           }
           while (k<fpt){
              wrtpf3 << real(Pf[j][k]) << "\t"
                   << imag(Pf[j][k]) << endl;
              k++;
           }
        }
     }
  break;

  default:
     cout << "program calculates two and three pulse experiments only"
        << endl;
```

```
            exit(0);
        break;
    }
    wrtp3.close();
    wrtt3.close();
    wrtpf3.close();
    wrtpp3.close();
    ofstream wrtwf3("wfor3.dat", ios::out);
    wrtwf3 << "1" << "\n" << fpt << "\n" << -1/(2*dt*cmfs) << "\n" << 1/(fpt*dt*cmfs) << endl;
    wrtwf3.close();
    delete [] Pt;
    delete [] Pf;
} // p3sum3

void rsum3(complex *ef[], complex *efc[], complex pt1[], complex ct[], complex cc[],
        complex ci[], double xT1[], double xT2[], int num, double dly1, double dly2,
        int diag[], int lowr, int uppr, int dt, double g[])
{
    int xx=num/2-1;
    int p[3], dly[3];
    complex cti, ctc, igl1, igl2, igl3;

    for (int i=0; i<3; i++){
        p[i]=diag[i+1]-1;
        dly[i]=0;
        if (p[i]==0)
            dly[i]=dly1;
        if (p[i]==1)
            dly[i]=dly2;
    }
    for (int t=lowr; t<uppr+1; t+=dt){
        for (int t1=lowr; t1<t; t1+=dt){
            for (int t2=lowr; t2<t1; t2+=dt){
                for (int t3=lowr; t3<t2; t3+=dt){
                    cti=ct[xx+t2-t3]*ct[xx+t1-t3]*ci[xx+t-t3];
                    igl1+=xT2[xx+t-t1+t2-t3]*g[xx+t-t1-t2+t3]*cti*ef[p[0]][t3-dly[0]];
                }
                cti=ct[xx+t-t2]*ci[xx+t1-t2];
                igl2+=xT1[xx+t1-t2]*dt*cti*efc[p[1]][t2-dly[1]]*igl1;
                igl1=complex(0,0);
            }
            ctc=cc[xx+t-t1]*efc[p[2]][t1-dly[2]];
            igl3+=dt*ctc*igl2;  // e1 in ctc
            igl2=complex(0,0);
        }
        pt1[t]=dt*igl3;
        igl3=complex(0,0);
    }
} // rsum3

void r3delta(complex *pt1[], complex ct[], complex cc[], complex ci[], double xT1[],
        double xT2[], int num, double dly[], int dpts, int diag[], int dly2, int lowr,
        int uppr, int dt, double g[])
{
    int xx=num/2-1, t;
    int p[3], d[3];
```

```
    complex cti;

    for (int i=0; i<dpts; i++){
        for (int j=0; j<3; j++){
            p[j]=diag[j+1]-1;
            d[j]=0;
            if (p[j]==0)
                d[j]=dly[i];
            else if (p[j]==1)
                d[j]=dly2;
            d[j]+=xx;
        }
        if (d[2] >= d[1] && d[1] >= d[0]){
            for (t=lowr; t<uppr+1; t+=dt){
                if (t >= d[2]){
                    cti=ct[xx+t-d[1]]*ct[xx+d[1]-d[0]]*ct[xx+d[2]-d[0]]*ci[xx+t-d[0]]
                        *ci[xx+d[2]-d[1]];
                    pt1[i][t]=xT2[xx+t-d[2]+d[1]-d[0]]*xT1[xx+d[2]-d[1]]*g[xx+t-d[2]-d[1]+d[0]]
                            *cti*cc[xx+t-d[2]];
                }
                else
                    pt1[i][t]=complex(0.0,0.0);
            }
        }
        else{
            for (t=lowr; t<uppr+1; t+=dt)
                pt1[i][t]=complex(0.0,0.0);
        }
    }
} // r3delta
```

```
// pcsum4.cpp
// functions to calculate one term (R4) of P3(t) in
// linear dipole response approximation.

#include "csum4.hpp"
#include "yehmath.hpp"

#include <complex.h>
#include <fstream.h>
#include <iostream.h>
#include <iomanip.h>
#include <math.h>
#include <stdlib.h>

#define kcm 0.695029    // boltzmann (cm*K)-1
#define pi 3.14159265358979
#define cmfs 2.99792458e-5      // speed of light (cm/fs)

void p3sum4(complex *ei[], complex *ec[], complex ldrc[], complex ldric[], double t[],
        double dT1[], double dT2[], int num, double *dlay[], int dpts[], double ewide[],
        int nplses, int low, int upp, int dgmn[], double gbrd[], complex *P3t[])
{
   extern int dt;
   extern double T2, ufact;
   int i,j,k,top,butt,npt,ind,dpt1=dpts[0],dpt2,pick=nplses,fpt,mpt,cft;
   double remain, test=0, dy1=0, dy2=0, hgh, lw;
   complex pp, pconj;
   complex **Pt=new complex*[dpt1],   // P3(t)
         **Pf=new complex*[dpt1];    // P3(w)
   for (i=0; i<dpt1; i++){
      Pt[i]=new complex[num];
      Pf[i]=new complex[num];
   }

   for (i=0; i<nplses; i++)
         test+=ewide[i];
   if (test==0){
      if (nplses==2)
         pick=101;
      else
         pick=102;
   }

   top=upp;
   butt=low;
   mpt=(top-butt)/dt+1;

   ofstream wrtp4("psum4.dat", ios::app);
   ofstream wrtt4("tsum4.dat", ios::app);
   ofstream wrtpf4("pfor4.dat", ios::app);
   ofstream wrtpp4("pp4.dat", ios::app);
   switch (pick){
      case 2:
         wrtp4 << dpt1 << "\t 0" << endl;
         wrtt4 << dpt1 << endl;
```

```
    wrtpf4 << dpt1 << "\t 0" << endl;
    for (i=0; i<dpt1; i++){
      if (dlay[0][i] > 0){
        upp=double((dlay[0][i]+T2*ufact-t[0])*(num-1)/(t[num-1]-t[0]));
        low=double((-2*ewide[1]-t[0])*(num-1)/(t[num-1]-t[0]));
        if ((dlay[0][i]-2*ewide[0]) < (-2*ewide[1]))
          low=double((dlay[0][i]-2*ewide[0]-t[0])*(num-1)/
                (t[num-1]-t[0]));
      }
      else{
        upp=double((T2*ufact-t[0])*(num-1)/(t[num-1]-t[0]));
        low=double((dlay[0][i]-2*ewide[0]-t[0])*(num-1)/(t[num-1]-t[0]));
        if ((dlay[0][i]-2*ewide[0]) > (-2*ewide[1]))
          low=double((-2*ewide[1]-t[0])*(num-1)/(t[num-1]-t[0]));
      }
      dy1=dlay[0][i];
      cft=(dy1-t[0])*(num-1)/(t[num-1]-t[0]);
      ind=dy1;
      remain=fmod(upp-low,dt);
      while (remain != 0){
        upp++;
        remain=fmod(upp-low,dt);
      }
      npt=(upp-low)/dt + 1;
      wrtt4 << npt << "\n" << t[low] << "\n" << dt << endl;
      rsum4(ei,ec,Pt[i],ldrc,ldric,dT1,dT2,num,dy1,dy2,dgmn,low,upp,dt,gbrd);
      fpt=cfour(Pf[i],Pt[i],npt,low,dt,mpt,cft);
      wrtp4 << npt << "\t 0" << endl;
      wrtpf4 << fpt << "\t 0" << endl;
      for (j=0; j<npt; j++){
        wrtp4 << real(Pt[i][low+j*dt]) << "\t"
            << imag(Pt[i][low+j*dt]) << endl;
        wrtpf4 << real(Pf[i][j]) << "\t"
            << imag(Pf[i][j]) << endl;
        P3t[i][low+j*dt]+=Pt[i][low+j*dt];
        pconj=conj(ei[0][low+j*dt-ind]);
        pp+=Pt[i][low+j*dt]*pconj;
      }
      wrtpp4 << real(pp) << "\t" << imag(pp) << endl;
      pp=complex(0,0);
      while (j<fpt){
        wrtpf4 << real(Pf[i][j]) << "\t"
            << imag(Pf[i][j]) << endl;
        j++;
      }
    }
  break;

  case 3:
    dpt2=dpts[1];
    wrtp4 << dpt1*dpt2 << "\t 0" << endl;
    wrtt4 << dpt1*dpt2 << endl;
    wrtpf4 << dpt1*dpt2 << "\t 0" << endl;
    for (i=0; i<dpt2; i++){
      ind=i*dpt1;
      dy2=dlay[1][i];
```

```
        hgh=T2*ufact;
        lw=-2*ewide[2];
        if (dy2+T2*ufact > hgh)
           hgh=dy2+T2*ufact;
        else if (dy2-2*ewide[1] < lw)
           lw=dy2 - 2*ewide[1];
        for (j=0; j<dpt1; j++){
           dy1=dlay[0][j];
           cft=(dy1-t[0])*(num-1)/(t[num-1]-t[0]);
           if (dy1+T2*ufact > hgh)
              hgh=dy1+T2*ufact;
           else if (dy1-2*ewide[0] < lw)
              lw=dy1 - 2*ewide[0];
           upp=double((hgh-t[0])*(num-1)/(t[num-1]-t[0]));
           low=double((lw-t[0])*(num-1)/(t[num-1]-t[0]));
           remain=fmod(upp-low,dt);
           while(remain != 0){
              upp++;
              remain=fmod(upp-low,dt);
           }
           npt=(upp-low)/dt + 1;
           wrtt4 << npt << "\n" << t[low] << "\n" << dt << endl;
           rsum4(ei,ec,Pt[j],ldrc,ldric,dT1,dT2,num,dy1,dy2,dgmn,low,upp,
              dt,gbrd);
           fpt=cfour(Pf[j],Pt[j],npt,low,dt,mpt,cft);
           wrtp4 << npt << "\t 0" << endl;
           wrtpf4 << fpt << "\t 0" << endl;
           for (k=0; k<npt; k++){
              wrtp4 << real(Pt[j][low+k*dt]) << "\t"
                   << imag(Pt[j][low+k*dt]) << endl;
              wrtpf4 << real(Pf[j][k]) << "\t"
                   << imag(Pf[j][k]) << endl;
              P3t[ind+j][low+k*dt]+=Pt[j][low+k*dt];
           }
           while (k<fpt){
              wrtpf4 << real(Pf[j][k]) << "\t"
                   << imag(Pf[j][k]) << endl;
              k++;
           }
        }
     }
break;

case 101:
   dy1=dlay[1][0];
   wrtt4 << "1" << endl;
   r4delta(Pt,ldrc,ldric,dT1,dT2,num,dlay[0],dpt1,dgmn,dy1,butt,top,dt,gbrd);
   npt=(top-butt)/dt+1;
   wrtt4 << npt << "\n" << t[butt] << "\n" << dt << endl;
   wrtp4 << dpt1 << "\t 0" << endl;
   wrtpf4 << dpt1 << "\t 0" << endl;
   for (i=0; i<dpt1; i++){
      cft=(dlay[0][i]-t[0])*(num-1)/(t[num-1]-t[0]);
      ind=num/2-1+dlay[0][i];
      pp=Pt[i][ind];
      wrtpp4 << real(pp) << "\t" << imag(pp) << endl;
```

```
            fpt=cfour(Pf[i],Pt[i],npt,butt,dt,mpt,cft);
            wrtp4 << npt << "\t 0" << endl;
            wrtpf4 << fpt << "\t 0" << endl;
            for (j=0; j<npt; j++){
               wrtp4 << real(Pt[i][butt+j*dt]) << "\t"
                    << imag(Pt[i][butt+j*dt]) << endl;
               wrtpf4 << real(Pf[i][j]) << "\t"
                     << imag(Pf[i][j]) << endl;
               P3t[i][butt+j*dt]+=Pt[i][butt+j*dt];
            }
            while (j<fpt){
               wrtpf4 << real(Pf[i][j]) << "\t"
                     << imag(Pf[i][j]) << endl;
               j++;
            }
         }
      break;

      case 102:
         dpt2=dpts[1];
         wrtt4 << "1" << endl;
         npt=(top-butt)/dt+1;
         wrtt4 << npt << "\n" << t[butt] << "\n" << dt << endl;
         wrtp4 << dpt1*dpt2 << "\t 0" << endl;
         wrtpf4 << dpt1*dpt2 << "\t 0" << endl;
         for (i=0; i<dpt2; i++){
            ind=i*dpt1;
            dy1=dlay[1][i];
            r4delta(Pt,ldrc,ldric,dT1,dT2,num,dlay[0],dpt1,dgmn,dy1,butt,top,dt,gbrd);
            for (j=0; j<dpt1; j++){
               cft=(dlay[0][j]-t[0])*(num-1)/(t[num-1]-t[0]);
               fpt=cfour(Pf[j],Pt[j],npt,butt,dt,mpt,cft);
               wrtp4 << npt << "\t 0" << endl;
               wrtpf4 << fpt << "\t 0" << endl;
               for (k=0; k<npt; k++){
                  wrtp4 << real(Pt[j][butt+k*dt]) << "\t"
                       << imag(Pt[j][butt+k*dt]) << endl;
                  wrtpf4 << real(Pf[j][k]) << "\t"
                        << imag(Pf[j][k]) << endl;
                  P3t[ind+j][butt+k*dt]+=Pt[j][butt+k*dt];
               }
               while (k<fpt){
                  wrtpf4 << real(Pf[j][k]) << "\t"
                        << imag(Pf[j][k]) << endl;
                  k++;
               }
            }
         }
      break;

      default:
         cout << "program calculates two and three pulse experiments only"
            << endl;
         exit(0);
      break;
   }
```

```
   wrtp4.close();
   wrtt4.close();
   wrtpf4.close();
   wrtpp4.close();
   ofstream wrtwf4("wfor4.dat", ios::out);
   wrtwf4 << "1" << "\n" << fpt << "\n" << -1/(2*dt*cmfs) << "\n" << 1/(fpt*dt*cmfs) << endl;
   wrtwf4.close();
   delete [] Pt;
   delete [] Pf;
} // p3sum4

void rsum4(complex *ef[], complex *efc[], complex pt1[], complex cc[], complex cic[],
        double xT1[], double xT2[], int num, double dly1, double dly2, int diag[], int lowr,
        int uppr, int dt, double g[])
{
   int xx=num/2-1;
   int p[3], dly[3];
   complex ctc, igl1, igl2, igl3;

   for (int i=0; i<3; i++){
      p[i]=diag[i+1]-1;
      dly[i]=0;
      if (p[i]==0)
         dly[i]=dly1;
      if (p[i]==1)
         dly[i]=dly2;
   }
   for (int t=lowr; t<uppr+1; t+=dt){
      for (int t1=lowr; t1<t; t1+=dt){
         for (int t2=lowr; t2<t1; t2+=dt){
            for (int t3=lowr; t3<t2; t3+=dt){
               ctc=cc[xx+t2-t3]*cc[xx+t-t3]*cic[xx+t1-t3]*efc[p[0]][t3-dly[0]];
               igl1+=xT2[xx+t-t1+t2-t3]*g[xx+t-t1+t2-t3]*ctc;      // e3 in ctc
            }
            ctc=cc[xx+t1-t2]*cic[xx+t-t2];
            igl2+=xT1[xx+t1-t2]*dt*ctc*ef[p[1]][t2-dly[1]]*igl1;
            igl1=complex(0,0);
         }
         ctc=cc[xx+t-t1]*efc[p[2]][t1-dly[2]];
         igl3+=dt*ctc*igl2;  // e1 in ctc
         igl2=complex(0,0);
      }
      pt1[t]=dt*igl3;
      igl3=complex(0,0);
   }
} // rsum4

void r4delta(complex *pt1[], complex cc[], complex cic[], double xT1[], double xT2[], int num,
         double dly[], int dpts, int diag[], int dly2, int lowr, int uppr,
         int dt, double g[])
{
   int xx=num/2-1, t;
   int p[3], d[3];
   complex ctc;

   for (int i=0; i<dpts; i++){
```

```
        for (int j=0; j<3; j++){
            p[j]=diag[j+1]-1;
            d[j]=0;
            if (p[j]==0)
                d[j]=dly[i];
            else if (p[j]==1)
                d[j]=dly2;
            d[j]+=xx;
        }
        if (d[2] >= d[1] && d[1] >= d[0]){
            for (t=lowr; t<uppr+1; t+=dt){
                if (t >= d[2]){
                    ctc=cc[xx+t-d[2]]*cc[xx+d[2]-d[1]]*cc[xx+d[1]-d[0]]*cc[xx+t-d[0]]
                          *cic[xx+t-d[1]]*cic[xx+d[2]-d[0]];
                    pt1[i][t]=xT2[xx+t-d[2]+d[1]-d[0]]*xT1[xx+d[2]-d[1]]*g[xx+t-d[2]+d[1]-d[0]]
                            *ctc;
                }
                else
                    pt1[i][t]=complex(0.0,0.0);
            }
        }
        else{
            for (t=lowr; t<uppr+1; t+=dt)
                pt1[i][t]=complex(0.0,0.0);
        }
    }
} // r4delta
```

## References


1. A. Juris, V. Balzani, F. Barigelletti, S. Campagna, P. Belser, A. Von Zelewsky, *Ru(II) Polypyridine Complexes: Photophysics, Photochemistry, Electrochemistry, and Chemiluminescence.* Coordination Chemistry Reviews, 1988. **84**: p. 85.
2. Cotton, F.A., *Chemical Applications of Group Theory.* 3rd ed. 1990, New York: John Wiley & Sons.
3. J.N. Demas, G.A. Crosby, Journal of the American Chemical Society, 1971. **93**: p. 2841.
4. J.N. Demas, D.G. Taylor, *"Intersystem Crossing" Yields in Ruthenium(II) and Osmium(II) Photosensitizers.* Inorganic Chemistry, 1979. **18**(11): p. 3177.
5. F.E. Lytle, D.M. Hercules, *The Luminescence of Tris(2,2'-bipyridine)ruthenium(II) Dichloride.* Journal of the American Chemical Society, 1969. **91**(2): p. 253.
6. D.P. Rillema, D.S. Jones, *Structure of Tris(2,2'-bipyridyl)ruthenium(II) Hexafluorophosphate, $[Ru(bipy)_3][PF_6]_2$; X-Ray Crystallographic Determination.* Journal of Chemical Society Chemical Communications, 1979: p. 849.
7. D. Braun, E. Gallhuber, H. Yersin, *Zeeman splittings of the two lowest excited states of $[Ru(bpy)_3](PF_6)_2$.* Chemical Physics Letters, 1990. **171**(1,2): p. 122.
8. H. Yersin, E. Gallhuber, *On the Lowest Excited States of $[Ru(bpy)_3](PF_6)_2$ Single Crystals.* Journal of the American Chemical Society, 1984. **106**(22): p. 6582.
9. J. Ferguson, E. Krausz, *Time-Resolved Luminescence and MCPL of $Ru(bpy)_3^{2+}$ in Glassy Solvents at the Fluid-Glass Transition.* Chemical Physics Letters, 1986. **127**(6): p. 551.
10. Krausz, E., *Excited-State Raman Spectra in the Luminescent States of $Ru(bpy)_3^{2+}$ in Solid Phases.* Chemical Physics Letters, 1985. **116**(6): p. 501.
11. N. Kitamura, H.-B. Kim, Y. Kawanishi, R. Obata, S. Tazuke, *Time-Resolved Emission Spectra of $Ru(bpy)_3Cl_2$ and cis-$Ru(bpy)_2(CN)_2$ at Low Temperature.* Journal of Physical Chemistry, 1986. **90**(8): p. 1488.
12. P.G. Bradley, N. Kress, B.A. Hornberger, R.F. Dallinger, W.H. Woodruff, *Vibrational Spectroscopy of the Electronically Excited State. 5. Time-Resolved Resonance Raman Study of Tris(bipyridine) ruthenium(II) and Related Complexes. Definitive Evidence for the "Localized" MLCT State.* Journal of the American Chemical Society, 1981. **103**(25): p. 7441.
13. P.J. Carroll, L.E. Brus, *Picosecond Raman Scattering Study of Electron Localization in the Charge-Transfer Excited State of Tris(bipyridine) ruthenium(II).* Journal of the American Chemical Society, 1987. **109**(25): p. 7613.

14. R.A. Malone, D.F. Kelley, *Interligand electron transfer and transition state dynamics in Ru(II)trisbipyridine.* Journal of Chemical Physics, 1991. **95**(12): p. 8970.
15. T. Yabe, L.K. Orman, D.R. Anderson, S.-C. Yu, X. Xu, J.B. Hopkins, *Picosecond Raman Investigation of Interligand Electron Transfer in Ruthenium(II) Complexes.* Journal of Physical Chemistry, 1990. **94**(18): p. 7128.
16. J. Van Houten, R.J. Watts, *Photochemistry of Tris(2,2'-bipyridyl)ruthenium(II) in Aqueous Solutions.* Inorganic Chemistry, 1978. **17**(12): p. 3381.
17. C. Creutz, M. Chou, T.L. Netzel, M. Okumura, N. Sutin, *Lifetimes, Spectra, and Quenching of the Excited States of Polypyridine Complexes of Iron(II), Ruthenium(II), and Osmium(II).* Journal of the American Chemical Society, 1980. **102**(4): p. 1309.
18. C.R. Bock, T.J. Meyer, D.G. Whitten, *Electron Transfer Quenching of the Luminescent Excited State of Tris(2,2'-bipyridine)ruthenium(II). A Flash Photolysis Relaxation Technique for Measuring the Rates of Very Rapid Electron Transfer Reactions.* Journal of the American Chemical Society, 1974. **96**(14): p. 4710.
19. D.K. Liu, B.S. Brunschwig, C. Creutz, N. Sutin, *Formation of Electronically Excited Products in Electron-Transfer Reactions: Reaction of Polypyridine Complexes of Cobalt(I) and Ruthenium(III) in Acetonitrile.* Journal of the American Chemical Society, 1986. **108**(8): p. 1749.
20. G.H. Allen, R.P. White, D.P. Rillema, T.J. Meyer, *Synthetic Control of Excited-State Properties. Tris-Chelate Complexes Containing the Ligands 2,2'-Bipyrazine, 2,2'-Bipyridine, and 2,2'-Bipyrimidine.* Journal of the American Chemical Society, 1984. **106**(9): p. 2613.
21. H.D. Gafney, A.W. Adamson, *Excited State Ru(bipyr)$_3^{2+}$ as an Electron-Transfer Reductant.* Journal of the American Chemical Society, 1972. **94**(23): p. 8238.
22. J.N. Demas, A.W. Adamson, *Tris(2,2'-bipyridine)ruthenium(II) Sensitized Reactions of Some Oxalato Complexes.* Journal of the American Chemical Society, 1973. **95**(16): p. 5159.
23. R. Ballardini, G. Varani, F. Scandola, V. Balzani, *Bimolecular Electron Transfer Processes of Electronically Excited Tris(2,2'-bipyridine)chromium(III).* Journal of the American Chemical Society, 1976. **98**(23): p. 7432.
24. E.M. Kober, T.J. Meyer, *Concerning the Absorption Spectra of the Ions M(bpy)$_3^{2+}$ (M = Fe, Ru, Os; bpy = 2,2'-Bipyridine).* Inorganic Chemistry, 1982. **21**(11): p. 3967.
25. C. Daul, E.J. Baerends, P. Vernooijs, *A Density Functional Study of the MLCT States of [Ru(bpy)$_3$]$^{2+}$ in $D_3$ Symmetry.* Inorganic Chemistry, 1994. **33**(16): p. 3538.
26. J. Ferguson, F. Herren, *A Model for the Interpretation of the Electronic Spectra of the Complex Ions M(bpy)$_3^{2+}$ (M = Fe, Ru, Os) in $D_3$ and $C_2$ Sites.* Chemical Physics, 1983. **76**: p. 45.

27. P.K. Mallick, G.D. Danzer, D.P. Strommen, J.R. Kincaid, *Vibrational Spectra and Normal-Coordinate Analysis of Tris(bipyridine)ruthenium(II).* Journal of Physical Chemistry, 1988. **92**(20): p. 5628.
28. S.K. Doorn, J.T. Hupp, *Preresonance Raman Studies of Metal-to-Ligand Charge Transfer in $(NH_3)_4Ru(2,2'\text{-bpy})^{2+}$. In Situ Bond Length Changes, Force Constants, and Reorganization Energies.* Journal of the American Chemical Society, 1989. **111**(13): p. 4704.
29. D.P. Strommen, P.K. Mallick, G.D. Danzer, R.S. Lumpkin, J.R. Kincaid, *Normal-Coordinate Analyses of the Ground and $^3$MLCT Excited States of Tris(bipyridine)ruthenium(II).* Journal of Physical Chemistry, 1990. **94**(4): p. 1357.
30. P.K. Mallick, D.P. Strommen, J.R. Kincaid, *Molecular Structure Determination of Transient Species from Vibrational Frequency Data. Application to the $^3$MLCT State of Tris(bipyridine)ruthenium(II).* Journal of the American Chemical Society, 1990. **112**(5): p. 1686.
31. R.F. Dallinger, W.H. Woodruff, *Time-Resolved Resonance Raman Study of the Lowest Excited State of Tris(2,2'-bipyridine)ruthenium(II).* Journal of the American Chemical Society, 1979. **101**(15): p. 4391.
32. U. Lachish, P.P. Infelta, M. Gratzel, *Optical Absorption Spectrum of Excited Ruthenium Tris-Bipyridyl ($Ru(bpy)_3^{2+}$).* Chemical Physics Letters, 1979. **62**(2): p. 317.
33. N.H. Damrauer, G. Cerullo, A. Yeh, T.R. Boussie, C.V. Shank, J.K. McCusker, *Femtosecond Dynamics of Excited-State Evolution in $[Ru(bpy)_3]^{2+}$.* Science, 1997. **275**: p. 54.
34. Z. Vardeny, J. Tauc, *Picosecond Coherence Coupling in the Pump and Probe Technique.* Optics Communication, 1981. **39**(6): p. 396.
35. W.T. Pollard, S.-Y. Lee, R.A. Mathies, *Wave packet theory of dynamic absorption spectra in femtosecond pump-probe experiments.* Journal of Chemical Physics, 1990. **92**(7): p. 4012.
36. W.T. Pollard, R.A. Mathies, *Analysis of Femtosecond Dynamic Absorption Spectra of Nonstationary States.* Annual Reviews in Physical Chemistry, 1992. **43**: p. 497.
37. C.H. Brito Cruz, J.P. Gordon, P.C. Becker, R.L. Fork, C.V. Shank, *Dynamics of Spectral Hole Burning.* IEEE Journal of Quantum Electronics, 1988. **24**(2): p. 261.
38. Mukamel, S., *Principles of Nonlinear Optical Spectroscopy.* 1995, New York: Oxford University Press.
39. A.T. Yeh, G. Cerullo, U. Banin, A. Mews, A.P. Alivisatos, C.V. Shank, *Dynamics of exciton localization in CdS/HgS quantum-dot quantum wells.* Physical Review B, 1999. **59**(7): p. 4973.
40. M. Yan, L. Rothberg, B.R. Hsieh, R.R. Alfano, *Exciton formation and decay dynamics in electroluminescent polymers observed by subpicosecond stimulated emission.* Physical Review B, 1994. **49**(14): p. 9419.

41. M. Yoshizawa, Y. Hattori, T. Kobayashi, *Femtosecond time-resolved resonance Raman gain spectroscopy in polydiacetylene.* Physical Review B, 1994. **49**(18): p. 13259.
42. T. Kobayashi, M. Yoshizawa, U. Stamm, M. Taiji, M. Hasegawa, *Relaxation dynamics of photoexcitations in polydiacetylenes and polythiophene.* Journal of Optical Society of America B, 1990. **7**(8): p. 1558.
43. W.B. Bosma, S. Mukamel, B.I. Greene, S. Schmitt-Rink, *Femtosecond Pump-Probe Spectroscopy of Conjugated Polymers: Coherent and Sequential Contributions.* Physical Review Letters, 1992. **68**(16): p. 2456.
44. A.B. Myers, R.A. Mathies, *Resonance Raman Intensities: A Probe of Excited-State Structure and Dynamics.* Biological Applications of Raman Spectroscopy: Vol. 2 - Resonance Raman Spectroscopy of Polyenes and Aromatics, ed. T.G. Spiro. 1987: John Wiley & Sons, Inc. 1-58.
45. M. Forster, R.E. Hester, *Resonance Raman Investigation of Electronically Excited Ru(Bipyridine)$_3^{2+}$ using a CW Laser.* Chemical Physics Letters, 1981. **81**(1): p. 42.
46. C. Turro, Y.C. Chung, N. Leventis, M.E. Kuckenmeister, P.J. Wagner, G.E. Leroi, *Resonance Raman Spectrum of the Phenanthroline Anion: Implications on Electron Delocalization in the MLCT Excited State of Ru(phen)$_3^{2+}$.* Inorganic Chemistry, 1996. **35**(17): p. 5104.
47. G.D. Danzer, J.R. Kincaid, *Resonance Raman Spectra of Homoleptic and Heteroleptic Complexes of Ruthenium(II) with Bipyridine and Bipyrazine in the Ground and $^3$MLCT Excited States.* Journal of Physical Chemistry, 1990. **94**(10): p. 3976.
48. P.A. Mabrouk, M.S. Wrighton, *Resonance Raman Spectroscopy of the Lowest Excited State of Derivatives of Tris(2,2'-bipyridine)ruthenium(II): Substituent Effects on Electron Localization in Mixed-Ligand Complexes.* Inorganic Chemistry, 1986. **25**(4): p. 526.
49. S.M. Treffert-Ziemelis, J. Golus, D.P. Strommen, J.R. Kincaid, *Resonance Raman and Time-Resolved Resonance Raman Studies of Tris(4-methyl-2,2'-bipyridine)ruthenium(II). Polarization of the Radical Fragment of the $^3$MLCT States.* Inorganic Chemistry, 1993. **32**(18): p. 3890.
50. L.K. Orman, J.B. Hopkins, *Re-evaluation of the Raman Assignments in the Ground and Excited Metal to Ligand Charge Transfer State of Tris-2,2'-Bipyridine Ru(II).* Chemical Physics Letters, 1988. **149**(4): p. 375.
51. Y.J. Chang, X. Xu, T. Yabe, S.-C. Yu, D.R. Anderson, L.K. Orman, J.B. Hopkins, *Picosecond Raman Measurements of Electron Transfer in the Metal-to-Ligand Charge-Transfer Excited States of 1,10-Phenanthroline-Ruthenium(II) Complexes.* Journal of Physical Chemistry, 1990. **94**(2): p. 729.
52. Y.J. Chang, L.K. Orman, D.R. Anderson, T. Yabe, J.B. Hopkins, *Picosecond Raman studies of dynamic charge localization following metal to ligand charge transfer excitation in tris (2,2'-bipyridyl) ruthenium (II).* Journal of Chemical Physics, 1987. **87**(5): p. 3249.

53. T. Yabe, D.R. Anderson, L.K. Orman, Y.J. Chang, J.B. Hopkins, *Picosecond Dynamics of Solvent Trapping following Electron Transfer in Transition-Metal Complexes.* Journal of Physical Chemistry, 1989. **93**(6): p. 2302.
54. J. Ferguson, E. Krausz, *Delocalization As Evidenced by Absorption, Luminescence, and Excitation Spectra of $Ru(bpy)_3^{2+}$ in $Zn(bpy)_3(PF6)_2$ and Ethanol/Methanol Glasses.* Inorganic Chemistry, 1987. **26**(9): p. 1383.
55. C.M. Carlin, M.K. DeArmond, *Temperature-Dependent Photoselection--Intramolecular Exciton Motion in $[Ru(bpy)_3]^{2+}$.* Journal of the American Chemical Society, 1985. **107**(1): p. 53.
56. E. Danielson, R.S. Lumpkin, T.J. Meyer, *Time-Resolved Emission at the Glass-to-Fluid Transition. Localization or Delocalization in Polypyridyl-Based Metal-to-Ligand Charge-Transfer Excited States of Ruthenium and Osmium?* Journal of Physical Chemistry, 1987. **91**(6): p. 1305.
57. E.M. Kober, B.P. Sullivan, T.J. Meyer, *Solvent Dependence of Metal-to-Ligand Charge-Transfer Transitions. Evidence for Initial Electron Localization in MLCT Excited States of 2,2'-Bipyridine Complexes of Ruthenium(II) and Osmium(II).* Inorganic Chemistry, 1984. **23**(14): p. 2098.
58. J. Van Houten, R.J. Watts, *Temperature Dependence of the Photophysical and Photochemical Properties of the Tris(2,2'-bipyridyl)ruthenium(II) Ion in Aqueous Solution.* Journal of the American Chemical Society, 1976. **98**(16): p. 4853.
59. G.R. Fleming, J.M. Morris, G.W. Robinson, *Direct Observation of Rotational Diffusion by Picosecond Spectroscopy.* Chemical Physics, 1976. **17**: p. 91.
60. C.V. Shank, E.P. Ippen, *Anisotropic absorption saturation with picosecond pulses.* Applied Physics Letters, 1975. **26**(2): p. 62.
61. Gordon, R.G., *Molecular Collisions and the Depolarization of Fluorescence in Gases.* Journal of Chemical Physics, 1966. **45**(5): p. 1643.
62. A.J. Cross, G.R. Fleming, *Analysis of Time-Resolved Fluorescence Anisotropy Decays.* Biophysical Journal, 1984. **46**: p. 45.
63. C. Galli, K. Wynne, S.M. LeCours, M.J. Therien, R.M. Hochstrasser, *Direct measurement of electronic dephasing using anisotropy.* Chemical Physics Letters, 1993. **206**(5,6): p. 493.
64. K. Wynne, R.M. Hochstrasser, *Coherence effects in the anisotropy of optical experiments.* Chemical Physics, 1993. **171**(1993): p. 179.
65. J. Ferguson, E. Krausz, *Absorption, Luminescence, and Magnetic Circular Polarized Luminescence of Dicarboethoxy Derivatives of $Ru(bpy)_3^{2+}$ in Rigid and Fluid Solutions: Evidence for Environmentally Induced Charge Localization.* Journal of Physical Chemistry, 1987. **91**(12): p. 3161.
66. M.L. Myrick, R.L. Blakley, M.K. DeArmond, M.L. Arthur, *Evidence for Static Localization in the Lowest Optically Excited States of Ruthenium(II) Diimine Complexes: A Solvent- and Time-Dependent Photoselection Study at 77 K.* Journal of the American Chemical Society, 1988. **110**(5): p. 1325.
67. K.K. Stavrev, M.C. Zerner, T.J. Meyer, *Outer-Sphere Charge-Transfer Effects on the Spectroscopy of the $[Ru(NH_3)_5(py)]^{2+}$ Complex.* Journal of the American Chemical Society, 1995. **117**(33): p. 8684.
68. Ege, S., *Organic Chemistry.* 2nd ed. 1989, Lexington: D.C. Heath and Company.

69. C.-P. Hsu, X. Song, R.A. Marcus, *Time-Dependent Stokes Shift and Its Calculation from Solvent Dielectric Dispersion Data.* Journal of Physical Chemistry B, 1997. **101**(14): p. 2546.
70. R.M. Stratt, M. Maroncelli, *Nonreactive Dynamics in Solution: The Emerging Molecular View of Solvation Dynamics and Vibrational Relaxation.* Journal of Physical Chemistry, 1996. **100**(31): p. 12981.
71. C.J. Bardeen, C.V. Shank, *Ultrafast dynamics of the solvent-solute interaction measured by femtosecond four-wave mixing: LD690 in n-alcohols.* Chemical Physics Letters, 1994. **226**: p. 310.
72. C.J. Bardeen, G.Cerullo, C.V. Shank, *Temperature-dependent electronic dephasing of molecules in polymers in the range 30 to 300 K.* Chemical Physics Letters, 1997. **280**: p. 127.
73. G.A. Crosby, K.W. Hipps, W.H. Elfring, *On the Appropriateness of Assigning Spin Labels to Excited States of Inorganic Complexes.* Journal of the American Chemical Society, 1974. **96**: p. 629.
74. K.W. Hipps, G.A. Crosby, *Charge-Transfer Excited States of Ruthenium(II) Complexes. III. An Electron-Ion Coupling Model for $d\pi^*$ Configurations.* Journal of the American Chemical Society, 1975. **97**(24): p. 7042.
75. H. Wang, M. Jiang, R. Merlin, D.G. Steel, *Spin-Flip-Induced Hole Burning in GaAs Quantum Wells: Determination of the Exciton Zeeman Splitting.* Physical Review Letters, 1992. **69**(5): p. 804.
76. J.B. Stark, W.H. Knox, D.S. Chemla, *Femtosecond Circular Dichroism Study of Nonthermal Carrier Distributions in Two- and Zero-Dimensional Semiconductors.* Physical Review Letters, 1992. **68**(20): p. 3080.
77. M.Z. Maialle, E.A. de Andrada e Silva, L.J. Sham, *Exciton spin dynamics in quantum wells.* Physical Review B, 1993. **47**(23): p. 15776.
78. R.C. Miller, D.A. Kleinman, *Excitons In GaAs Quantum Wells.* Journal of Luminescence, 1985. **30**: p. 520.
79. S. Bar-Ad, I. Bar-Joseph, *Exciton Spin Dynamics in GaAs Heterostructures.* Physical Review Letters, 1992. **68**(3): p. 349.
80. Levine, I.N., *Physical Chemistry.* 3rd ed. 1988, New York: McGraw-Hill Book Company.
81. M. Ziegler, A. von Zelewsky, *Charge-transfer excited state properties of chiral transition metal coordination compounds studied by chiroptical spectroscopy.* Coordination Chemistry Reviews, 1998. **177**: p. 257.
82. X. Hua, A. von Zelewsky, *Enantiomerically Pure Chiral $Ru^{II}(L\hat{}L)_2$ Building Blocks for Coordination Compounds.* Inorganic Chemistry, 1995. **34**(23): p. 5791.
83. Ziegler, M., *Personal Communication*, 2000.
84. J.S. Gold, S.J. Milder, J.W. Lewis, D.S. Kliger, *Transient Circular Dichroism of the Luminescent State of $[Ru(bpy)_3]^{2+}$.* Journal of the American Chemical Society, 1985. **107**: p. 8285.
85. A. Ceulemans, L.G. Vanquickenborne, *On the Charge-Transfer Spectra of Iron(II)- and Ruthenium(II)-Tris(2,2'-bipyridyl) Complexes.* Journal of the American Chemical Society, 1981. **103**(9): p. 2238.

86. C.A. Daul, J. Weber, *The Electronic Structure and Low-Lying Excited States of the Ruthenium(II)Tris(Diimine) Complex.* Chemical Physics Letters, 1981. **77**(3): p. 593.
87. D.H. Oh, M. Sano, S.G. Boxer, *Electroabsorption (Stark Effect) Spectroscopy of Mono- and Biruthenium Charge-Transfer Complexes: Measurements of Changes in Dipole Moments and Other Electrooptic Properties.* Journal of the American Chemical Society, 1991. **113**(18): p. 6880.
88. F. Felix, J. Ferguson, H.U. Gudel, A. Ludi, *Electronic Spectra of $M(bipy)_3^{2+}$ Complex Ions (M=Fe, Ru, and Os).* Chemical Physics Letters, 1979. **62**(1): p. 153.
89. G.D. Hager, R.J. Watts, G.A. Crosby, *Charge-Transfer Excited States of Ruthenium(II) Complexes. II. Relationship of Level Parameters to Molecular Structure.* Journal of the American Chemical Society, 1975. **97**(24): p. 7037.
90. J.V. Caspar, T.D. Westmoreland, G.H. Allen, P.G. Bradley, T.J. Meyer, W.H. Woodruff, *Molecular and Electronic Structure in the Metal-to-Ligand Charge-Transfer Excited States of $d^6$ Transition-Metal Complexes in Solution.* Journal of the American Chemical Society, 1984. **106**(12): p. 3492.
91. P. Belser, C. Daul, A. Von Zelewsky, *On the Assignment of the MLCT Transition in the $Ru(bpy)_3^{2+}$ Complex Ion.* Chemical Physics Letters, 1981. **79**(3): p. 596.
92. Y. Tanabe, S. Sugano, *On the Absorption Spectra of Complex Ions. I.* Journal of the Physical Society of Japan, 1954. **9**(5): p. 753.
93. Y. Tanabe, S. Sugano, *On the Absorption Spectra of Complex Ions. II.* Journal of the Physical Society of Japan, 1954. **9**(5): p. 766.

Ernest Orlando Lawrence Berkeley National Laboratory
One Cyclotron Road · Berkeley, California 94720

Prepared for the U.S. Department of Energy under Contract No. DE-AC03-76SF00098